Università degli Studi di Bergamo, Italy
Department of Engineering and applied Sciences

Collision Detection for Industrial Applications

Fabio Angeloni

in fulfillment of the requirements
for the degree of

Doctor of Philosophy in
Mechatronics, Information Technology,
New Technologies and Mathematical Methods

XXIX Cycle

Advisor: Prof. Fabio Previdi

April, 2017

Everything should be made as simple as possible,
but no simpler.

ALBERT EINSTEIN

Abstract

In the manufacturing industry, the request of complex products and the decreasing of production time have led to more and more sophisticated CNC-controlled multi-axis machines. Often their setup process is affected by different mistakes caused by the persons responsible that lead to collisions inside the working area. Those collisions often lead to damage the tool and the work piece.

The thesis deals with this problem, providing new insights for a fast and robust collision detection. Imagining to start from scratch, through a dynamic analysis of the impact in a mechanical transmission, we reached to identify the sensors which provide the optimal trade-off between the quality of impact information measured, feasibility and costs. Then, we propose two new collision detection algorithms able to identify the unwanted event as fast as possible, with the goal to reduce the impact force and containing the damage. Furthermore, their performance are compared with the most successful algorithm found in literature on two different mechanical systems: a heavy automatic access gate and the laboratory's robotic arm.

Keywords. *Collision Detection, Inertial Platforms, Mechatronic Systems, Sensor Fusion, Estimation, Kalman Filtering, Robotics, Safe Physical Human Robot Interaction, Observing Generalized Momentum.*

Contents

Chapter 1

Introduction

(a) Physical Human-Robot Interaction.

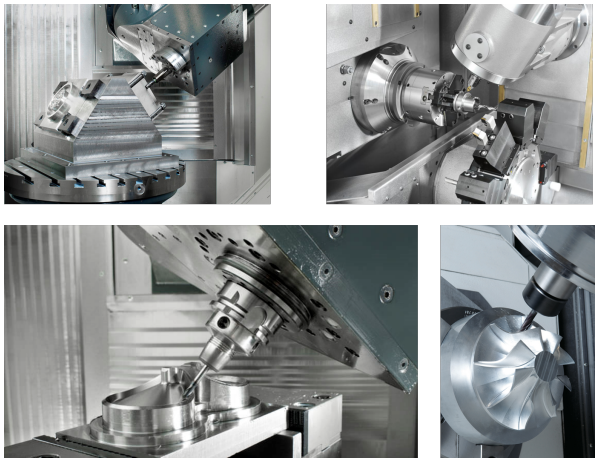

(b) Complex manufacturing process.

Figure 1.1: Two examples of collision detection industrial applications.

The impact is a very complex phenomenon which occurs when two or more bodies undergo a collision, or come in touch each other.

This topic has always attracted the interest of scientists and engineers from different areas of knowledge for years. The first studies go back to 1639 with Marci [32], who derived the first relations on impact mechanics based

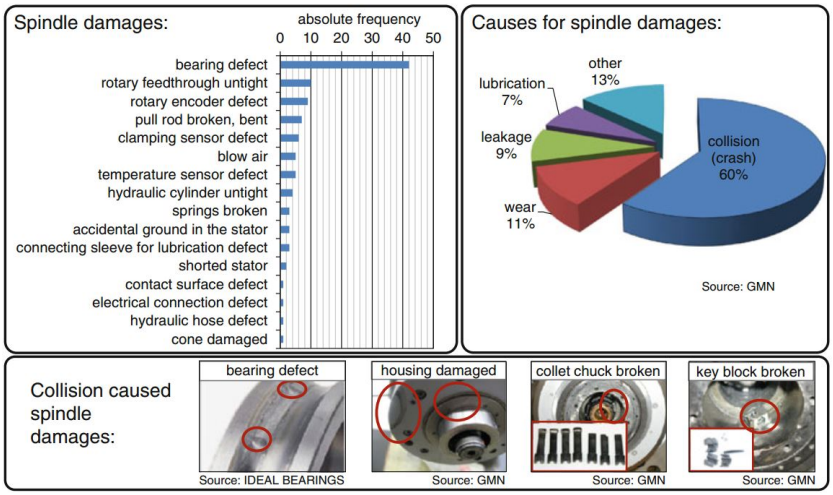

Figure 1.2: Damages of main spindle units and their causes [2].

on experiments, and have continued until nowadays with the developing of several methods for detecting and avoiding a collision.

In the manufacturing industry, the increasing product complexity and decreasing production time have led to more and more complex manufacturing processes. Therefore, collisions within the working area of the machine tools occur more often.

Those collisions often lead to damage the tool and the work piece. Especially in cases of machining processes very large and complex work pieces, e.g. in the Aerospace Industry, where such a damage might be very expensive. Additionally, these collisions could cause the breakage of the whole machine, which will lead to downtime and high costs [44].

In Figure 1.2 we report the results of a survey on spindle damages. It comprises the analysis of 231 spindle systems and their causes of failure. Ninety-seven out of two hundred failures in the observation period can be attributed to process loads. The remaining failures are the consequence of direct or indirect faulty operation and crashes [2].

While CAM software automatically generate complex machining programs, the process itself may still be erroneous. These errors range from wrong NC programs for specific NC control units [46], wrong or missing considerations of the whole machine tool, or clamping devices, caused by human errors[46].
The first two error sources (wrong NC program, wrong or missing consideration of machine parts) can be prevented by using machine simulation programs prior to the real production process at the real machine tool with its adjusted control unit. However, operator errors, which increasingly appear as the process gets more and more complex, cannot be prevented by simulation.
In Figure 1.3 we report a schematic illustration of the setup process of a CNC-controlled multi-axis machine for a new machining task. In particular, the setup process can be especially affected by different mistakes caused by the persons responsible. Such errors may result in collisions of the machine tool, work piece or clamping devices. These collisions not only damage the work piece or the clamping device, but may also lead to damages at the machine tool and, consequentially, lead to downtimes and high costs. Obviously, the damage depends on the kind and strength of the collision.

For the last decades, a lot of strategies have been researched and implemented to decrease the impact of collisions on the manufacturing processes [4]). Figure 1.4 shows an overview of currently existing collision protection measures.
Newly generated, the NC software are usually tested thoroughly with simulation programs prior to the real production process. They simulate the whole machine tool, coupling the 3D-CAD model of the real machine and the workpiece with the NC-code in terms of boundary representation models. Some

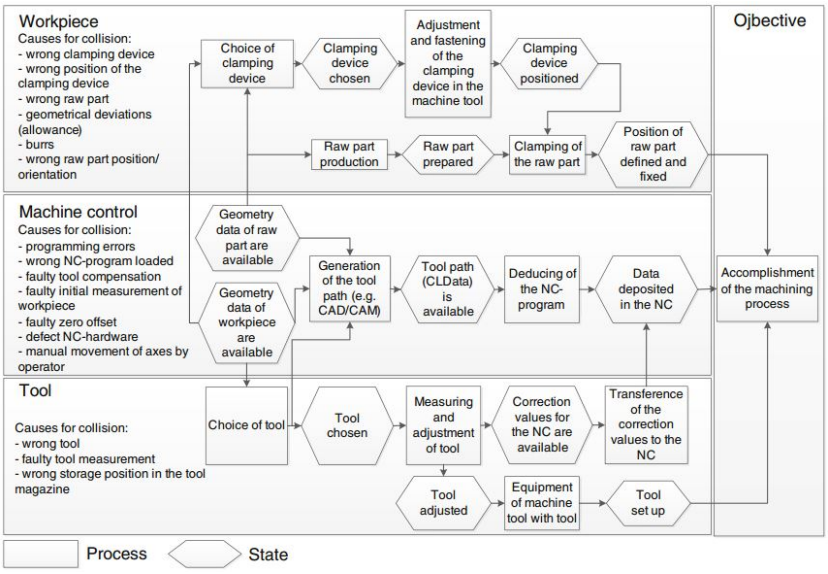

Figure 1.3: Setup process of a CNC-controlled multi-axis machine for a new machining task and possible collision causes [2].

of them also use Virtual Reality or Augmented Reality to enhance an effect close-to-reality [37,38,41,47]. An integration of the real NC control unit into the simulation environment is also possible [61]. These machine simulation programs detect most errors of the NC program. However, during the real production process on a real machine tool there are still a lot of tasks that cannot be simulated with machine simulation software. As mentioned before, these operations are all manual user operations, setup of new work pieces or new tools and a change of the clamping device during the production process. Another approach to prevent collisions, even during the operation, uses external sensors like a camera system [53] or laser systems to monitor the working space. These systems are limited to the sensor detection fields.

To reduce the collisions on the process and therefore to limit the costs of a crash, some systems do not prevent the collision itself but decrease the strength of the collision. Sensorless solutions allow collision detection without additional sensors, just by analyzing the signals of the motor current of

the main spindle and the feed axes. In case of a crash the current of the spindle engine increases and a stop signal will be sent automatically to all moving machine axes [3].
Sensor-based measures use additional sensor elements which are applied to the machine structure. In [9] different solutions are described using spindle-integrated piezo force sensors for the identification of collision situations. In [43] a sensor-based method coupled with mechanical overload protection elements for contact detection between tool and workpiece to initiate the emergency reaction is presented. Another strategy to avoid damages caused by collisions is to integrate mechanical overload elements into the force flux of the machine tool. One example is the use of overload clutches which are integrated in the feed axes between axis drive and ball screw. In case of collision, the torque in the feed drive chain rises to a critical limit and the overload clutches separate the ball screw from the drive. Compared to sensorless solutions, sensor-based collision detection is in general much faster because of the fast reaction time of the sensor systems [12].

An industrial sector where the collision detection topic has come of key interest is that of Robotics.
For more than half a century it was predicted that robots will eventually interact and work closely with humans in diverse everyday environments as well as support them in industrial scenarios. However, despite large efforts in all major robotic fields, only recently have robots gained capabilities in both sensing and actuation, which may enable operation in the proximity of humans.
Recently, some significant contributions in control, design, motion planning, and safety were achieved to provide a solid basis for *physical Human-Robot*

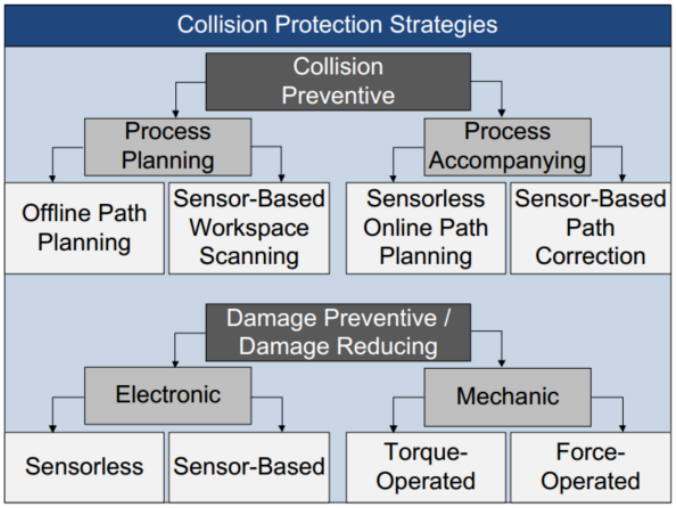

Figure 1.4: Overview of different collision protection measures [4].

Interaction (pHRI) [17].

There have been initial investigations of robot-human collisions and their related impact characteristics. The resulting contact forces during the impact phase may be reduced by pursuing a lightweight robot design [20], by adding soft visco-elastic covering to the links [59], or by introducing compliance in the driving system so as to mechanically decouple the heavy motor inertia from the link inertia [7, 58]. Others approaches focus on the developing of algorithms, able to detect a collision merging the information from different sensors – i.e. motor torque and speed [11, 17].

These innovations are expected to lead to entirely new application domains that will require highly flexible and autonomous robotic systems, like:

- support of humans in heavy industrial jobs,
- elderly care in elderly-dominated societies,
- rehabilitation robotics,
- tele-presence systems during lack or high cost of local human expertise,

- and unmanned warfare with human augmentation.

1.1 Contribution of the thesis

In Figure 1.4 the collision detection strategies are classified in two categories: the Collision Preventive and Damage Preventive, or Reducing.

Focusing on the second category, the present thesis provides new insights for a fast and robust collision detection addressing to industrial applications. Through a dynamic analysis of the impact in a mechanical transmission, we reach to identify the types of sensor which provide the optimal trade-off between the quality of information measured on the impact, feasibility and costs.
Furthermore, we propose two new collision detection algorithms, which performance are compared to the top algorithm found in literatures on two different mechanical systems: a heavy automatic access gate 1.5a and the laboratory's robotic arm 1.5b.

(a) DEIMOS automatic access gate.

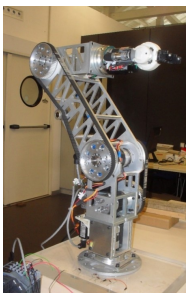

(b) Laboratory's robot arm.

Figure 1.5: Application cases considered in this thesis.

1.2 Structure of the thesis

The Robotics, with the *physical Human-Robot Interaction* theme, appears to be the industrial sector where the Damage Preventive strategy is investigated and innovated more, with the development and testing of different approaches. Thus, as a first work step we investigated the algorithms used in this field, with goal to become aware of the main Damage Preventive strategies and identify the most successful current solution to use as a benchmark for testing our proposed approaches.

To develop our algorithms, we decided to start from scratch, going to review the main literatures about the impact mechanics, and its modeling approaches, with the goal to get a deeper understanding of the phenomenon. As next step, after identifying a suitable contact math model for our scopes, we analyzed the impact dynamics in a generic controlled mechanical system to find the sensors able to provide a good information on the collision event. Finally, based on the knowledge achieved, we developed our collision detection strategies based on two different application cases – that are a heavy automatic access gate and the laboratory's robotic arm.

In the following, a summary of the chapters is reported.

Chapter 2: State of the art on collision detection algorithms

In this chapter we present the solutions and methods adopted for the collision detection in Robotics. First, the main structure of a collision detection algorithm is given, then the results of the literature investigation on the impact detection in Robotics are reported.

Chapter 3: Fundamental of impact dynamics

In this chapter we review the main literatures about the impact mechanics and its modeling approaches with the goal to get a deeper understanding of the phenomena and identify a specific modeling approach with which study the collision phenomena in a mechanical transmission in the next chapter.

Chapter 4: Impact dynamics on a controlled mechanical system

In this chapter we investigate the effects of a collision on controlled mechanical system with the scope of identifying the optimal sensors for developing a reliable and generalizable strategy for the collision detection problem.

Chapter 5: Friction estimation approach to the collision detection

In this chapter we present a new collision detection approach applied to the industrial application case of the safety in the automatic access gate. Furthermore, we compare its performance with the *Generalized Momenta* algorithm, the most successful collision detection algorithm used in Robotics.

Chapter 6: Inertial Generalized Momenta algorithm

In this chapter we propose an evolution of the Generalized Momenta which merges the inertial information of the load with its approach. Furthermore, we apply and compare its performance respect the FEEFK and standard Generalized Momenta algorithm on a robot arm application case.

Chapter 2

State of the Art on collision detection algorithms

This thesis deals with the collision detection issues and wants to propose new innovative solutions with the traits to be reliable and generalizable to any type of controlled mechanical system, such as a manufacturing machine or a robot.

The Robotics, with the *physical Human-Robot Interaction* theme, appears to be the industrial sector where the *Damage Preventive* strategy is investigated and innovated more, with the development and testing of different approaches.

Exactly starting from the Robotics, in this chapter we present the solutions and methods adopted in this field. The goal is to become aware of the main strategies and identify the most successful current solution to use as a benchmark for testing our proposed approaches.

At the beginning of this chapter, we present the main structure of a collision detection algorithm, describing its main parts and defining the aims of this work. Afterward, the main approaches used in Robotics are reported.

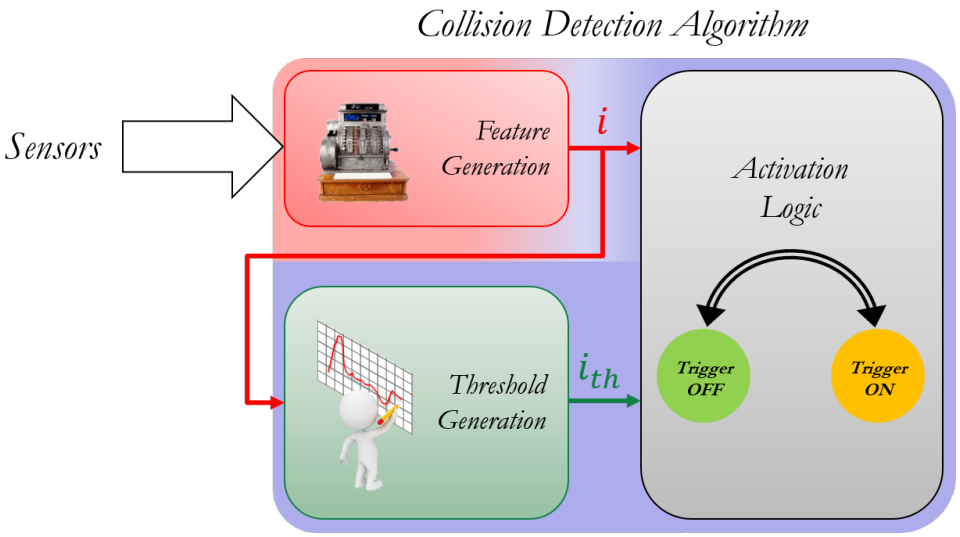

Figure 2.1: Collision detection algorithm general block diagram

2.1 Structure of a collision detection algorithm

In this section the main structure of a collision detection algorithm is described.

The collision detection problem can be seen as a type of fault detection task where the fault is a collision, an unwanted external event that might be detect as fast as possible. Accordingly, the algorithm is composed mainly by two part: the *Feature Generation* and *Fault Detection*. In Figure 2.1 they are represented by the red and blue area.

The Feature Generation block takes the sensor data to extract useful, or compacted, information with which is possible to detect the unwanted event. In our case, this part consist in a sensor fusion algorithm which gives as output the signal i, that we define as *collision detection signal*.

The Fault Detection part can be divided in others two subsystems: the

Threshold Generation and the *Activation Logic*.
The first, as the name suggest, generates a threshold with which it is possible to discriminate the occurrence of a collision based on the Activation Logic. The threshold, indicated with i_{th}, represents the system's behavior in the nominal conditions. The Activation Logic detects the occurrence of a collision based on a specific math law, which formulates and identities the difference between the signal i and the threshold i_{th}.

In literature is possible to find different methods to develop the Fault Detection block. Often the chosen solution depends on the specific application. Differently, the Feature Generation can be the same independently from the scenario. Moreover, the Threshold Generation influence more the robustness of the algorithm than the rapidity of detecting an impact, on contrary of the Feature Generation.

One of the main proposes of our work is to develop an algorithm usable in the most different applications where is present a controlled system with a body in movement which might collide, or we want it to collide, with an another physical object.

For these reasons, our work focus mainly on the study of innovative methods for the feature generation than the way to discriminate the unwanted event itself. For the detection part and how to generate the threshold, we address the reader to more specific literature, like the source in [25]. For completeness, we limit ourselves to mention some of them.

In the following we report the main collision detection algorithm used in Robotics.

2.2 Collision detection schemes in Robotics

The main objective of this thesis is the study of the impact detection problem for industrial applications, in particular the development of a reliable and generalizable strategy for its identification.

One of the industrial areas where the theme of collision detection is of great interest, and as consequence it is the most studied, is that of Robotics. In these years the idea of a physical interaction between robots and humans, with different proposes, is emerging. It can be intended as a working collaboration, support of humans in heavy industrial jobs, support for health care needs, rehabilitation robotic, or again as entertainment robotics. This has led to a development and design of new mechanical systems and automatic control strategies to ensure a safety physical interaction.

This part of the chapter intends to provide the background on the main collision detection methods used in Robotics. First, it briefly provides the basic notions on robot dynamics description, requirement for understanding the methods reported afterwards.

2.2.1 Robot dynamics background

For sake of clarify, we consider a serial robot (Figure 2.2), having n joints with associated generalized coordinates $\mathbf{q}$, that may collide with the environment. Moreover, the mechanical structure is assumed rigid and for each joint is associated a commanded torque τ_J^i.

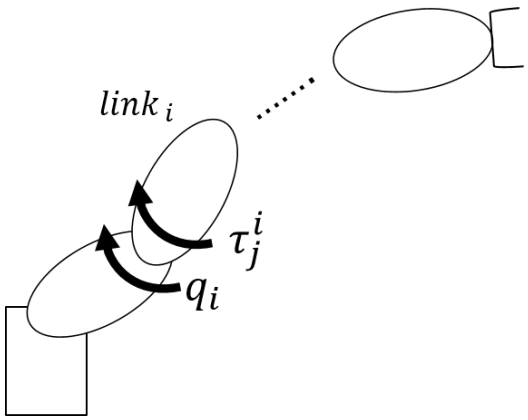

Figure 2.2: Scheme of a generic serial robot.

Collision-free dynamics

During normal operation the standard robot dynamic model is described by the following matrix equation [45],

$$M(\mathbf{q})\ddot{\mathbf{q}} + C(\mathbf{q}, \dot{\mathbf{q}})\dot{\mathbf{q}} + \boldsymbol{g}(\mathbf{q}) = \boldsymbol{\tau_J} \tag{2.1}$$

where

- $\mathbf{q} \in \mathbb{R}^n$ are the generalized coordinates associated to the position of the links;
- $M(\mathbf{q}) \in \mathbb{R}^{n \times n}$ is the symmetric and positive definite inertia matrix;
- $C(\boldsymbol{q}, \dot{\boldsymbol{q}})\dot{\boldsymbol{q}} \in \mathbb{R}^n$ is the centripetal and Coriolis vector;
- $\boldsymbol{g}(\mathbf{q}) \in \mathbb{R}^n$ is the gravity vector;
- $\boldsymbol{\tau_J} \in \mathbb{R}^n$ are the joint torques supplied by motors.

During collision dynamics

When the robot collides with a standing or a moving obstacle in its workspace, an external force appears in the dynamics equation. For simplicity, it is assumed that there is at most a single link involved in the collision. Let

$$\dot{\boldsymbol{x}}_{\boldsymbol{c}} = \begin{bmatrix} \boldsymbol{v_c} \\ \boldsymbol{\omega_c} \end{bmatrix} = J_c(\boldsymbol{q})\dot{\boldsymbol{q}} \in \mathbb{R}^6 \tag{2.2}$$

be the construct vector of the vector of the linear velocity, $\boldsymbol{v_c}$, at the contact point and the angular velocity, $\boldsymbol{\omega_c}$, of the associated robot link. $J_c(\boldsymbol{q})$ is the Jacobian referred to the impact contact point. The Cartesian collision forces, $\boldsymbol{f_c}$, and moments, $\boldsymbol{m_c}$, are denoted by

$$\boldsymbol{F_c} = \begin{bmatrix} \boldsymbol{f_c} \\ \boldsymbol{m_c} \end{bmatrix} \in \mathbb{R}^6 \tag{2.3}$$

When a collision occurs, the robot dynamics (2.1) becomes

$$M(\mathbf{q})\ddot{\mathbf{q}} + C(\mathbf{q}, \dot{\mathbf{q}})\dot{\mathbf{q}} + \boldsymbol{g}(\mathbf{q}) = \boldsymbol{\tau_J} - \boldsymbol{\tau_c} \tag{2.4}$$

with $\boldsymbol{\tau_c} \in \mathbb{R}^n$ is the collision torque, which is associated to the Cartesian collision force $\boldsymbol{F_c}$ by

$$\boldsymbol{\tau_c} = J_c^T(\boldsymbol{q})\boldsymbol{F_c} \tag{2.5}$$

2.2.2 Direct derivation method

Using the equation (2.4) the impact force $\boldsymbol{F_c}$ can be estimated as

$$\hat{\boldsymbol{\tau}}_{\boldsymbol{c}} = \boldsymbol{\tau_J} - M(\mathbf{q})\ddot{\mathbf{q}} - C(\mathbf{q}, \dot{\mathbf{q}})\dot{\mathbf{q}} - \boldsymbol{g}(\mathbf{q}) \tag{2.6}$$

The most simple estimation of the impact force is obtained by using joint torques and link positions information. However, this approach is usually not applicable in practice because $\mathbf{q}$ cannot be differentiated two times due to the presence of non-negligible noise.
A solution to evade this problem can be achieved using the position reference information instead of the measure. As described afterwards, this method can be used for a robot that is being controlled by a high performance position controller.

2.2.3 Derivation from desired dynamics

For a planned trajectory with smooth derivatives of higher order and a well parameterized position controller, it can be assumed that

$$\boldsymbol{q_{ref}} \approx \mathbf{q} \tag{2.7}$$

where $\boldsymbol{q_{ref}} \in \mathbb{R}^n$ is the joint position reference. $\boldsymbol{q}$ and its derivatives can be approximated by $\boldsymbol{q_{ref}}$ and its derivatives. An estimate of the collision joint torque is given by

$$\hat{\boldsymbol{\tau}}_{\boldsymbol{c}} = \boldsymbol{\tau_J} - M(\boldsymbol{q_{ref}})\ddot{\boldsymbol{q}}_{\boldsymbol{ref}} - C(\boldsymbol{q_{ref}}, \dot{\boldsymbol{q}}_{\boldsymbol{ref}})\dot{\boldsymbol{q}}_{\boldsymbol{ref}} - \boldsymbol{g}(\boldsymbol{q_{ref}}) \tag{2.8}$$

Even though this method suffices for stiff position control and smooth desired motions, the scheme is not a general estimation of collision torques since it is not independent from the controller and desired trajectories.

In the next sections three different disturbance observers that neither suffer from the problem of requiring $\ddot{\boldsymbol{q}}$ nor from the demanded a priori knowledge of $\boldsymbol{q_{ref}}$ are proposed. The methods may be interpreted as a "virtual sensor"

for external torques along the robot structure [18].

2.2.4 Energy based detection

In order to recognize the occurrence of a collision, observing the energy of mechanical system can be sufficient [17].
The method is based on the following scalar quantity

$$\hat{r}(t) = k \cdot \left[E(t) - \int_0^t (\dot{\boldsymbol{q}}\boldsymbol{\tau_J} + \hat{r}) ds - E(0)) \right] \tag{2.9}$$

where

- its initial value $\hat{r}(0) = 0$;
- $k > 0$ is the observer gain;
- $E(t)$ is the total robot energy. It is defined by the sum of robot kinetic energy T and potential energy due to gravity U:

$$T = \frac{1}{2}\dot{\boldsymbol{q}}^T M(\boldsymbol{q})\dot{\boldsymbol{q}}$$
$$U = \sum_{i=1}^{n} m_i \cdot h(\mathbf{q})_i \cdot g$$

  where m_i and h_i are respectively the center of mass and its vertical position than the absolute reference system, g is the gravitational constant.

The parameter $\hat{r}$ is called *collision detection signal* and essentially monitors the energy changes of the robot. During free motion, $\hat{r} = 0$, up to measurement noise and unmodeled disturbances. In response to a generic collision, $\hat{r}$ raises exponentially and detection occurs as soon as $\hat{r} \geq r_{TH}$. The scalar r_{TH} is a suitable threshold whose actual value depends on the

noise characteristics in the system. Dynamic thresholding can be used to avoid false detection due to spurious spikes in noisy signals, as shown in [10]. Note that $\hat{r}$ can be computed using the measured joint position $\mathbf{q}$, the joint velocities $\dot{\boldsymbol{q}}$ (possibly obtained through numerical differentiation), and the commanded motor torques. No acceleration measurements is needed.
It is possible to show [17] the resulting dynamics of $\hat{r}$ is

$$\dot{\hat{r}} = -k\hat{r} + k\dot{\boldsymbol{q}}^{\boldsymbol{T}}\boldsymbol{\tau_c} \tag{2.10}$$

i.e., that of a first-order stable linear filter driven by the work performed by the joint torques due to collision. $1/k$ is the time constant of the filter.
This method has the advantage of very low computational complexity. However, not all possible collision situations are detected by this scheme. With the robot at rest ($\dot{\boldsymbol{q}} = 0$), the instantaneous value of $\boldsymbol{\tau_c}$ does not affect $\hat{r}$, but begins as soon as the robot starts moving. As a consequence, with the robot at rest, true impulse collision forces/torques cannot be detected with this scheme. On the other hand, when the robot is in motion, collision can be detected if the Cartesian collision force $\boldsymbol{F_c}$ produces motion at the contact.

2.2.5 Observing joint velocity

In Figure 2.3 is shown the scheme of the joint velocity observer. The underlying idea is to construct an nonlinear disturbance observer, as proposed in [29], based on the velocity [17].
Assuming the joint velocities as state of the system, $\boldsymbol{x} = \dot{\boldsymbol{q}}$, and the impact force is constant,

$$\begin{aligned} \dot{\hat{\boldsymbol{r}}} &= 0 \\ \hat{\boldsymbol{r}} &= \boldsymbol{\tau_c} \end{aligned} \tag{2.11}$$

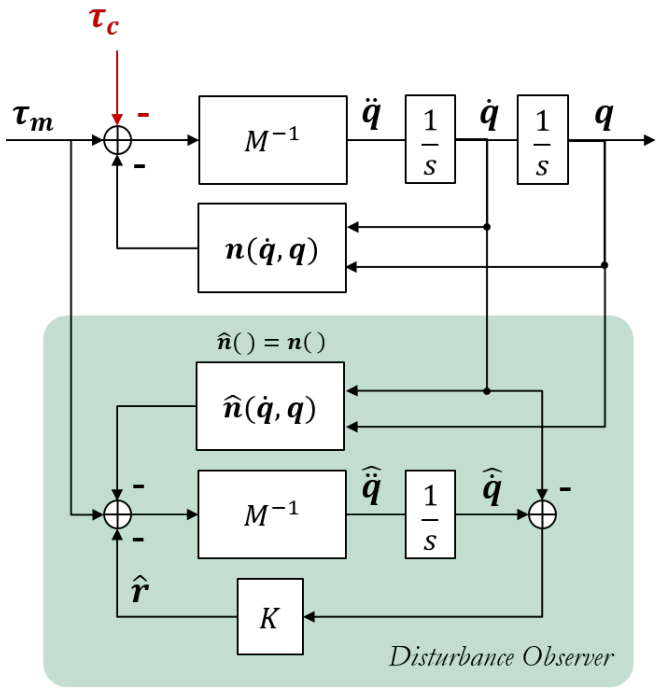

Figure 2.3: Joint velocity disturbance observer

according to [29] it is possible to build the following disturbance observer:

$$\hat{\dot{\boldsymbol{x}}} = M^{-1}\left(\boldsymbol{\tau_J} - \boldsymbol{n}(\boldsymbol{q}, \dot{\boldsymbol{q}}) - \hat{\boldsymbol{r}}\right) \tag{2.12}$$

$$\hat{\boldsymbol{r}} = K \cdot (\hat{\boldsymbol{x}} - \boldsymbol{x}) \tag{2.13}$$

where $K = diag\{k_i\}$ is the observer gain matrix and $\boldsymbol{n}(\boldsymbol{q}, \dot{\boldsymbol{q}})$ is defined as

$$\boldsymbol{n}(\boldsymbol{q}, \dot{\boldsymbol{q}}) = C(\boldsymbol{q}, \dot{\boldsymbol{q}})\dot{\boldsymbol{q}} + \boldsymbol{g}(\boldsymbol{q}) \tag{2.14}$$

As shown in [17], it is possible to obtain the transfer function between the collision torque $\boldsymbol{\tau_c}$ and the observed disturbance [17] $\hat{\boldsymbol{r}}$:

$$\hat{\boldsymbol{r}} = \left(sI + KM^{-1}\right)^{-1} KM^{-1} \cdot \boldsymbol{\tau_c} \tag{2.15}$$

In other words, a filtered version of $\boldsymbol{\tau_c}$ with a variable filter frequency is obtained.
Unlike the previous, this method is independent from the trajectory and motion control performances. However, it suffers of two main disadvantages:

- it requires the computation of $M^{-1}(\mathbf{q})$;
- a nonlinear filter dynamics between $\hat{\boldsymbol{d}}$ and $\boldsymbol{\tau_c}$ are introduced. Due to the term $M^{-1}(\mathbf{q})$, the filter has a variable cut-off frequency, which is difficult to determine.

In the following section the concept of estimating the collision torques based on the observation of the generalized momentum $\mathbf{p}$ is introduced. Thanks to this choice of changing the state variable describing the system dynamics, it is possible to obtain a linear filter behavior between $\hat{\boldsymbol{r}}$ and $\boldsymbol{\tau_c}$, evading the problems mentioned above.

2.2.6 Observing generalized momentum

This method has a similar structure to the previous one. However, in contrast to the velocity observer its basic concept is to observe the *generalized angular momentum* [11]:

$$\boldsymbol{p} = M(\boldsymbol{q})\dot{\boldsymbol{q}} \tag{2.16}$$

First, the physical relationship between $\boldsymbol{p}$ and $\boldsymbol{q}$ of the robot equation needs to be explicated. The robot dynamics (2.4) can be rewritten to

$$\begin{aligned} \dot{\boldsymbol{p}} &= \frac{\mathrm{d}M(\boldsymbol{q})\dot{\boldsymbol{q}}}{\mathrm{d}t} = \dot{M}(\boldsymbol{q})\dot{\boldsymbol{q}} + M(\boldsymbol{q})\ddot{\boldsymbol{q}} \\ \dot{\boldsymbol{p}} &= \boldsymbol{\tau_J} - \boldsymbol{\beta}(\boldsymbol{q}, \dot{\boldsymbol{q}}) - \boldsymbol{\tau_c} \end{aligned} \tag{2.17}$$

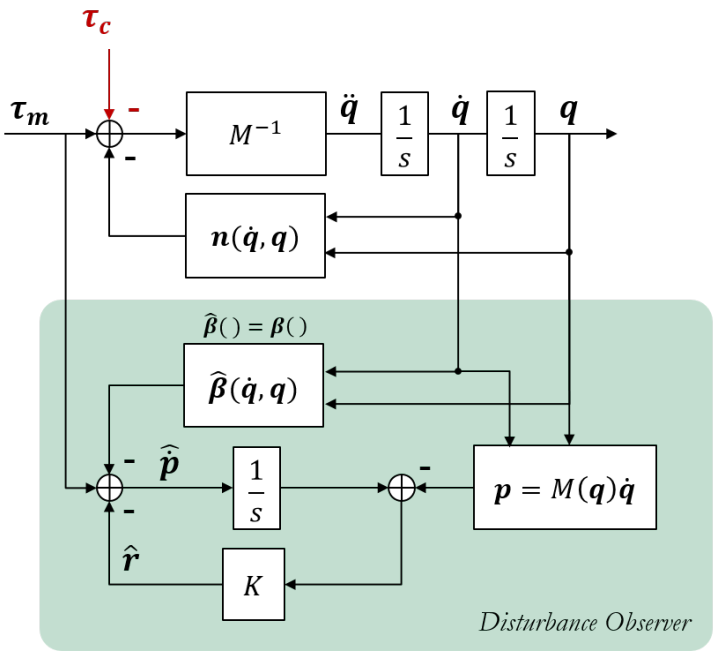

Figure 2.4: Generalized momentum disturbance observer

where

$$\begin{aligned}\beta(q, \dot{q}) &= n(q, \dot{q}) - \dot{M}(q)\dot{q} \\ &= C(q, \dot{q})\dot{q} + g(q) - \dot{M}(q)\dot{q} \\ &= C(q, \dot{q})\dot{q} + g(q) - \left(C(q, \dot{q}) + C(q, \dot{q})^T\right)\dot{q} \\ &= g(q) - C(q, \dot{q})^T\dot{q}\end{aligned} \tag{2.18}$$

These relations can be found in most standard robotics textbooks as [45]. Now, assuming the generalized angular momentum as state of the system, $x = p$, and the impact force is constant, according to [29] it is possible to build the following disturbance observer:

$$\begin{aligned}\dot{\hat{x}} &= \tau_m - \beta(q, \dot{q}) - r \\ \hat{r} &= K \cdot (\hat{x} - x)\end{aligned} \tag{2.19}$$

where $K = diag\{k_i\}$ is the observer gain matrix.
Combining (2.19) and (2.17), it is shown in [17] that the observed disturbance is a component-wise filtered version of the real external torque. The dynamics of $\hat{\boldsymbol{r}}$ is therefore

$$\dot{\hat{\boldsymbol{r}}} = -K\hat{\boldsymbol{r}} + K\boldsymbol{\tau_c} \tag{2.20}$$

and its components can be written as

$$\hat{r}^i = \frac{k^i}{s + k^i}\tau_c^i \tag{2.21}$$

where $\forall i \in \{1, ..., n\}$, with n is the number of joints. Each k^i can be interpreted as a filter constant $T^i = \dfrac{1}{k^i}$ of the ith external joint torque signal component. In order to ensure fast collision detection a high observer filter frequency is needed, i.e. large K. In ideal conditions

$$K \to \infty \Rightarrow \hat{\boldsymbol{r}} \approx \boldsymbol{\tau_c}$$

However, the presence of sensor noise can compromise a clear collision detection, leading to false trigger activations. Thus, certain low pass filter characteristics are needed.

2.3 Threshold generation methods

In this section, for completeness, we report some methods to generate and check the threshold.

2.3.1 Limit checking of absolute values

The simplest and frequently used method is the limit checking of the collision detection signal $i(t)$. The signal is monitored and checked if its absolute value exceeds certain thresholds, a maximal value I_{max} and a minimal value I_{min}. The normal state is when

$$I_{min} < i(t) < I_{max}$$

which means that the process is in normal situation if the signal stays within a certain tolerance zone.
This simple method is applied in the almost all process automation system. Examples are the oil preassure, the coolant water of combustion engine or the control error of a control loop. The thresholds are mostly selected based on experience and represent a compromise. On one side false alarms through normal fluctuations of the variable should be avoided, on the other side faulty deviations should be detected early. Therefore, a trade-off between too narrow and too wide thresholds exists.

A further improvement of limit checking can be realized by applying signal prediction. By using polynomial regression models

$$i(k) = a_0 + a_1 k + a_2 k^2 + ...$$

with $k = t/T_s$, and recursive least squares parameters estimation a prediction of the signal can be made for N sample ahead. The predicted signal then shows relatively early danger of exceeding a threshold of avoids a false alarm if the signal returns to normal zone without action. The prediction can also be made by using stochastic difference equations for the randomly changing

monitored signal [24].

2.3.2 Trend checking

A further simple solution is to calculate the first derivative of $i(t)$, the trend of the signal and to check if

$$\dot{I}_{min} < \dot{i}(t) < \dot{I}_{max}$$

If relative small threshold are selected, an alarm can be obtained earlier than for limit checking of the absolute value. Trend checking is for example applied for the oil pressure for vibration problem in bearings, turbines of wear of machines. Limit checking of absolute values and trends can be combined. One solution is to make the threshold of absolute values dependent on the trend – e.g. $I_{max} = f(\dot{I}_{max})$, $I_{min} = f(\dot{I}_{min})$ – in order to detect fast developing deviations early and to avoid false alarms for small trend, if the value is far from the threshold possibility to make the threshold adaptive, that is function of the other variables [25].

2.3.3 Adaptive thresholds

The use of an adaptive threshold, instead of a fixed one, can improve the performance of a fault-detection module significantly with respect to delay of detection and false alarm rate [51].
The threshold consists of a filter with lead-lag behaviour which is driven by the input signal. This causes the filter output to be zero for steady-state inputs: otherwise it is a measure for the dynamic input excitation. In order to rectify this signal the absolute value is computed. If more input signals are involved for each input the highpassfiltering and the rectification has to

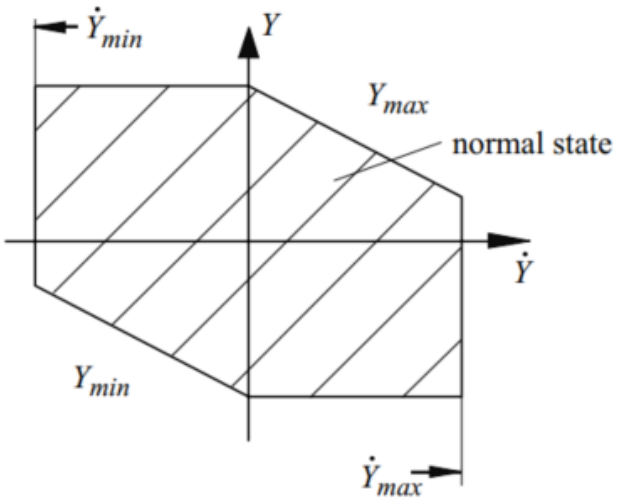

Figure 2.5: Combination of limit checking for absolute values and trends [25].

be performed. A constant value is added due to the effects of measurement noise on the residual. Optionally a first-order low-pass filter can be applied in order to smooth the adaptive threshold. In Figure 2.6 is reported the scheme of the approach.

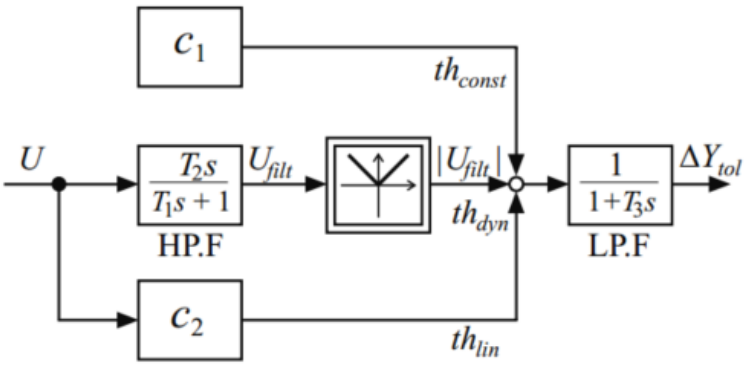

Figure 2.6: Adaptive threshold main structure [25].

2.4 Conclusion

In this chapter we described the main structure of a collision detection algorithm. Further, we investigated the main algorithm currently used in Robotics for the safe human robot interaction. In particular, the *Generalized Momenta* appears to be the most successful algorithm. For this reason, it was chosen as benchmark to test our future solutions.

In the next chapter, we go more in deep in analyzing the impact phenomena. First we study the physical aspect of the event and its modeling approaches. Afterward, we investigate the collision effect on a controlled mechanical system, with the aims to find the best information, thus sensors, with which to develop our approaches.

Chapter 3

Fundamental of impact dynamics

The impact is a complex phenomenon that occurs when two or more bodies undergo a collision.

This topic has always attracted the interest of scientists and engineers from different areas of knowledge for years – from the physics, machines design, robotics, multi-body simulation – these are just a few examples. The first studies go back to 1639 with Marci [32], who derived the first relations on impact mechanics based on experiments, and have continued until nowadays [1, 14, 16, 33, 39]. The goal is to develop theories that can predict the dynamics of colliding objects in term of: velocities before and after the impact, contact force and energy losses.

In this chapter we review the main literatures on this topic. At the beginning, we present the fundamentals of impact mechanical theory. Next, we report an overview of its modeling approaches focusing on the methods which are results most suitable in the description of the collision phenomenon

for multibody systems.

Focusing on our final goals, the scope of this survey is to get a deeper understanding of the phenomenon and identify a modeling approach with which analyze the impact in a controlled mechanical system, described in the next chapter.

3.1 Basic Impact Theory

3.1.1 Types of impact

By definition, Impact is a complex physical phenomenon which occurs when two or more bodies collide with each other [42]. It is a brief duration event where the corps are subject to high force levels and sudden changes of velocity. As a consequence, the bodies are subject to dissipation of energy in various forms [15]: plastic deformation, damping of material, wave propagation, friction, sound and heat.

In order to classify collisions into specific types which require distinct methods of analysis, we need to think about the deformations that develop during collision, the distribution of these deformations in each of the colliding bodies, and how these deformations affect the period of contact [49]. Reading the literature is possible to identify two macro classification about the impact: *rigid impacts*, or *slow speed impacts*, and *plastic impacts*, or *high speed impacts*. The first type of impact is characterized by small deformations in the contact area of the colliding bodies in comparison to their both the cross-sectional dimensions and the depth. The kinetic energy of the colliding bodies is not enough high to produce a relevant deformation in the contact area [6, 14, 49]. On contrary, the second consider the domain of high velocity impact, generally associated with explosives and projectiles. In these case

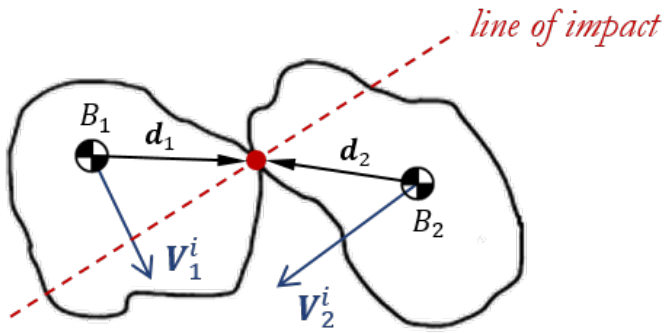

(a)

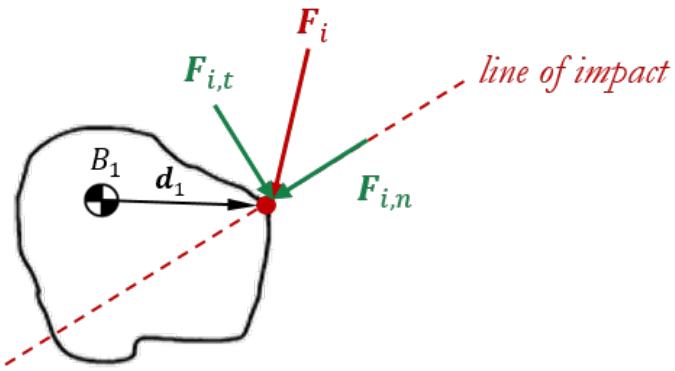

(b)

Figure 3.1: An oblique-eccentric collision between two bodies (B_1, B_2) is shown in 3.1a. $\mathbf{V}^i$ indicates the initial velocity of the bodies, $\mathbf{d}_i$ is the distance of the center of mass from contact point. In Figure 3.1b is shown the components of the impact force acting on the body B_1.

there are a plastic strains which are not more negligible and associable with the mechanical assumption of "small deformation" [16, 49]. We point up that this work focuses on the first class of collisions.
For the rigid impacts is possible identify subclasses depending on the material property of the colliding bodies and the modeling assumptions. In general, there are three types of analysis for low speed collisions, associated with particle impact, impact with compliant contact region and impact on flexible bodies [6, 14, 49]. Particle impact is an analytical approximation that considers the bodies as particles, which by definition are smooth and spherical, with a symmetric position of the center of gravity. The second type, in contrast to the first, considers the bodies as physical bodies with their own geometries and positions of the center of gravity. The analysis of the impact is realized considering the contact stresses resulting from the impact of two bodies. The last class investigates the collision in flexible body (e.g. transverse impact on a beam, longitudinal impact of two rods, ...etc.), where elastic wave propagation phenomenon is relevant. Here, the impact is accompanied by a stress wave that propagates in the impacting bodies away from the region of impact. The energy is transformed into vibrations which becomes an important fraction of the total energy.

Another kind of classification focuses on the dynamics of the colliding bodies. In Figure 3.1 is shown a generic collision between two bodies with a single contact point. The line represents the direction of the impact, normal to the tangential plane at the contact point [42]. Depending on the mass center position of the bodies and the direction of their initial velocity than the line of impact, four types of collision can be defined:

- *central* or *collinear*: the mass centers of the two bodies are on the line

of impact;

- *eccentric*: the mass centers of one or both bodies are not on the line of impact;
- *direct*: the initial velocities of the two bodies are along the line of impact;
- *oblique*: if the initial velocities of one or both bodies are not along the line of impact.

Obviously, the most general and predominant collision scenario is *oblique-eccentric* impact [14].
The type of collision determines in a unique way the dynamics of bodies. For example, in case of a *direct-eccentric* collision the impact force acts mainly along the normal to the contact surface. Due to the non-alignment between the center of gravity of the bodies and the line of impact, the force generates a momentum on the bodies which puts on them in rotation.
A different scenario is the *oblique-central* impact. In this case the contact force is composed by two components: tangential and normal to the contact surface,

$$\mathbf{F}_i = \mathbf{F}_{i,t} + \mathbf{F}_{i,c} \tag{3.1}$$

with $\mathbf{F}_i$ is indicates the contact force, while $\mathbf{F}_{i,t}$, $\mathbf{F}_{i,n}$ are respectively the tangential and normal component. The first term is given by the friction phenomenon generated by the sliding between the two bodies during the contact. It depends on the relative tangential speed, i.e. the angle of impact than the line of impact, and by the surface roughness of bodies. The second is the impact force's main component, related to the impact physical phenomenon which will be described later.

The friction phenomenon becomes more prominent less the collision is central. In literature is reported that is modeled using the traditionally Coulomb's law [14, 16, 39, 48, 49]. In this work is not reported this aspect since it is unnecessary for our aims. For more detailed information about the effects of the friction on impact dynamics and its modelling approach, we address the reader to the reference literature.

3.1.2 Mechanics of impact

In this section we report the mechanics of impact described by Stronge in [14]. Referring to Figure 3.2a, he considers a collinear-direct impact of two rigid bodies, labeled B_1 and B_2, respectively with initial speed V_1^i and V_2^i. The friction is not considered, thus the impact force is given entirely by its normal component: $F_i \equiv F_{i,n}$.

The contact points are separated by an infinitesimal deformable particle with diameter λ. The particle is the lumped representation of the small local deformation of the bodies in the contact region. With δ is indicated the indentation or compression of the deformable particle.

By and large, two phases can be identified: the *compression*, or loading phase, and the *restitution*, or unloading phase [14].

As soon as the colliding bodies come in contact the first phase begins. The impact force $F_i(t)$ rises as the deformable particle is compressed (Fig. 3.2b). The maximum deformation δ_c and maximum impact force $F_{i,max}$ occur simultaneously when the relative velocity v vanishes ($v = V_2 - V_1$) (Fig. 3.2c). During this phase, the kinetic energy of relative motion is converted into internal energy of deformation by the contact force. The work of compression, W_c equals the area under the loading curve (Fig. 3.2d).

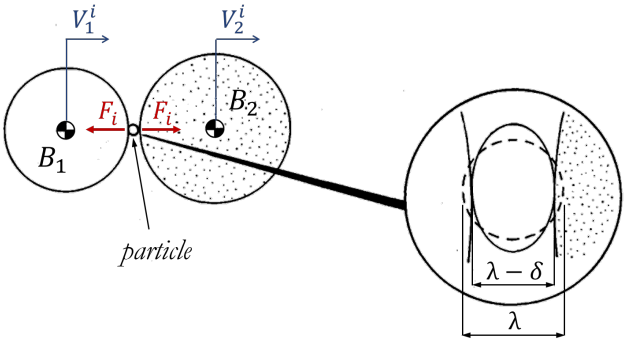

(a) Collinear impact of two rigid bodies with contact points separated by an infinitesimal deformable particle. The particle represents small local deformation of the contact region.

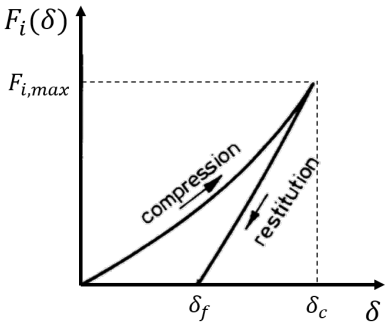

(b) Normal contact force F_i as a function of relative displacement δ.

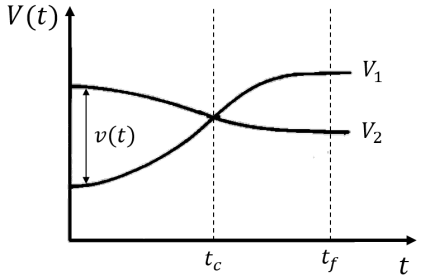

(c) Changes of normal velocities V_1, V_2 as functions of time. v is the relative velocity between the bodies ($v = V_2 - V_1$)

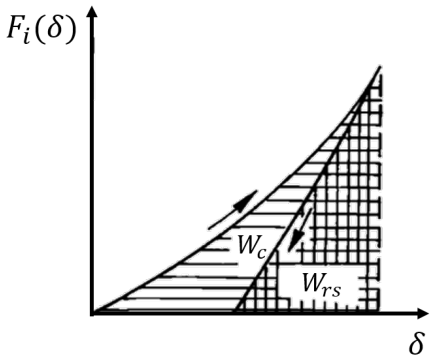

(d) Work W_c done by normal contact force F_c against bodies during period of compression, and work W_{rs} recovered during restitution, as functions of normal relative displacement δ at contact point.

Figure 3.2: Mechanics of impact

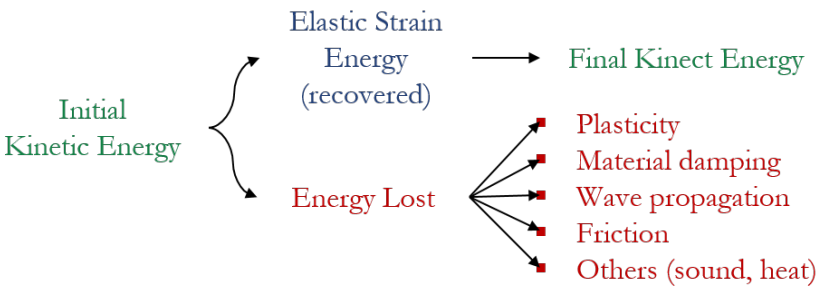

Figure 3.3: Energy conversions during the impact

The compression phase terminates and restitution begins at time t_c, when the normal relative velocity of the contact points vanishes. In this phase, the particle internal energy is released. The elastic strain energy stored during compression generates a force which restores the initial kinetic energy of relative motion of the bodies, or at least part of it. Unless the impact speed is extremely small, part of the initial kinetic energy is dissipated during the collision. This can be due to plastic deformation, elastic vibrations, rate-dependent processes such as viscoplasticity, friction, sound and heat (Fig. 3.3) [6, 8, 15, 56].

Whatever the cause, it results in an inelastic or irreversible relation between the F_i and the compression δ. The compliance of the deforming region during restitution is smaller than that during compression, so when the contact terminates there is some residual compression δ_f of the deformable particle. This fact can be observed in Figure 3.2d from an energetic point of view, where the W_{rs} is clearly lower than W_c: the area under the unloading curve is less than the area under the loading curve.

3.1.3 Coefficient of restitution

As mentioned in the previous section, a fraction of the initial kinetic energy is dissipated during the collision. Not whole the elastic strain energy stored in the compression phase is released in the restitution phase. Part of it could remain trapped in the bodies as permanent deformation or dissipated in other forms.

The energy loss about the relative motion in the normal direction can be expressed in terms of a *coefficient of restitution*, usually denoted by e. It represents a sort of the efficiency index of energy conversions during the impact:

- *perfectly elastic*: for $e = 1$, when no energy is lost;
- *perfectly plastic*: for $e = 0$, when all energy is lost and the deformation is permanent;
- *partially elastic*: for $e > 0.5$, when energy is lost but no permanent deformation;
- *partially plastic*: for $e < 0.5$, when energy is lost and permanent deformation.

Newton first defined this impact parameter on the basis of his measurements of energy loss in collisions between identical balls. He proposed a kinematic coefficient of restitution defined as:

$$e = -\frac{v_f}{v_i} \tag{3.2}$$

where v_i and v_f are respectively the normal component of the relative velocity of the colliding bodies at the beginning and at the end of event:

$$\begin{aligned} v_i &= V_2^i - V_1^i \\ v_f &= V_2^f - V_1^f \end{aligned} \tag{3.3}$$

Newton presumed incorrectly that the coefficient of restitution is a material property. In his Principia (1686) he gave values for spheres made of steel ($e = 5/9$), glass ($e = 15/16$), cork ($e = 5/9$) and compressed wool ($e = 5/9$). Poisson, in 1835, improved the theory dividing the impact into a compression and restitution phase and postulates the impulse hypothesis [56]. According Poisson the coefficient of restitution is defined by:

$$e = -\frac{p_f - p_c}{p_c} \tag{3.4}$$

where p_c is the impulse relative to the compression phase, whilst p_f is the total impulse of the impact. Thus, p_c and p_f are respectively

$$\begin{aligned} p_c &= \int_0^{t_c} F_i(t)dt \\ p_t &= \int_0^{t_f} F_i(t)dt \end{aligned} \tag{3.5}$$

It can be shown [14] they are equal to

$$\begin{aligned} p_c &= -mv_i \\ p_f &= mv_f - mv_i \end{aligned} \tag{3.6}$$

where m is the effective mass during the collision. Considering the scenario in Figure 3.2a, m is given by

$$m = \frac{M_1 M_2}{M_1 + M_2} \tag{3.7}$$

Poisson also recognized that his definition is equivalent to the kinematic coefficient of restitution for direct impact between rough bodies if the direction of slip remains the same.

Finally, in 1991, Stronge formalized the coefficient of restitution relying on the *internal energy dissipation hypothesis*: the square of the coefficient of restitution, e, is the negative of the ratio of the elastic strain energy released during restitution to the internal energy of deformation absorbed during compression,

$$e^2 = -\frac{W_{rs}}{W_c} \tag{3.8}$$

The internal energy of compression W_c and the energy released in the restitution phase W_{rs} are defined as

$$\begin{aligned} W_c &= -\frac{1}{2} m v_i^2 \\ W_{rs} &= \frac{m v_i^2}{2} \left(1 - \frac{p_f}{p_c}\right) \end{aligned} \tag{3.9}$$

Stronge in [50, 56], through an energetic analysis of a planar impact of two bodies, put in evidence that the three restitution models are equivalent unless the bodies are rough, the configuration is eccentric and the direction of slip varies during collision. In these case, it appears that the Stronge's hypothesis of restitution is the better of the three theories, since Poisson's and Newton's models show a paradox when it is considered an impact with $e = 1$. Their methods produce non-zero energy dissipation in the normal direction,

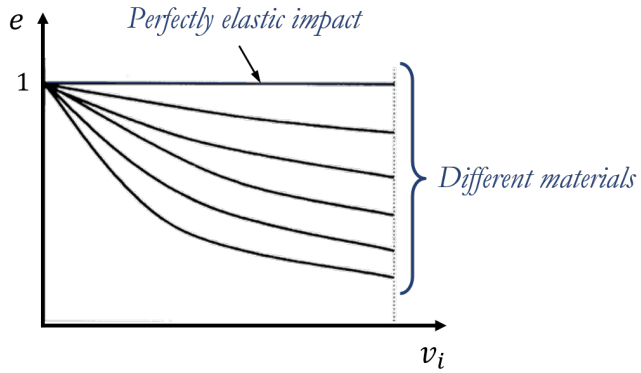

Figure 3.4: Coefficient of restitution as a function of the initial relative velocity of the colliding bodies and their materials

fact in contrast with the meaning represented by the coefficient of restitution.

It has been widely experimentally proved that the coefficient of restitution depends on many elements, not just by the relative initial velocity, such as the geometry of bodies in contact, the material properties, the duration of contact and, possibly, friction [15, 23, 33, 39, 40, 48, 54, 60]. In Figure 3.4 is shown qualitatively the relationship between the coefficient of restitution and impact velocity for a central-direct collision of two spheres of different materials: it tends to level out with increase in impact velocity. Based on the studies reported by Goldsmith [15], it is worth to report the following relationship:

$$e^2 = 1 - \alpha \dot{v}_i^{\beta} \tag{3.10}$$

where parameter α and the exponent β depend on the material and geometry. Usually, bodies with a low ratio of surface area to volume (like spheres) present this kind of behavior [6, 15].

3.1.4 Wave propagation phenomenon

Related to the energy loss and coefficient of restitution is the phenomenon of wave propagation. Since real bodies are not perfectly rigid, their parts are not instantaneously subjected to the same change of motion following the impact. The disturbance generated at the contact point travels in the body as stress (and deformation) waves with a finite velocity [6, 49]. These waves produce oscillations and part of the impact (kinetic) energy is converted to the energy associated with this vibration. A useful parameter to quantify this situation is the ratio between the duration of impact and the period of the fundamental natural mode of vibration of the impacting bodies. The greater is this ratio, the smaller is the energy dissipation associated with the elastic waves since they can travel across the bodies many times before the impact ends. If this ratio is large enough, a quasi-equilibrium state is reached [6]. These observations are complemented by Stronge [49] who states that stress waves contribute to energy dissipation during collision if the relative size of the bodies is different from unity. In this case, the waves in the larger body do not have sufficient time to reflect from any boundary and, in essence, remain "trapped" in the body. Experimental results of this fact can be found in [23, 28, 40, 60]. The authors, trying to predict the impact dynamics of flexible bodies, such as flexible beam, using discrete models approach, confirmed the strong dependency of the energy lost during impact on vibrations of the contacting bodies.

Summarizing, if the two impacting bodies are similar in size and material properties, the vibration energy lost is negligible [49]. The coefficient of restitution is mainly determined by the plastic deformation near the impact, which depends on the approach relative velocity of the colliding bodies.

Whereas, for slender bodies like beams or plates, the time of impact tends to be short compared with the period of propagation of stress waves. Thus, a more significant portion of the initial kinetic energy remains in the bodies in the form of vibration. In this case the coefficient of restitution may be significantly influenced by this factor [6].

Until now it has been reported an overview of the impact physical phenomenon, its classification and its characteristics. Furthermore, it has been presented an important parameter, easily determined experimentally, which gives an energetic evaluation of the losses due to the impact.
The following section will deal with the issues modeling of impact dynamics.

3.2 Survey on impact modeling approaches

Furthermore, it has shown the complexity of the physical phenomenon with the main mechanical aspects: wave propagation, elastic and plastic deformations at the contact. The literature reports two different approaches which trying to cope the description of this tough physical phenomena: *discrete* approach and *continuous* approach. As it will be noted, the first type of methods is inadequate reference for our aims. Thus, this work focuses on the second approach.

3.2.1 Discrete approach

The first approach is referred to as *Impulse–Momentum method*, *Rigid Body Contact Modeling* or *Piecewise Analysis Method*. It based on the *Impulse-Momentum law* and mainly aims to predict the velocities of the colliding

bodies after impact.

The basic assumption underlying such analysis is that the impact occurs instantaneously. It is justified if the duration of the contact period is small enough such that the configuration of the system does not change much during that period. This scenario shows when the colliding bodies are very rigid. The phenomenon is treated as discontinuous and the dynamic analysis is divided into two intervals: the beginning and the end of impact. Integration of the system equations of motion is carried out while checking for the contact between the different components of the system. At the time of contact, the dynamic analysis is stopped and a balancing of the system momenta is performed to obtain the jump in the velocities (or momenta) of the different bodies due to the impact. Integration of the system equations of motion is restarted with the new velocities (or momenta) until the next impact occurs. The energy dissipations during the event are taken into account through the coefficient of restitution. Thus, its accuracy is crucial to obtaining sufficiently good results.

Goldsmith, in his classic work [15] devotes a chapter to the application of this theory to several problems. Brach uses this approach exclusively in [8] to model numerous problems of practical value.

The algebraic nature of this method makes the mathematical development easy and accessible to most engineers as can be seen in Brach's work, but the unknown duration of the impact limits its application, since for large enough contact periods the system configuration changes significantly [36]. This is very common in multibody systems like robots. The manipulator is inherently flexible and when it comes into contact with its environment, independently at how could be rigid, the impact duration cannot be assumed to be instantaneous. That because part of kinematic energy is dissipated by

the flexible components of the system.

Moreover, as it is mentioned in the previous section, although the coefficient of restitution is capable of capturing the energy losses, it depends on many factors and it is difficult to use for general impact scenarios.

Another drawback emerges in presents of friction. According to this approach, there are not an unequivocal use of Coulomb's law to model friction during impact. Several authors have noted the inconsistencies that arise when rigid body models are used with Coulomb's empirical law of friction. Examples are described by Wang and Kumar [55] and Mason and Wang [34] where the aforementioned inconsistencies are demonstrated by either no feasible solution or by multiple solutions for particular initial conditions. This has been attributed to the approximate nature of Coulomb's model and to the inadequacy of rigid body model, but no clear explanation has been found.

Despite these disadvantages, in the cases where rigid-body hypothesis is valid, this approach has been used to solve the intermittent motion problem in mechanical systems [27] and it is still the most commonly used approach in vehicle accident reconstruction [1]. Also, it has been used to predict the impact dynamics of flexible bodies, such as flexible beams.

Summarizing, it is difficult to make general statements on the validity of discrete impact dynamics models. They depend on the applicability of the rigid-body hypothesis, more specifically, whether it is reasonable to neglect deformation at the contact point [23, 28, 40, 60].

3.2.2 Continuous approach

The second approach is referred to as *continuous analysis* or *force based methods*. The collision is assumed as continuous phenomenon: the contact force

and the relative deformations vary in a continuous manner. So the dynamic analysis may be performed in the usual way, by simply adding the contact force to the equations of motion during their action period. This approach allow a better description of the real behavior of the system, especially in scenarios where friction may not be neglected, in presence of complex environments with multiple contacts collision and, especially, with respect to impact with long duration they are effective and accurate.

For the most general collision, i.e. the oblique-eccentric collision (section 3.1.1), the contact force is modeled as the sum of two components:

$$F_i(t) = F_{i,n}(t) + F_{i,t}(t) \tag{3.11}$$

where F_i is the impact force, whilst $F_{i,n}$ and $F_{i,t}$ are respectively the components of force normal and tangential at the contact surface.

The first term, in general, is modeled as a spring-damper element as function of a fictitious penetration, δ, between the colliding bodies at the contact point and its rate, [6, 8]:

$$F_{i,n} = F_k(\delta) + F_b(\delta, \dot{\delta}) \tag{3.12}$$

It represents the main aspects of the phenomenon mentioned in the previous section 3.1.2. The second term of 3.11 takes into account the friction phenomenon. It is mainly model through the Coulomb's law or using more sophisticate models like Bristol friction approaches [16]. Since this work it does not have as main goal the modelling and simulation of the collision event, we address the reader to more specialized literatures about the modelling aspect about the friction.

The first published work about contact modeling was written by Hertz in

1896, which is based on the theory of elasticity [52]. It relates the contact force with a nonlinear spring behavior. Although his work is one of the most important example of analysis of the contact between two elastic bodies, Goldsmith proved experimentally that Hertz's theory provides a good description for impact of two spheres or a sphere and a plate, that is if the materials are hard and the initial speed is low, but it is not valid in most impact situations where some plastic deformation and energy dissipation always takes place. To overcome this problem Kelvin and Voigt [15, 36] proposed as solution the Kelvin-Voigt model: the spring-dashpot model with a linear behavior. It provides a reasonable method for representing the energy dissipation related to the contact force without considering the plastic deformation issues. Although its simplicity has made it a popular choice [21, 30, 35], it is not represents the impact dynamics with accuracy. Finally, with Hunt and Crossley (1975), it was introduced the nonlinear spring-dashpot, which catches the benefit of the previous methods and overcame their issues.

In the following is reported more in deep the modeling aspects of these last approach.

3.3 Continuous contact dynamics models

The discussion from the previous section indicates that the continuous model approach is better suited for aims of this work. This section looks in more detail at the literature regarding the implementation of continuous analysis methods [36]. These models are essentially non-linear spring models used to predict the force acting to separate the colliding bodies. Since in the following paragraphs we consider only the normal component of the contact

force, it will be hereafter declared as F_n, instead of $F_{i,n}$.

3.3.1 Hertz's contact model

The Hertz Theory was developed basing on the theory of elasticity and analyzing the collision between two spheres [14, 26, 36]. The bodies are assumed to be homogeneous, isotropic and linearly elastic, and the plastic flows are treated quasi-statically. The impact process is assumed as two rigid bodies interacting via a non-linear spring along the line of impact. The relative deformations are concentrated in the proximity of the contact area and elastic wave motion is neglected. In other words, the use of Hertz Theory, and the contact models derived from it, should be restricted to contact between bodies with non-conformal geometries, i.e., where the shape of the two bodies have sufficiently dissimilar profiles, such that the contact regions are small in comparison to the size of either body. Moreover, Hertz's model does not take into account any dissipation phenomena. This involves, referring to Goldsmith work [15], this model can be used only for low impact speeds and hard materials.

In general, the contact force according to Hertz is given by:

$$F_n(t) = k \cdot \delta^n \tag{3.13}$$

where δ is relative local penetration. k and n are constants which take into account the material and geometric properties of the colliding bodies. In case of central collision between two spheres of isotropic materials, analyzed by Hertz, $n = 3/2$ and k is directly related with the geometry and material

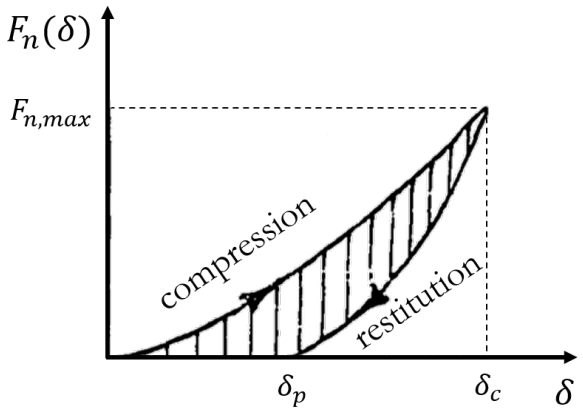

(a) Hertz contact force model with permanent indentation

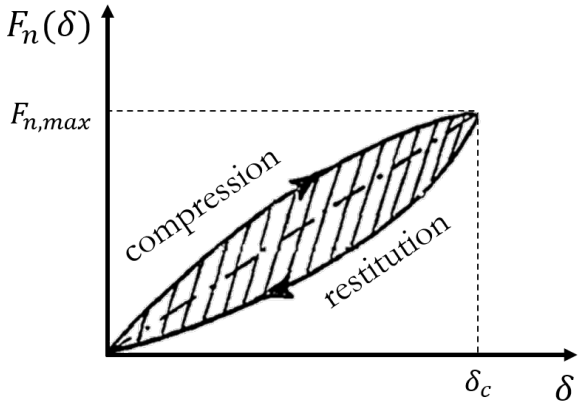

(b) Kelvin-Voigt contact model with hysteresis damping.

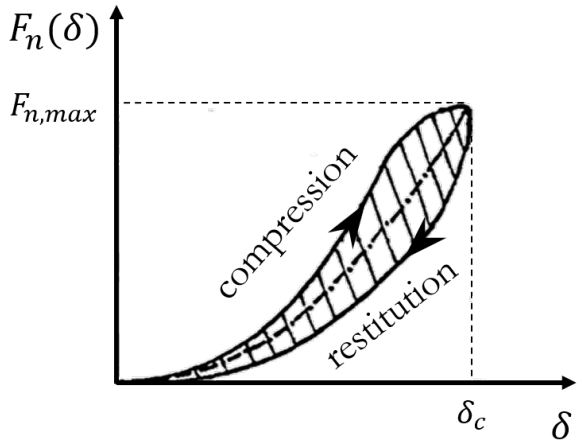

(c) Force-indentation law with nonlinear spring-damping.

Figure 3.5: Hertz contact force model with damping.

properties of the bodies:

$$k = \frac{4}{3\pi(h_i + h_j)} \left(\frac{R_i R_j}{R_i + R_j} \right)^{1/2} \tag{3.14}$$

where R_i e R_j are respectively the radii of the spheres, while h is defined by:

$$h_m = \frac{1 - \nu_m^2}{\pi E_m} \qquad with \quad m = i, j \tag{3.15}$$

The variables ν_m and E_m are the Poisson's ratio and the Young's modulus associated with each sphere respectively.

The Hertz model can be extended to account the plastic deformation by introducing hysteresis in the contact force law. This is obtained using a different force-indentation relationship for the unloading phase of the contact which generally takes the following form [57]:

$$F_n(t) = F_{n,max} \left(\frac{\delta(t) - \delta_p}{\delta_c - \delta_p} \right)^2 \qquad for \quad t > t_c \tag{3.16}$$

where F_n $F_{n,max}$ and δ_c are respectively the maximum normal force and penetration reached during the loading phase (Fig. 3.5a). δ_p is the permanent indentation which must be specified as an additional parameter. t_c is the instant when the compression phase ended (section 3.1.2).

It is clear that the proposed model assumes that the permanent indentation is the sole factor accounting for the energy loss during impact. This is not an unreasonable assumption for most impact problems.

3.3.2 Hysteresis damping model

The simplest model of the contact force between two bodies was suggested by Kelvin and Voigt [15]. The model incorporates a linear spring and damper in

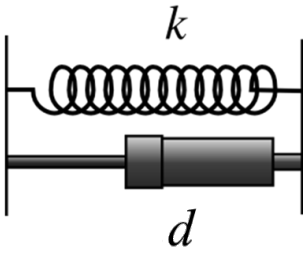

Figure 3.6: Kelvin-Voigt contact force model

parallel connecting the two contact points of the colliding bodies (Fig. **??**). The contact force is evaluated from:

$$F_n = k\delta + d\dot{\delta} \tag{3.17}$$

where δ is the relative penetration of the surfaces of two colliding bodies in the direction of impact. The parameter k is the stiffness coefficient of the spring, and the parameter d is the damping coefficient of the damper. Actually this model was born to describe the mechanics behavior of polymer materials. Solids whose follows the equation (3.4) are referred to as Kelvin-Voigt solids [36].

In order to guarantee that the damping force $d\dot{\delta}$ satisfies both boundary conditions at the time of initial contact and at the time of separation, the coefficient d is chosen such that the damping force is in phase with the indentation velocity but proportional to the indentation. This model is referred to as a *hysteresis damping* model [36], and may be expressed as

$$F_n = k\delta + \mu\delta \cdot \dot{\delta} \tag{3.18}$$

where the terms $\mu\delta$ is the hysteresis damping terms. the parameter μ is called the hysteresis damping factor. In Figure 3.5b is shown the trends of the contact force during the compression and the restitution phases of contact. During the compression period, the contact force follows the loading path shown. The contact force is increased from zero to its maximum value 1m at which point the amount of indentation is δ_c. During the restitution period, the contact force follows the unloading path for which the force and the indentation are both reduced from $F_{n,max}$ and δ_c to zero. Therefore, the hatched area represents the dissipated energy during impact. The boundary of the area is called the hysteresis loop.

As the figure suggests, the bodies exert tension on each other right before separation. The process of separation, though, must be a smooth one. Thus, intuitively this model may not be an accurate force model. Even for linear elastic materials, the impact force must be nonlinear due to the nonlinear nature of impact [36].

A more accurate model of the contact force is discussed next.

3.3.3 Hertz contact model with damping

Hunt and Grossley (1975) proposed a sort of extension of Hertz's model with the idea of represent the energy loss in impact as damping function similar to the one in the Kelvin-Voigt model. The contact force model will then be of the form [22]:

$$F_n = k\delta^n + D\dot{\delta} \tag{3.19}$$

Where D is the hysteresis damping coefficient proposed by Hunt and Grossley as

$$D = \mu\delta^n \tag{3.20}$$

The damping parameter μ can be related to the coefficient of restitution, since both are related to the energy dissipated by the impact process.
Assuming that the energy dissipated during the compressive phase and during expansion phase are equal and basing on the Goldsmith results 3.10, Hunt and Crossley [22] approximated the hysteresis damping factor as a function of the restitution coefficient e and the normal relative velocity v_i at the start of impact phase:

$$\mu = \frac{3}{2}\alpha k \tag{3.21}$$

where α is the parameter which taken into account the material and geometry of the bodies (section 3.1.3), whilst k is the stiffness coefficient of the spring representing the impact stiffness.
Lankarani and Nikravesh [31] performed a similar analysis, but they instead assumed that the amount of energy dissipated was much less then the energy stored in compression. According to their work, hysteresis damping factor is defined as:

$$\mu = \frac{3}{2}\alpha k \left(1 - \frac{\alpha v_i}{2}\right) \tag{3.22}$$

Chapter 4

Impact dynamics on a controlled mechanical system

In the previous chapter it was conducted a survey on impact mechanics and its modeling methods. About the second aspect we showed there are two different approaches: discrete and continuous. The first considers the event occurs instantaneously and aims to predict the velocities of the colliding bodies after impact only as function on their initial velocities. The mathematical development is easy and accessible to most engineers, but since it assumes of impulsive duration of the impact, where the system configuration is considered unchanged, it is limited to collisions between rigid bodies. The continuous approach describes the dynamics of a collision by modeling the interaction between the bodies as nonlinear spring-dashpot element. The impact is represented by a force which dynamics depends on the element parameters and the virtual penetration between the bodies. Thus, the dynamic analysis may be performed simply adding the contact force in the equations of motion. Compared to the discrete approach, it allows a more general description of the real behavior of the system, since it does not require as-

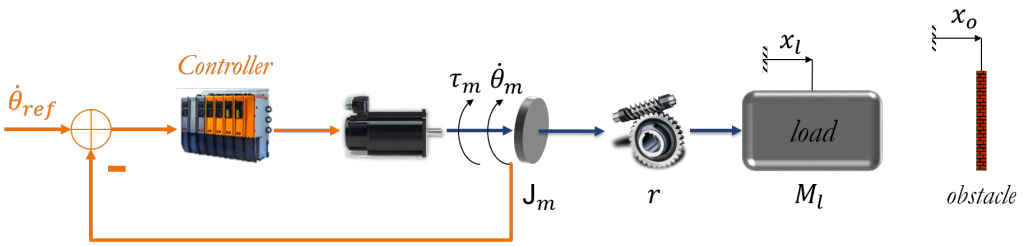

Figure 4.1: Impact scenario taken as example to study the impact dynamics on a actuated system.

sumptions which limit its application. For these reasons, we concluded that the continuous approach is more suitable for our proposes.

Starting from this point, in this chapter we analyze the impact on controlled mechanical system with the scope of identifying the suitable types of sensor for the development of our collision detection strategies.

4.1 Collision scenario

In order to analyze the dynamics of a collision on a generic mechanical system, as a paradigmatic example, it is considered the scenario shown in Figure 4.1. An actuator, through a linear transmission, moves a cart with a mass M_l towards an obstacle at constant speed. The obstacle is motionless. In Figure 4.1 the actuator and the obstacle are straightforwardly represented by an electrical motor and a wall. With x_l and $\dot{x}_l$ are indicated the absolute velocity and position of the load, while with x_o the obstacle absolute position. The motion is considered along one direction. Thus, the type of collision is direct-central impact.

Since our work addresses to the industrial world with a generalized point of view, the actuator is considered commanded by means of a closed-loop

speed control.
The transmission converts the motor rotary motion, θ_m, to linear one of the load x_l. With r is indicated the transmission ratio which is given by

$$r = \frac{\dot{x}_l}{\dot{\theta}_m} \tag{4.1}$$

In a real transmission there may be different phenomena which degrade the performance, both from an energetic and dynamic point of view. To describe these aspects we take into account the elasticity of transmission. At certain frequencies it produces a decoupling effect between the motor and load position.
As components of energy dissipation or elements which oppose to the motion, the model takes into account a viscous friction term both on the motor and load side.

About the collision event, the following assumptions are made. The impact dynamic is defined by Hunt and Crossley's nonlinear contact model:

$$F_c : \begin{cases} 0 & if \quad x_o > x_l \\ k_c \left(x_l - x_o\right)^n + d_c \left(x_l - x_o\right)^n \cdot \dot{x}_l & if \quad x_o \leqslant x_l \end{cases} \tag{4.2}$$

where F_c is the impact force, whilst k_c and d_c represent respectively the stiffness and damping of the contact element. As a contact surface geometry we consider the obstacle flat, while the cart a sphere of radius $R_s = 10mm$. Thus, k_c is defined as

$$k_c = \frac{4}{3\left(\sigma_s + \sigma_f\right)} \sqrt{R_s} \tag{4.3}$$

in which the material parameters σ_s and σ_f are given by

$$\sigma_i = \frac{1 - v_i^2}{E_i} \qquad (i = s, f) \tag{4.4}$$

and the quantities v_i and E_i are, respectively, the Poisson's ratio and Young's modulus associated with sphere and the flat surface. About the damping coefficient d_c of contact, according to Hunt and Crossley, is defined as

$$k_c = \frac{3\,(1-e)\cdot k_c}{2}\sqrt{R_s} \tag{4.5}$$

where e is the impact coefficient of restitution.

In the next section the analysis of collision through a rigid transmission is performed.

4.2 Impact with rigid transmission

In this section we investigate the dynamics of a rigid transmission during a collision.

In Figure 4.2a is shown the scenario taken into account where δ represents the virtual penetration between the bodies, needed for the impact modeling (review the chapter two).

The analysis is split in two parts. Defining with t_c the time when the bodies come in touch, the first part considers the system before the impact occurs, that is at time $t < t_c$. The second part deals with the studying of collision effects on the mechanical system, thus for $t \geq t_c$.

The motion equation before the collision occurs, that is till $x_o \leq x_l$, is defined by the following differential equation,

$$\begin{cases} \tau_m = J_t\ddot{\theta}_m + d_t\dot{\theta}_m \\ \dot{\theta}_m(0) = 0 \\ \theta_m(0) = 0 \end{cases} \tag{4.6}$$

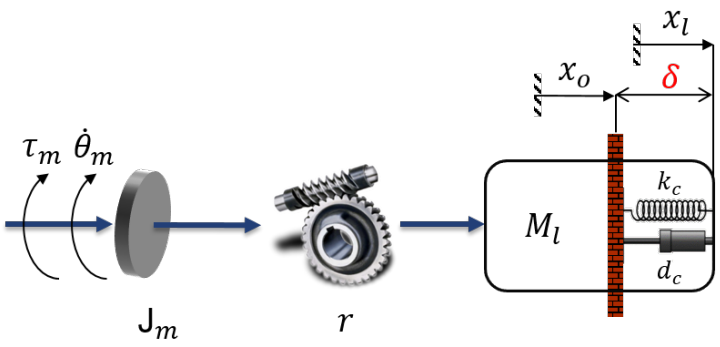

(a) Collision scenario in case of rigid transmission.

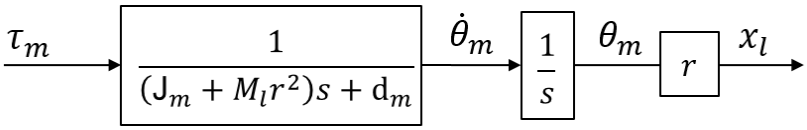

(b) Dynamics of the system before the collision.

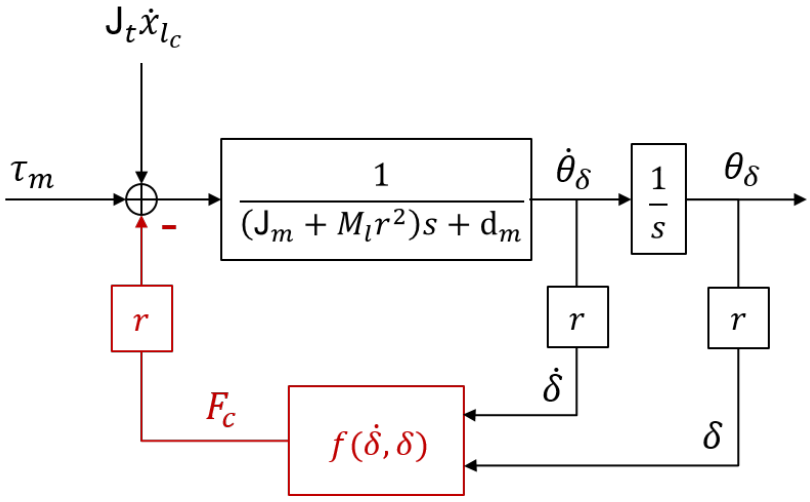

(c) Block diagram of the system during the impact.

Figure 4.2: Block diagram of the system during the collision.

where,

- τ_m is the motor torque;
- J_t is the overall inertia of the system: $J_m + M_l r^2$. The term $M_l r^2$ indicates the load inertia reduced at motor side, whilst J_m is the motor inertia.
- d_t is the overall friction of the system: $d_m + d_l r^2$. The terms d_m and $d_l r^2$ are respectively the viscous friction coefficient of the motor and load.

The dynamics represented in the Laplace domain is given by,

$$\Theta_m(s) = (\tau_m(s)) \cdot G(s) \tag{4.7}$$

where $G(s)$ is the transfer function of the mechanical system,

$$G(s) = \frac{1}{J_t s^2 + d_t s} \tag{4.8}$$

It is a standard second order dynamics with a pole in the origin, $p_1 = 0$, and the other in $p_2 = -\dfrac{d_t}{J_t}$. The generalized gain is $\mu_g = \dfrac{1}{d_t}$.

In Figure 4.2b is shown the block diagram of the dynamic system, where it is possible to observe how the motor torque and the loading forces act as input to $G(s)$ giving as output the motor position and, by the transmission ratio r, the position of load mass.

At the instant when the load mass collides with the obstacle, the dynamics changes significantly. On the load mass appears the impact force F_c described by,

$$F_c = k_c \delta^n + d_c \delta^n \cdot \dot{\delta} \tag{4.9}$$

where $\delta = x_l - x_o$ and represents the virtual penetration between the bodies. k_c and d_c are respectively the stiffness and damping of the impact model. Since the obstacle is assumed motionless, the penetration and the load mass velocity are coincident: $\dot{\delta} = \dot{x}_l$.

In figure 4.2c is reported the block diagram of the system which helps to put in evidence the difference between the two situations.

Although the model adopted allows to represent the collision event as continuous phenomenon, the instant of first contact between the bodies, that is the instant at which appears the contact force in the model dynamics equation, remains a discontinuous event.
To properly formalize the dynamic description, we rewrite the motion equation beginning from the instant at first contact. Remembering that t_c is the instant when $x_o = x_l$, the dynamic equation during the impact is given by

$$\begin{cases} \tau_m - F_c \cdot r = J_t \ddot{\theta}_m + d_t \dot{\theta}_m \\ \dot{\theta}_m(t_c) = \dot{\theta}_{m_c} \\ \theta_m(t_c) = \theta_{m_c} \end{cases} \tag{4.10}$$

where θ_{m_c} and $\dot{\theta}_{m_c}$ are respectively the motor position and velocity at first instant of the impact. Since the transmission is rigid, θ_{m_c} and $\dot{\theta}_{m_c}$ are directly related to the load mass kinematics by the ratio transmission r:

$$\begin{aligned} \dot{\theta}_{m_c} &= \frac{\dot{x}_l(t_c)}{r} \\ \theta_{m_c} &= \frac{x_l(t_c)}{r} = \frac{x_o}{r} \end{aligned} \tag{4.11}$$

Substituting the expression of contact model (4.9) the dynamics equation

becomes

$$\begin{cases} \tau_m - \left[k_c \left(x_l - x_o\right)^n + d_c \left(x_l - x_o\right)^n \cdot \dot{x}_l\right] \cdot r = J_t \ddot{\theta}_m + d_t \dot{\theta}_m \\ \dot{\theta}_m(t_c) = \dot{\theta}_{m_c} \\ \theta_m(t_c) = \theta_{m_c} \\ \dot{x}_l(t_c) = \dot{x}_{l_c} \\ x_l(t_c) = x_o \end{cases} \tag{4.12}$$

As final step, we describe the evolution of dynamic system starting from the impact time t_c. That is

$$\begin{aligned} x_l(t) &= \delta(t) + x_l(t_c) = \delta(t) + x_o \\ \theta_m(t) &= \theta_\delta(t) + \theta_m(t_c) = \theta_\delta(t) + \theta_{m_c} \end{aligned} \tag{4.13}$$

Replacing x_l and θ_m with the previous relations in (4.12), we obtain the motion equation of the system during the collision:

$$\begin{cases} \tau_m - \left(k_c \delta^n + d_c \delta^n \dot{\delta}\right) \cdot r = J_t \ddot{\theta}_\delta + d_t \dot{\theta}_\delta \\ \dot{\theta}_\delta(t_c) = \dot{\theta}_{m_c} \\ \theta_\delta(t_c) = 0 \\ \dot{\delta}(t_c) = \dot{x}_{l_c} \\ \delta(t_c) = 0 \end{cases} \tag{4.14}$$

Finally, since the transmission is rigid ($\delta = \theta_\delta \cdot r$), it is possible to re-write

the motion equation in a more compact form,

$$\begin{cases} \tau_m = J_t\ddot{\theta}_\delta + d_t\dot{\theta}_\delta + d_c\theta_\delta^n\dot{\theta}_\delta r^{(2+n)} + k_c\theta_\delta^n r^{(1+n)} \\ \dot{\theta}_\delta(t_c) = \dot{\theta}_{m_c} \\ \theta_\delta(t_c) = 0 \end{cases} \tag{4.15}$$

In Figure 4.3 we report the results of an impact simulation example in *Simulink*, whose parameters are shown in table 4.1. Referring to our collision scenario, we consider an impact between a plastic sphere of 10 mm toward a steel wall at the constant speed of 0.25 m/s. As it possible to observe by the graph, the collision begins at time of 408 ms, as soon as the contact force rises, and lasts for 63 ms. The event does not cease with a unique phase of impact. The initial kinetic energy is dissipated on several stages of contact. About the first, it presents a loss of kinetic energy of 52% of the initial one. It has a duration of 1.2 ms during which the contact force reaches the peak value of 864 N. About the virtual penetration δ, it reaches the maximum value of 0.091 mm.
As is it possible to observe, the type of collision simulated is a quite rigid impact.

To gain a deeper understanding of the system dynamics can be useful to graph the Bode diagram.
Since it is a nonlinear system, first of all, we need to linearize it. Reviewing dynamic equation 4.15 on the following form

$$\ddot{\theta}_\delta = f(\theta_\delta, \dot{\theta}_\delta, \tau_m, F_l)$$

and applying the Taylor expansion, we get the equation of the linearized

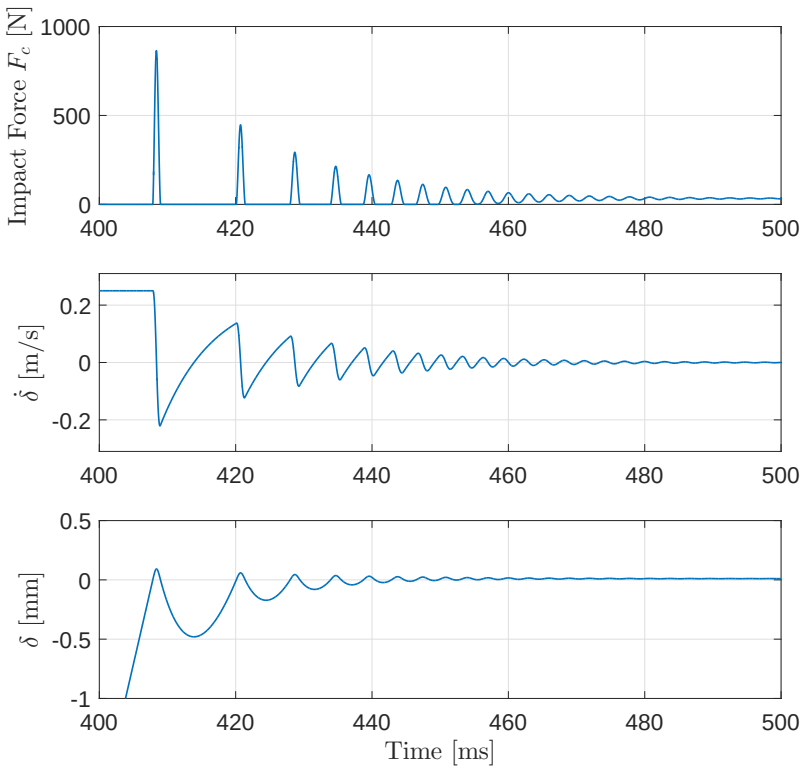

Figure 4.3: Results of an impact simulation in Simulink of the collision scenario.

Table 4.1: Parameters used for the Simulink simulation of the collision scenario.

T_m (Nm)	0.5
J_t (kgm^2)	2.3500e-04
d_m (Nms/rad)	0.03
τ	0.0150
k_c (N/m)	9.8261e+08
d_c (Ns/m)	2.9478e+08
n	1.5

system:

$$\Delta\tau_m = J_t\Delta\ddot{\theta}_\delta + \left(d_t + D_\Delta(\bar{\dot{\theta}}_\delta, \bar{\theta}_\delta)\right)\Delta\dot{\theta}_\delta + K_\Delta(\bar{\dot{\theta}}_\delta, \bar{\theta}_\delta)\Delta\theta_\delta \tag{4.16}$$

$\bar{\dot{\theta}}_\delta$ and $\bar{\theta}_\delta$ are the speed and motor position at the linearization point. With $\Delta\cdot$ are indicated the "smal" deviation variables round the linearization point. The terms $K_\Delta(\bar{\dot{\theta}}_\delta, \bar{\theta}_\delta)$ and $D_\Delta(\bar{\dot{\theta}}_\delta, \bar{\theta}_\delta)$ represent, respectively, the linearized contact parameters of stiffness and damping, whose expression are

$$\begin{aligned} K_\Delta(\bar{\dot{\theta}}_\delta, \bar{\theta}_\delta) &= k_c \cdot n \cdot r^{n+1} \cdot \bar{\theta}_\delta^{n-1} + d_c \cdot n \cdot r^{n+2} \cdot \bar{\theta}_\delta^{n-1} \cdot \bar{\dot{\theta}}_\delta \\ D_\Delta(\bar{\dot{\theta}}_\delta, \bar{\theta}_\delta) &= d_c \cdot r^{n+2} \cdot \bar{\theta}_\delta^{n} \end{aligned} \tag{4.17}$$

It is interesting to note how they change depending on the states of system. In particular, the increase of δ leads a more rigid and viscous contact properties. About the speed $\dot{\delta}$, its increase involves only an increment of the contact stiffness. These observations come out to be very useful to understand the physic phenomenon and to tune the contact parameters for simulation propose.

Now, representing the equation 4.16 in Laplace domain is possible to obtain the transfer function of the linearized system,

$$G_\Delta(s) = \frac{\Delta\Theta_\delta(s)}{\Delta\tau_m} = \frac{1}{J_t s^2 + (d_t + D_\Delta)\, s + K_\Delta} \tag{4.18}$$

It is a second order mass-spring-damper system with two poles in

$$p_{1,2} = \frac{-\left(d_t + D_\Delta\right) \pm \sqrt{\left(d_t + D_\Delta\right)^2 - 4J_tK_\Delta}}{2J_t}$$

and gain

$$\mu = \frac{1}{K_\Delta}.$$

In a more useful parametric formulation, $G_\Delta(s)$ can be rewritten as,

$$G_\Delta(s) = \frac{\omega_n}{s^2 + 2\xi\omega_n s + \omega_n^2} \tag{4.19}$$

where

$$\omega_n = \sqrt{\frac{K_\Delta}{J_t}} \quad \text{and} \quad \xi = \frac{(d_t + D_\Delta)}{2\omega_n}$$

are respectively the natural frequency and damping factor of the linearized system.

Observing this last expression, it is possible to perceive how the dynamics change over the collision. The increase of penetration between the bodies and its rate leads a faster dynamic behavior and more damped. This fact can be seen in Figure 4.4. We report the G_Δ Bode diagram for the previous simulation example considering different linearization point. In particular, we consider five configurations of the dynamic system, starting from the instant before the impact to the first peak of the load cell. We can observe clearly that the increase of δ and $\dot{\delta}$ involve an increment of the rigid behavior of the system. Thus, an increase of the system bandwidth and faster dynamics of the collision in the motor position.

To conclude this analysis, for completeness, we invite to observe that the overall system dynamics is a *Switching Dynamic System*, where the switching variable is the relative position between the cart and obstacle δ. In particular, before the collision, for $\delta < 0$, the dynamics is described by a classic Linear Time-Invariant system. Differently, for $\delta \geqslant 0$, we have a Nonlinear dynamic

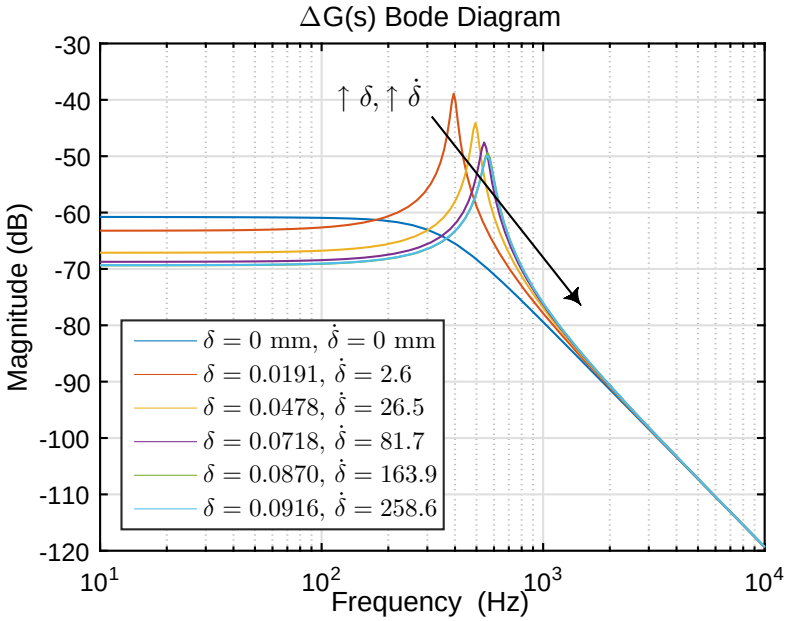

Figure 4.4: Bode diagram of system dynamics during the collision with rigid transmission.

system. In mathematical form the overall dynamics is described by,

$$SYS: \begin{cases} \tau_m = J_t\ddot{\theta}_m + d_t\dot{\theta}_m & if \quad \delta < 0 \\ \tau_m - \left(k_c\delta^n + d_c\delta^n\dot{\delta}\right)\cdot r = J_t\ddot{\theta}_\delta + d_t\dot{\theta}_\delta & if \quad \delta \geqslant 0 \end{cases} \tag{4.20}$$

4.3 Impact with elastic transmission

In the previous case we considered a rigid connection between the motor and load. This involves the motor torque is able to act instantly on the load dynamics and, vice versa, an external load force is able to act directly on the motor dynamics. In other words, the transmission has a infinity bandwidth.

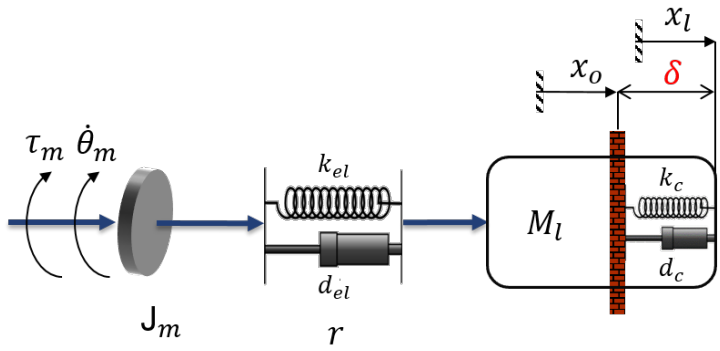

(a) Collision scenario in case of elastic transmission.

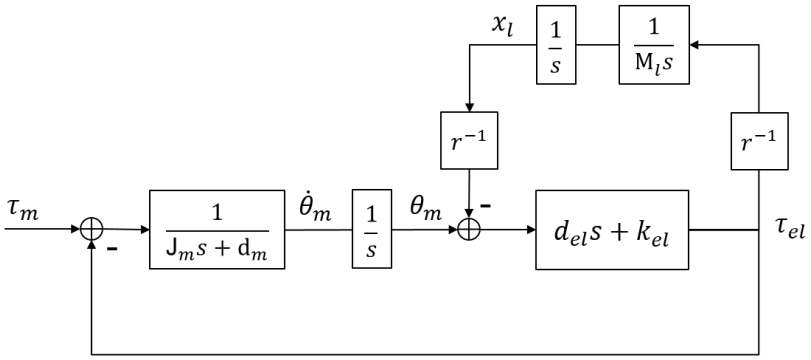

(b) Block diagram of the system before the collision.

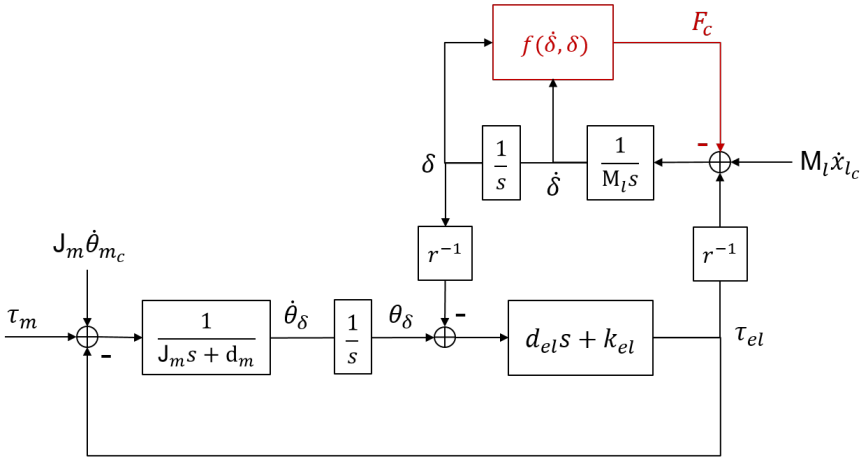

(c) Block diagram of the system during the impact.

Figure 4.5: System dynamic analysis in case of elastic transmission during a collision.

Obviously, this is an ideal condition. In a real transmission there are different phenomena which degrade the performance from an energetic and dynamic point of view. The most common are the elasticity, irregularities (affect the transmission ratio), backlash and nonlinear friction.
Trying to get closer at real scenario, without unnecessarily complicating the analysis regarding our goals, in this section we study the impact dynamics in a elastic transmission. We remove the rigid connection hypothesis and consider the motor torque generated through spring-dashpot element (fig. 4.5a).

For this scenario the motion at time before the collision is described by the following system of equations:

$$\begin{cases} \tau_m - \tau_{el} = J_m\ddot{\theta}_m + d_m\dot{\theta}_m \\ \dfrac{\tau_{el}}{r} = M_l\ddot{x}_l \\ \tau_{el} = k_{el}\left(\theta_m - \dfrac{x_l}{r}\right) + d_{el}\left(\dot{\theta}_m - \dfrac{\dot{x}_l}{r}\right) \\ \dot{\theta}_m(0) = 0 \\ \theta_m(0) = 0 \\ \dot{x}_l(0) = 0 \\ x_l(0) = 0 \end{cases} \tag{4.21}$$

where τ_{el} is the internal reaction of the elastic transmission represented on motor side. k_{el} and d_{el} are respectively the stiffness and damping of the spring-dashpot element.
As it is possible to note the system dynamics is decoupled by the elastic transmission. The first equation describes the dynamics between the motor and the transmission. The second one, between the transmission and the load.

The next equation describes the dynamics of the spring-dashpot element, or rather how the motor and load are decoupled. The last four relations are the initial condition of the system.
The description of dynamics in Laplace domain is given by,

$$\begin{cases} \tau_m(s) - \tau_{el}(s) = J_m \Theta_m(s) s^2 + d_m \Theta_m(s) s \\ \dfrac{\tau_{el}(s)}{r} = M_l X_l(s) s^2 \\ \tau_{el}(s) = k_{el} \left(\Theta_m(s) - \dfrac{X_l(s)}{r} \right) + d_{el} s \left(\Theta_m(s) - \dfrac{X_l(s)}{r} \right) \end{cases} \tag{4.22}$$

In Figure 4.5c is shown the system block diagram where is possible to catch graphically the decoupling between the motor and the load dynamics.

As in the rigid transmission scenario, when the collision occurs a new term in the motion equation appears. In the second equation of (4.21) we add contact force, F_c, expression. Thus, the dynamics in time domain is described by

$$\begin{cases} \tau_m - \tau_{el} = J_m \ddot{\theta}_m + d_m \dot{\theta}_m \\ \dfrac{\tau_{el}}{r} - \left[k_c \left(x_l - x_o \right)^n + d_c \left(x_l - x_o \right)^n \cdot \dot{x}_l \right] = M_l \ddot{x}_l \\ \tau_{el} = k_{el} \left(\theta_m - \dfrac{x_l}{r} \right) + d_{el} \left(\dot{\theta}_m - \dfrac{\dot{x}_l}{r} \right) \\ \dot{\theta}_m(t_c) = \dot{\theta}_{m_c} \\ \theta_m(t_c) = \theta_{m_c} \\ \dot{x}_l(t_c) = \dot{x}_{l_c} \\ x_l(t_c) = x_o \end{cases} \tag{4.23}$$

As in the previous scenario, we rewrite the evolution of system dynamics

starting from the impact time t_c obtaining the following representation,

$$\begin{cases} \tau_m - \tau_{el} = J_m\ddot{\theta}_\delta + d_m\dot{\theta}_\delta \\ \dfrac{\tau_{el}}{r} - \left(k_c\delta^n + d_c\delta^n\dot{\delta}\right)\cdot r = M_l\ddot{\delta} \\ \tau_{el} = k_{el}\left(\theta_\delta - \dfrac{\delta}{r}\right) + d_{el}\left(\dot{\theta}_\delta - \dfrac{\dot{\delta}}{r}\right) \\ \dot{\theta}_\delta(t_c) = \dot{\theta}_{m_c} \\ \theta_\delta(t_c) = 0 \\ \dot{\delta}(t_c) = \dot{x}_{l_c} \\ \delta(t_c) = 0 \end{cases} \tag{4.24}$$

As for the rigid scenario, we face *Switching Dynamic System* where the dynamics is described by a classic Linear Time-Invariant system for $\delta < 0$ (that is before the collision occur), whilst for $\delta \geqslant 0$ (during the impact) the dynamics is nonlinear.

Comparing this last expression with the motion equation of the rigid transmission scenario (eq. (4.21)), it is possible to note the collision acts differently on the system. The load dynamics is affected directly by the impact force, while the motor senses the collision through the elastic reaction of the transmission. As it is possible to figure out, the impact dynamics on the motor position might be slower compared to that on the load.

In the following we put more in evidence this fact, going to study the system dynamics in Laplace domain. Differently from the rigid scenario, where we linearized the dynamics about the normal trajectory, we decide to simplify the impact model considering a linear behavior instead of nonlinear one for sake of computation. We underline this implication does not change significantly the considerations we get from this analysis.

From the previous chapter, we have seen that the nonlinear impact model

is better than the linear one, since it approximates better the phenomena from the energetic point of view. As it is possible observe from the Figure 4.5a, we are studying the case of a mechanical system dynamics with two elastic elements in series. Since, we are interest in deepening the impact dynamic aspects, then the energic one, the simplification for this analysis can be considered valid.

To describe the system dynamics during the collision in Laplace domain, we reformulate the contact model as

$$F_c = K_c \left(x_l - x_o\right) + D_c \left(x_l - x_o\right) \cdot \dot{x}_l \tag{4.25}$$

where K_c and D_c are respectively the stiffness and damping of the linear contact element.

Applying the Laplace transform at eq. 4.24 with the linear contact model we get,

$$\begin{cases} \tau_m(s) - \tau_{el}(s) + J_m \dot{\theta}_{m_c} = J_m \Theta_m(s) s^2 + d_m \Theta_m(s) s \\ \dfrac{\tau_{el}(s)}{r} + M_l \dot{x}_{l_c} = M_l \delta(s) s^2 + D_c \delta(s) s + K_c \delta(s) \\ \tau_{el}(s) = k_{el} \left(\Theta_\delta(s) - \dfrac{\delta(s)}{r} \right) + d_{el} s \left(\Theta_\delta(s) - \dfrac{\delta(s)}{r} \right) \end{cases} \tag{4.26}$$

In Figure 4.5c is shown the block diagram of the elastic transmission dynamics during the collision where is possible to observe how the decoupling effect influence the impact dynamics than the rigid transmission scenario (Fig. 4.2c). It is clear that the feedback reaction of the contact acts primarily on the load dynamics. Thus, for the analysis of the impact dynamics through the transmission, we observe the system starting from the load side. In particular, we study the dynamics of the system considering as input only

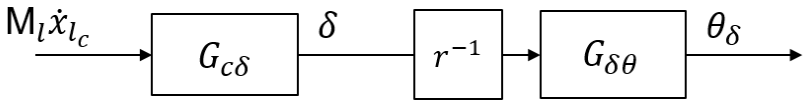

Figure 4.6: Block diagram of system dynamics during the collision considering as input only $M_l\dot{x}_{l_c}$.

$M_l\dot{x}_{l_c}$, that is the initial momentum of the load mass. Physically, this fact is like to study the scenario where the load mass is initially stationary and the obstacle collides to the system at the initial velocity $\dot{x}_{l_c}$. From this point of view, the assumption of consider as input $M_l\dot{x}_{l_c}$ makes sense, since our main aim in this chapter is to investigate the dynamic effects of collision inside the mechanical system, specially, identify the measurable system information from which is possible detect the impact. Under this view, we can state that $M_l\dot{x}_{l_c}$ is the input of the impact phenomenon.

Thus, considering $M_l\dot{x}_{l_c}$ as the only input and setting the others at zero value, it is possible to review the block diagram 4.5c obtaining that in Figure 4.6. Where the two transfer function of the system are:

$$G_{c\delta} = \frac{b_2 s^2 + b_1 s + b_0}{a_4 s^4 + a_3 s^3 + a_2 s^2 + a_1 s + a_0} \tag{4.27}$$

$$G_{\delta\theta} = \frac{d_{el} s + k_{el}}{J_m s^2 + d_t s + k_{el}} \tag{4.28}$$

where $d_t = d_m + d_{el}$ and the coefficients a_i, b_i are:

$$a_i = \begin{cases} a_0 = & K_\delta k_{el} \\ a_1 = & d_t K_c + D_c k_{el} + \dfrac{J_m}{r^2} d_{el} + \dfrac{d_m}{r^2} k_{el} \\ a_2 = & J_m K_c + D_c d_t + k_{el} M_l + \dfrac{J_m}{r^2} k_{el} + \dfrac{d_m}{r^2} d_{el} \\ a_3 = & J_m D_c + d_t M_l + \dfrac{J_m}{r^2} d_{el} \\ a_4 = & J_m M_l \end{cases} \tag{4.29}$$

$$b_i = \begin{cases} b_0 = & k_{el} \\ b_1 = & d_t \\ b_2 = & J_m \end{cases} \tag{4.30}$$

The first transfer function describes the system dynamics between the load side input and the load position. The second describes the dynamic relation between the motor position and the load position. Observing the block diagram 4.6, and in particular the transfer function $G_{\delta\theta}$, it is noted two facts. First, it is possible to appreciate more clearly the decoupling effect between the motor and the load position due to the elastic transmission. Second, the motor position senses a filtered dynamics of the collision.

To investigate in more detail this last point, it's convenient to neglect the viscous terms of the system. Thus, the previous transfer functions become:

$$G_{c\delta} = \frac{J_m s^2 + k_{el}}{J_m M_l s^4 + \left(J_m K_c + k_{el} M_l + \dfrac{J_m}{r^2} k_{el} \right) s^2 + K_\delta k_{el}} \tag{4.31}$$

$$G_{\delta\theta} = \frac{k_{el}}{J_m s^2 + k_{el}} \tag{4.32}$$

In the following are reported the analytic expression of the $G_{c\delta}$'s gain and singularities:

$$\begin{aligned} z_{1,2} &= \pm\sqrt{\frac{k_{el}}{J_m}} \\ p_{1,2,3,4} &= \pm \left(-\frac{B \pm \sqrt{B - 4AC}}{2A} \right)^{1/2} \\ \mu &= \frac{k_{el}}{K_c k_{el}} \end{aligned} \tag{4.33}$$

where,

$$\begin{aligned} A &= J_m M_l \\ B &= J_m K_\delta + k_{el} M_l + \frac{J_m k_{el}}{\tau^2} \\ C &= K_\delta k_{el} \end{aligned} \tag{4.34}$$

Instead, $G_{\delta\theta}$ is standard second order filter with two imaginary poles positioned in

$$p_{1,2} = \pm\sqrt{\frac{k_{el}}{J_m}}. \tag{4.35}$$

In Figure 4.7 are shown the bode diagrams of $G_{\delta\theta}$ and $G_{c\delta}$ for different values of K_c. Observing the changing of resonance positions than the natural frequency of $G_{c\delta}$, it is possible to identify two cases. The first is when the resonance positions of $G_{\delta\theta}$ are located before the imaginary poles of $G_{c\delta}$, or rather they are inside the $G_{\delta\theta}$ bandwidth. In this case the elastic transmission does not affect on the impact dynamics sensed by the motor position. That is, the transmission can be assumed rigid. On contrary, when the resonance positions of $G_{\delta\theta}$ are located after the imaginary poles of $G_{c\delta}$, the transmission filters the higher frequency components of the impact. So, the collision dynamics sensed by δ and θ will be different.

Analyzing what has been achieved so far, it is possible to formulate a stiffness condition of K_c so the system dynamics can be assumed as rigid, that is:

$$K_c \leq \frac{k_{el} \cdot J_t}{J_m \cdot r^2}. \tag{4.36}$$

In conclusion, in case of elastic transmission, the measure of position at load side, where the collision occurs, might contain more information on the impact dynamics than the measure at motor side.

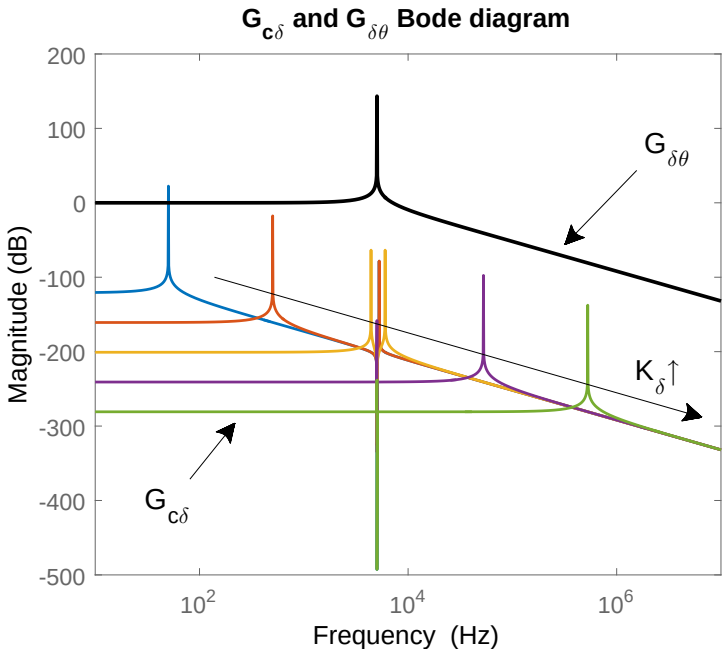

Figure 4.7: Bode diagram of $G_{\delta\theta}$ and $G_{c\delta}$ for different values of the impact stiffness parameter, K_c.

4.4 Impact with control system

In this section, we aim to study the collision effects in a controlled mechanical system.

As anyone might figure out, the information which guarantees the fastest collision detection, obviously, is the force. The use of load cells or torque sensors close to the impact allows a direct measurement of the contact force. In a controlled system another solution might be estimate the impact through the control action the actuator exerts on the system. At the time of collision, a difference between the reference signal and the measure is generated, which results in a control action on the system to restore the wanted motion.

In this analysis, we want to highlight the dynamic relationship between the impact force and the control action. Clearly, the exact math expression

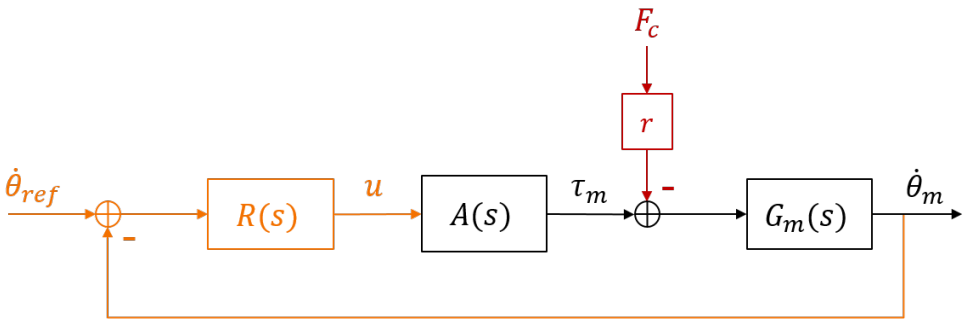

Figure 4.8: Block diagram of the system.

Figure 4.9: Dynamic analysis in case of speed-controlled system during the collision.

describing the system dynamics depend on the type of the actuator and the motion control law. This work wants to be a qualitative analysis with the goal to investigate the effectiveness of the control action information for detecting a collision.

We recall that the final goal of this chapter is to determine which are the most reliable information, thus types of sensor, with which develop an algorithm for impact detection.

For this analysis we consider the scenario reported in Figure 4.1, where the mechanical system is ideal (it is rigid) and, as example, controlled in speed.

Starting from the Figure 4.2b, let's add the transfer functions representing the dynamic of the controller and actuator. In Figure 4.8 is shown the block diagram under analysis. The dynamic model of the mechanical system is indicated with $G_m(s)$ (equation (4.8)), the actuator dynamics with $A(s)$ and the regulator with $R(s)$.

In most of the cases $G_m(s)$ is generalizable with a transfer function shown in eq. 4.8). The dynamic behavior of the actuator, $A(s)$, can be approximated

as a a first order low pass filter:

$$A(s) = \frac{\mu_a}{\tau_a s + 1} \tag{4.37}$$

The regulator is modeled as a generic transfer function with the constraint to be at least proper. A famous example of regulator is the PID controller:

$$R(s) = E(s) \cdot \left(K_P + K_D s + \frac{K_I}{s} \right) \tag{4.38}$$

Studying the effect of the impact force on the control action involves to deduce the transfer function between F_c and τ_m, and between F_c and u:

$$\begin{aligned} G_{F_c,\tau_m}(s) &= \frac{L(s)}{1 + L(s)} \\ G_{F_c,u}(s) &= \frac{1}{A(s)} \frac{L(s)}{1 + L(s)} \end{aligned} \tag{4.39}$$

where $L(s) = G_m(s)R(s)A(s)$ is the open loop transfer function of the system.

Refering at basic theory of control systems, more the poles of $L(s)$ are positioned in the high frequency, more the control action u, or the actuator effort τ_m, will be sensitive to impact dynamics. This implies the following design requirements of the system:

- a light and rigid mechanical system;
- a driver and actuator with a high bandwidth;
- tuning a regulator with high dynamics performance.

The first two points depend on the designing of mechanical system, thus on the application and economy reason. Whilst the controller dynamic perfor-

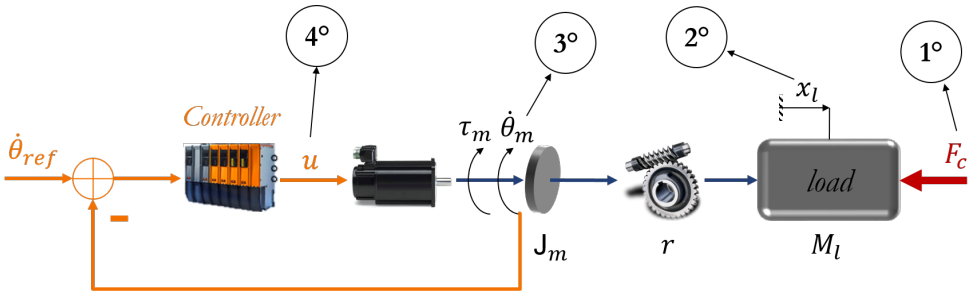

Figure 4.10: Sensors used for detecting a collision, sorted by how fast they allow to detect the event.

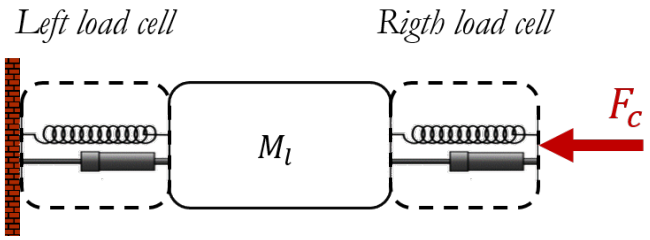

Figure 4.11: Application example about the principle of load cell measurement.

mance are limited by the stability of closed loop system.

4.5 Sensors for collision detection

Up to now, we studied and formalized the impact dynamics on a mechanical system considering different scenarios: a collision with a rigid transmission, a collision with an elastic transmission and a collision in presence of a speed loop control. In particular, we investigated its effects on the state variables of the system.

Based on the results obtained, in this section we identify the sensors which guarantee the optimal trade-off between the quality of information measured on the impact, feasibility and costs.



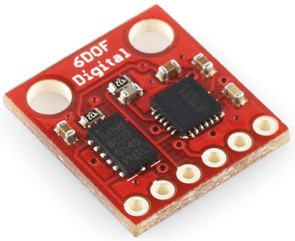

Figure 4.12: Types of sensor for collision detection

The Figure 4.10 summarize the sensors that can be used for detecting a collision, sorted by how fast they allow to detect the event.

The fastest collision detection can be achieved measuring directly the impact force using torque sensors or load cells in the mechanical system. It is important to underline that more the sensor is located close to the impact, more the measure of the collision will be effective. This can be easily explained by the following example. Let's take into account the case in Figure 4.11. A mass M is situated between two load cell. The sensors are modeled as two spring. A force F_c, hit the first load cell. The question is *what the sensors measure*. It is very clear the load on the left measures exactly the impact force, while the load cell on the right measures the impact force minus the inertia of the mass:

$$F_{rl} = F_c$$
$$F_{ll} = F_c - M \cdot \ddot{x}$$

About this solution we can state that the main drawback is given by the high cost of the sensors, their location and setting up on the system. It might require to make important changes to the mechanical system. This fact is especially true for the torque sensors, which required to be integrate

into the force flux of the machine.

At second place there are the kinematic data at load side, where the collision occurs. We saw the kinematic data in case of elastic transmission contains more information on the impact dynamics than those at the motor side.
Respect the previous solution we are not able to catch the complete impact dynamics. The impact's higher frequency components are filtered by the mechanical system. This fact has been shown on the study of impact in a rigid transmission.
The kinematic information considered to detect a collision are the speed and acceleration. Thus, as type of sensors we mention the encoder and the inertial platform.
The encoder is the most common transducer to measure the position of a shaft or a linear axle. In literature is possible to find different methods to estimate the speed by differencing the position; however, all of them present an issue very relevant for our scopes. In [5] is shown, for a fixed a quantization, the Root Mean Square Error of estimated speed increases with the inverse square of the sampling period. Trying to reduce the error would increase the delay between two data and consequently the amount of the impact frequency components observable. Furthermore, it would limit the achievable closed-loop control bandwidth and slowing down the collision data from the control action variable of the regulator.

The inertial measurement platform, as the name suggests, are sensors based on inertia, able to measure accelerations. In industrial mechatronic systems, the IMU sensors can increase the knowledge of the system, permit-

ting an increment of performance in terms of safety, maintainability, efficiency and productivity. Their peculiarity is they required a specific signal processing since the raw data are often noisy. They are so sensitive to catch the natural vibration frequency of the mechanical system, often unwanted for the main scopes of their application. In [13] are reported different uses of the inertial sensor in industrial applications, where is possible to appreciate this fact.

At third place, there are the kinematic data at motor side. As mention before, in case of elastic transmission they might contain less impact dynamic information than the load side. As type of kinematic data, we take into account, again, the speed and acceleration. Thus, as type of sensors we mention, again, the encoders and inertial platforms. However, for practical reason, the using of encoders on the actuators is more common.

In final position, obviously, there is the control action of the regulator. This variable presents less frequency components of the impact. In the relative section of this chapter, we saw that the bandwidth of the control action depends on the mechanical system and the control law of the regulator. About the transducers, it is more difficult identify a technology since it depends on the actuator used.

Final considerations

Observing what has been achieved so far, we are now able to identify the sensors needed for designing a collision detection algorithm that guarantees the fastest performance. Excluding the torque/force sensors for costs and practical reasons, we find three types of sensors:

- a position sensor at actuator side – e.g. encoder sensors;
- an information related to the regulator control action – e.g. PWM in the case of electrical motor;
- an inertial measurement unit positioned at load side.

It is important to note the sensors considered individually do not represent an optimal solution. Each of them has its own limits. The IMU provides the fastest information about the collision, but it is often noisy. On contrary, the actuator encoder guarantees a cleaner data on the event, but its dynamics depends on the mechanical system (the presence of clearance or elastic deformations). The regulator control action is the most robust information, but it also the slowest to detect the event. It has also the property to inherit the same physical interpretation of the collision: e.g. for a DC motor the current can be described as a torque and, consequentially as a contact force.

Based on the results obtained and these last considerations, in the next chapters we present two innovative collision detection algorithms. As it will be possible to observe, at the base of these new solutions there is the sensor fusion concept, which contemplates a smart merging of the sensor data to get a new information that takes the main advantages of the raw data and compensates the drawbacks.

Chapter 5

Friction estimation approach to the collision detection

In the previous chapter, we investigated the effects of a collision on controlled mechanical system identifying four type of sensor for a reliable measurement: force sensors, encoders, accelerometers and sensors related to measure the control action of the regulator.
We reported that the force sensors allow the fastest measure of the impact force, but they have the drawback to be not very practical due to the cost and their setting up on the system. So, this solution was excluded. The using of accelerometers at load side we get an information with the highest impact dynamics, but the data are often noisy. On contrary, the actuator encoders show a cleaner information but dependent on the mechanical system. Finally, the slower but robust information is given by control action, related to the error between reference point and the measure, generated by the collision.

In this chapter we present a new collision detection approach applied to the industrial application case of the safety in the automatic access gate.

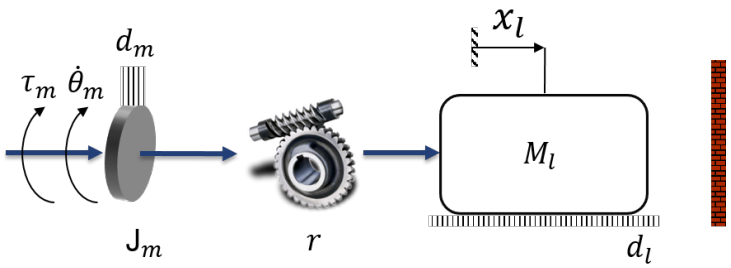

Figure 5.1: Collision scenario

Furthermore, we compare its performance with the *Generalized Momenta* algorithm, the successful collision detection algorithm used in Robotics.

5.1 FEEFKF algorithm

To introduce the proposed method, let's resume the collision scenario of the previous chapter (Figure 5.1).

A speed controlled actuator moves a cart with a mass M_l towards an obstacle at constant speed. The transmission is considered rigid and as components of energy dissipation a viscous friction term both on the motor and load side is taken into account.

We have seen that the dynamics of the system before the collision occurs is given by

$$\tau_m = J_t\ddot{\theta}_m + d_t\dot{\theta}_m \tag{5.1}$$

where τ_m is the motor torque, J_t and d_t are respectively the overall inertia and the overall friction of the system.

Afterwards, we have seen that during the collision a force term relative to the contact force appears in the equation,

$$\tau_m - F_c \cdot r = J_t\ddot{\theta}_m + d_t\dot{\theta}_m \tag{5.2}$$

The core idea of this approach is modeling the impact force as a viscous friction and identify the collision as virtual change of the wear condition of the mechanical system. Thus, the contact force is now described as

$$F_c = d_c \cdot \dot{x}_l \tag{5.3}$$

while the dynamic equation becomes

$$\tau_m = J_t \ddot{\theta}_m + d_{t'} \dot{\theta}_m \tag{5.4}$$

where $d_{t'} = d_t + d_c r^2$ is the new global viscosity friction coefficient of the system during the collision.
In other word, the problem of detecting an impact force is expressed as estimation of the viscous friction coefficient of the mechanical system.

Starting from the last model equation (5.4), the goal is to estimate the friction coefficient d_t of the system, given the measurement of the motor torque (τ_m), the speed (ω_m) and acceleration ($\dot{\omega}_m$). The motor speed is considered to be measured using an encoder on the motor, whilst the motor acceleration is measured using an inertial measurement unit on the cart (at load side) and from knowledge of the transmission ratio, r.
Since the model is nonlinear, in order to solve the estimation problem, the Extended version of the Kalman filter must be used. As reported in [19], *EKF* consists in applying linearization techniques about the estimated trajectory, to get simple approximation of the system and then compute the Kalman filter gain respect these points.
Thereby to formulate the Extended Kalman filter problem, there are three main steps to follow:

1. basing on the model equation, define the state space model of the sys-

tem;

2. linearize the system;

3. define the noise covariance matrix Q and R.

About the first step, given the measurement of the motor torque, the speed and the acceleration, the state variables of the system are defined as:

About the first step, the state variables of the system are,

$$\boldsymbol{x} = \begin{cases} x_1 = d_t \\ x_2 = \ddot{\theta}_m \\ x_3 = \dot{\theta}_m \end{cases}$$

while the observation are given by,

$$\boldsymbol{z} = \begin{cases} z_1 = \omega_m \\ z_2 = \dot{\omega}_m = \frac{a_x}{r} \end{cases}$$

where a_x is the acceleration measurement of the cart. The motor torque τ_m is the input u of the system.
Hence, the state space model in discrete time is:

$$\begin{cases} x_1(k+1) & = x_1(k) + w_1(k) \\ x_2(k+1) & = \frac{u(k) - x_1(k)x_3(k)}{J_t} + w_2(k) \\ x_3(k+1) & = x_3(k) + T_s x_2(k) + w_3(k) \\ z_1(k) & = x_2(k) + v_1(k) \\ z_2(k) & = x_3(k) + v_2(k) \end{cases} \tag{5.5}$$

where w_n represents the uncorrelated noise of the plant, v_m the uncorrelated noise in the measurement and T_s is the sampling time.
The second step consists in linearize our model. Starting from the classic state space description of nonlinear system,

$$\begin{cases} \mathbf{x}(k+1) & = f(\mathbf{x}(k+1), \mathbf{u}(k)) \\ \mathbf{z}(k) & = h(\mathbf{x}(k), \mathbf{u}(k)) \end{cases}$$

the system is linearized in the following manner:

$$\delta F = \frac{\delta f(x,u)}{\delta x} = \begin{bmatrix} 1 & 0 & 0 \\ -\frac{x_3}{J_t} & 0 & -\frac{x_1}{J_t} \\ 0 & T_s & 1 \end{bmatrix} \tag{5.6}$$

$$\delta H = \frac{\delta h(x,u)}{\delta u} = \begin{bmatrix} 0 & 1 & 0 \\ 0 & 0 & 1 \end{bmatrix} \tag{5.7}$$

Finally, to complete the formulation the covariance matrix of the model is defined as:

$$Q = \begin{bmatrix} w_1 & 0 & 0 \\ 0 & w_2 & 0 \\ 0 & 0 & w_3 \end{bmatrix}, \; R = \begin{bmatrix} v_1 & 0 \\ 0 & v_2 \end{bmatrix} \tag{5.8}$$

where Q represent the covariance matrix related to the plant noise while R is linked to the measurement noise. They are considered diagonal as simplified assumption.

Comparing from the mathematical point of view the FEEFKF with the Generalizes Momenta algorithm, we can state both are model based approaches which assume the mechanical system is rigid. Our solution introduces a little computational complexity than the robotic algorithm, and it doesn't work in every collision situation. With the mechanical system at rest (the motor speed is zero) is not possible to detect an impact, since is not possible to get an estimate of the virtual friction coefficient. On the other hand, we believe these drawbacks are a low price to pay for getting the performance shown in the next sections.

The strong point of FEEKF is to be able to merge the data in a unique parameter with physical meaning easily understandable and interpretable. Furthermore, it requires only low-cost sensors. It only needs to add the accelerometer sensor, since in a controlled system the others two information (the motor speed and the torque for the scenario considered) are already present.

About its functioning limit, we argue the resting scenario is not a dangerous case in every industrial application. Thinking about a collision with a human, it corresponds at the situation where is the person which collides to the system. A case where the responsibility rests with the human. In the next chapter, we will go more in deep about this problem and we will propose a second approach which solves this problem.

In the following section, we finally show the performance of the FEEKF algorithm, also compared to GM, for an application case well designed for our goals.

5.2 Application case: safety in automatic access gate

In this section a particular application case is presented, which highlights the potential of the sensor fusion solution proposed in this work.

(a) DEIMOS automatic access gate.

(b) Rubber bumper.

Figure 5.2: Image of the mechanical system used for the tests.

5.2.1 Problem description

The electromechanical system used to test the algorithm is a heavy automatic access gate (Figure 5.2). The gate has a weight of 620 Kg and a operative speed of 12 meters per minute. The goal is to detect in the minimum time the collision of the gate against a person, a car or any other object. Obviously, from a safety point of view, the impact with a human is the most significant to detect.

This lead to an examination of two types of impact:

- *Stiff*: it relates to collisions between a gate and rigid objects (*e.g.* a car or human bones);
- *Soft*: this type of impact refers to collisions among the gate and soft

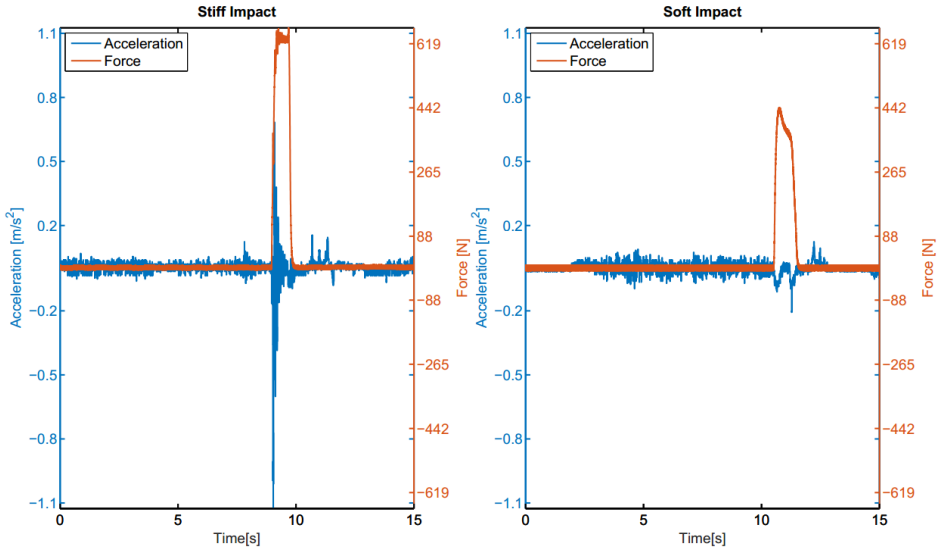

Figure 5.3: Comparison of the two different impacts. The stiff one has an higher impact force and, consequentially an higher deceleration.

items (*e.g.* obese people). Another crucial condition, modeled as soft impact, happens when a person remain stuck between the gate and the barrier at the end of the track, being pressed by the gate.

Since the system now is completely described is easy to deduce that the *stiff impact* will produce an higher deceleration compared to the *soft* one, as visible in figure 5.3.. On the other side, a *soft impact* will be more visible on the torque signal, due to the slow increase of the force needed to overcome the obstacle.

Due to these remarks, the sensor fusion algorithm proposed perfectly meets the requirements, promising better performance than Generalized Momenta, which uses only the information on the motor side.

5.2.2 Experimental setup

The mechanical structure of the gate consists of four components:

- motor: typically a synchronous brushless motor, with the speed of the rotor calculated by the resolver;
- transmission: reduce the rotational speed, increasing the torque produced in output;
- rack: transform the motion from rotational to linear;
- moving mass: this is effectively the gate, which moves forward and backward, opening and closing the access.

The Extended Kalman Filter requires three measurements from the system:

1. acceleration: using an accelerometer placed on the moving part of the gate. Since the derivative of the angular speed is needed, using the following equation the linear acceleration is transformed into a rotational one:
$$\dot{\omega}_m = \frac{\ddot{x}}{r} \tag{5.9}$$
where r is the gear ratio and $\ddot{x}$ the longitudinal acceleration;
2. torque: in this case, the torque is estimated directly from the motor current:
$$T_m(t) = K_t \cdot i_m(t) \tag{5.10}$$
where i_m is the current in the motor and K_t is the coefficient which relate the current to the torque;

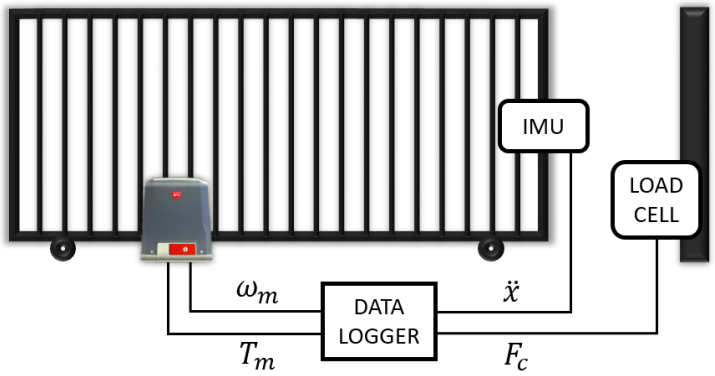

Figure 5.4: Schematic of the experimental layout. The position of the IMU and the load cell reflect the real location during the tests.

3. angular velocity, ω_m: this variable is acquired through a resolver connected to the motor.

In addition to these data and only for validation propose, the force of the impact is acquired using a load cell. This sensor permits to understand when the collision begins and, as a consequence, an evaluation of the time required by the algorithm to identify the impact. The load cell chosen has a stiffness of 500 N/mm which approximate the rigidity of human cranium.
The experimental layout described is shown in Figure 5.4.
The two type of collision defined in the previous section are recreated in this way:

- *Stiff*: using the load cell previously described;
- *Soft*: placing a rubber bumper in front of the gate, which absorb a part of the impact force.

All these data are acquired using a dedicated electronics which runs the algorithm in real-time. The embedded system permits to stop the gate in case of detection of the impact.

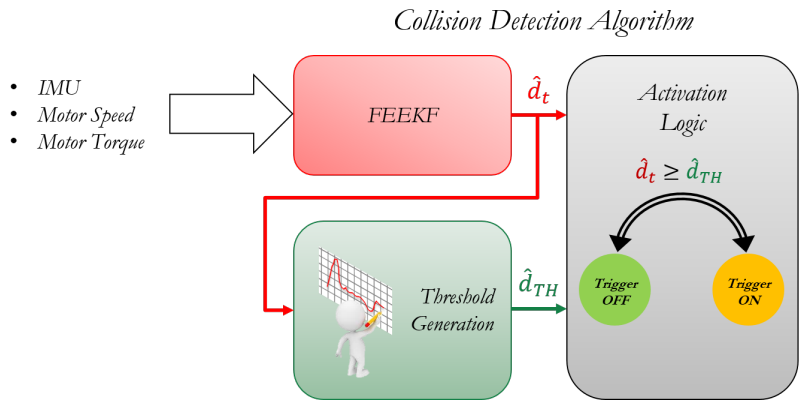

Figure 5.5: The structure of the algorithm is briefly resumed in the figure. The torque, the angular speed and the acceleration permit to estimate the friction coefficient. Then this parameter is used for the creation of the *signature* and the identification of the impact.

5.2.3 Collision detection algorithm

The algorithm for the collision detection (resumed in figure 5.5) can be divided in two parts. The first is the *FEEKF* algorithm, which generates the friction coefficient. The second part is the collision detection logic.

The math model of the gate is the same of the scenario taken into account in section 5.1; as well as the relative application of the FEEKF algorithm.

About the collision detection logic, since the behavior of the system is deterministic, the impact can be detected simply comparing the actual value of the friction coefficient with a threshold curve which represent the normal behavior of the system without collision. This threshold curve is defined as the *signature* of the gate.

In the following, the *threshold* generation process and the impact detection logic are presented.

Signature creation and update

In this phase a number (> 10) of closing operation without impact has been carried out, estimating for each operation a friction coefficient curve. The threshold is then created taking the mean of these curves and increasing it by a safe-factor, in this case the standard deviation. Each time the gate completes a closing operation without impact the *signature* is updated with the new values; in this way the behavior of the gate is updated, matching the changes in the environment (weather, aging of the components etc.).

Impact detection

Once the reference behavior is created the impact can be detected simply identifying when the friction coefficient exceeds the *signature*, as visible in figure 5.6.

5.2.4 Results

In this section we present the performance of the FEEKF algorithm for the application case considered. In particular, we compare our solution with other three approaches.

A solution based on only the measure from the inertial platform, that we called *Pure Inertial* algorithm. A second one, which is based only the torque data, that we called *Pure Torque* algorithm. Finally, the *Generalized Momenta* algorithm used in Robotics, presented in the first chapters of this thesis.

It is important to underline the method used to generated the threshold for these last approaches is the same of the FEEKF algorithm. Therefore, the only difference in performance between the algorithms is given by the

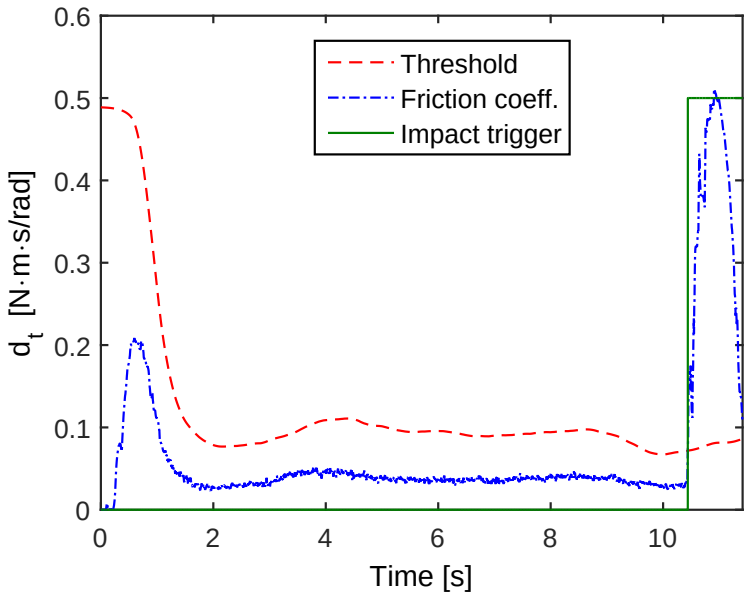

Figure 5.6: The figure illustrates how the algorithm identify the impact. In red (dashed line) is visible the *signature* created during the setting up of the system. In blue (dashed-dotted line) there is the friction coefficient estimated during a closing operation. In green (solid line) is visible the trigger which identifies the impact. It is clear that when the blue line exceeds the red one the impact is detected.

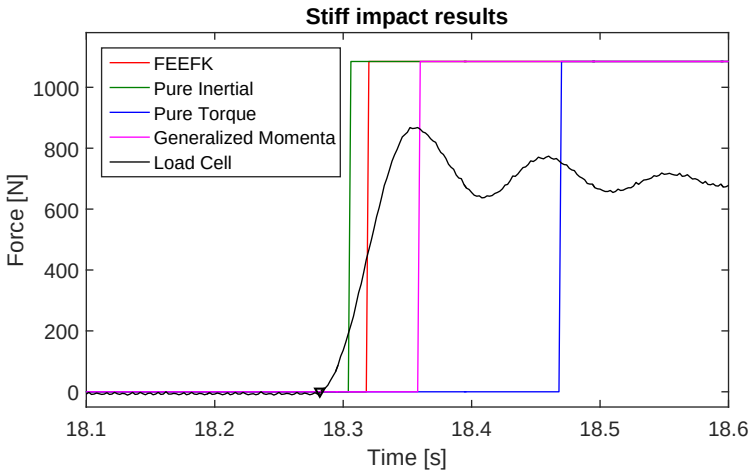

Figure 5.7: Trigger of activation of the algorithm during a stiff impact at maximum speed. The red line is the FEEKF, the green line is the PI algorithm, the blue line is the PT algorithm and the violet line the GM algorithm. The black continuous line is the force of the impact measured by the load cell.

different data about the collision contained in the measures, or in the main information with which the threshold is generated.

The benchmark used to test the performance consists in a closing operation at the maximum speed reachable by the gate, that is 12 meters per minutes. In particular, the reliability of the algorithm is tested for the two-different type of impact described.

Stiff impact

The trigger activations for the stiff impact which, recalling the concept, represents a collision with a rigid object, are shown in figure 5.7 and the performance of the algorithms are summarized in the table 5.1.
In case of stiff impact, high level of acceleration is detected and, as a consequence, the Pure Inertia algorithm, which uses only the accelerometer signals, is the fastest to detect the collision. Some milliseconds later, we get the Fric-

tion Estimation Extended Kalman Filter. It takes the advantages from the accelerometer signals and identifies the impact very quickly. The Generalized Momenta detects the collision after the PI and the FEEKF since it doesn't have any measure at load side. The Pure Torque algorithm identifies the collision much later compared to the new algorithms. It detects the collision only when the regulator increases the current in order to overcome the obstacle.

In conclusion, for this type of impact, the best performance are achieved by the FEEKF and the PI algorithm.

Algorithm type	Activation time [ms]	
	Mean	Std deviation
Pure Inertia	21	3
FEEKF	36	3
GM	76	5
Pure Torque	186	20

Table 5.1: Performance of the algorithms in case of stiff impact. The mean and the std deviation are computed using 30 impact test.

Soft impact

A soft impact happens when the stiffness of the object against whom the gate hits is low. In the application presented, this type of impact is recreated placing a rubber bumper on the moving part of the gate. The performance are summarized in Table 5.2, while in Figure 5.8 the activations of the triggers, compared to the force of the impact, are shown.

The effect of the bumper is visible in Figure 5.8; in fact the slope of the force is not continuous, it has two steps. The first is related to the force absorbed by the bumper, while the second starts when the bumper has ended

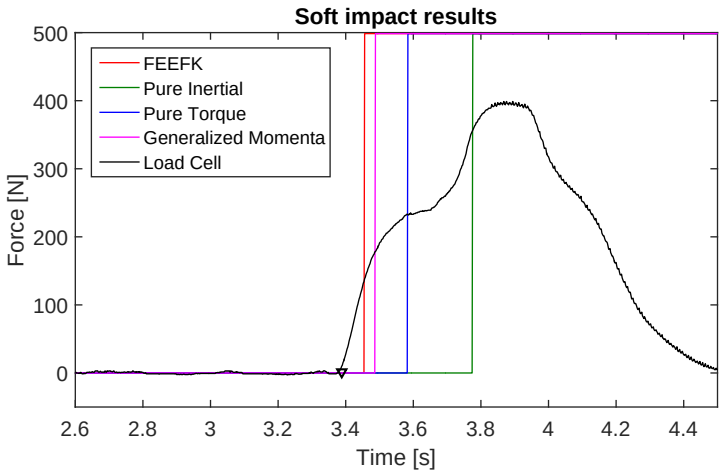

Figure 5.8: Trigger of activation of the algorithm during a soft impact at maximum speed. The red line is the FEEKF, the green line is the PI algorithm, the blue line is the PT algorithm and the violet line the GM algorithm. The black continuous line is the force of the impact measured by the load cell.

its work.

The first algorithm to identify the impact is the FEEKF, which is able to perfectly mix the information from the accelerometer and the torque. Then we get the GM, which, thanks to the speed information, is faster than the PT solution. The worst performance is achieved by the Pure Inertia algorithm, since in this type of impact the amount of acceleration measured is very low and it mixes up with the noise.

Algorithm type	Activation time [ms]	
	Mean	Std deviation
FEEKF	66	10
GM	98	6
Pure Torque	193	15
Pure Inertia	386	14

Table 5.2: Performance of the algorithms in case of soft impact. The mean and the std deviation are computed using 30 impact tests.

Considerations

The two types of collision considered are drastically. The stiff collision presents, obviously, a high impact dynamics with a fast increase of the contact force and high deceleration of the gate. On contrary, the soft collision presents very slow dynamics, indeed it can be separated in two steps. The first, when the bumper absorbs most of the impact energy producing a lower reaction force on the loadcell and low deceleration on the gate. The second, when the bumper is completely compress and the remaining kinetic energy of the gate goes directly on the load cell.

For this reasons, the PI solution is the fastest to detect the collision, while its worst scenario is the soft collision where the acceleration data of the impact are mixed up with the noise.
About the PT algorithm, in the stiff collision shows the worst performance. The impact dynamics is so fast the regulator is not able to update immediately its control action. Opposite situation happens during the soft collision, where the dynamics is slower.

More interesting is to compare the FEEFK with the GM algorithm. The first performs better in the stiff impact, while they show similar performance in the soft impact. The reason behind this fact has been explained in the previous chapter. The main difference between the solutions comes from the different frequency component information of the impact contained in the IMU data at the load side and in the encoder data at motor side. In the stiff collision, due to some clearances and elastic deformations of the mechanical system, some high frequency components of the impact are lost at motor side.

In the end, the algorithm which performs better and is more robust for the different collisions is that one which uses and merges more information,

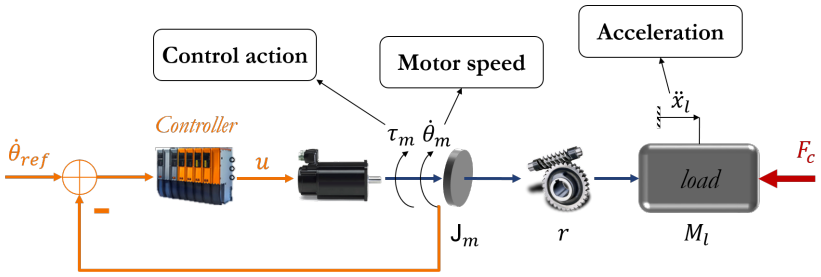

Figure 5.9: Sensors identified to measure a collision.

that is the FEEKF algorithm.

5.3 Conclusion

Based on the result of the previous chapter, in this one we presented a new the collision detection algorithm which merges the data of three different sensors to obtain a unique information with which generating the collision threshold and detect the unwanted event. Moreover, we shew it performs better than the Generalized Momenta, the top collision detection algorithm used robotics and taken into account here as benchmark.

Summarizing, the sensors used by FEEKF are:

- position sensor at the actuator side;
- inertial measurement unit positioned at the load side;
- an information related to the effort of actuator – e.g. the torque for an electrical motor.

The collision detection signal is a virtual viscous friction coefficient. In Figure 5.9 is reported the usual controlled mechanical system considered with highlighted the information used.

In the next chapter we present a second new collision detection algorithm applied on more complicate mechanical system, a robot arm. In particular, it is an evolution of the Generalized Momenta algorithm with the using of acceleration data.

Chapter 6

Inertial Generalized Momenta algorithm

In the previous chapter, we presented the *Friction Estimation Extended Kalman Filter* collision detection algorithm. A novel approach which merges the data of three different sensor types – i.e. the load inertial measures, where the collision occurs, the speed and torque data of the motor, before the mechanical transmission chain – to obtain a unique information with which generating the collision threshold and detect the unwanted event. In particular, it based on the concept to model the collision as a virtual viscous friction. Thus, studying the change in the wear condition of the mechanical system is possible to identify a collision.

Analyzing its performance on an automatic gate access application case, we saw it shows better performance than the *Generalized Momenta* algorithm, the currently most successful collision detection algorithm used in Robotics. However, as drawback, it can be applied only when the mechanical system is in movements, or, in other words, when the motor speed is different from zero.

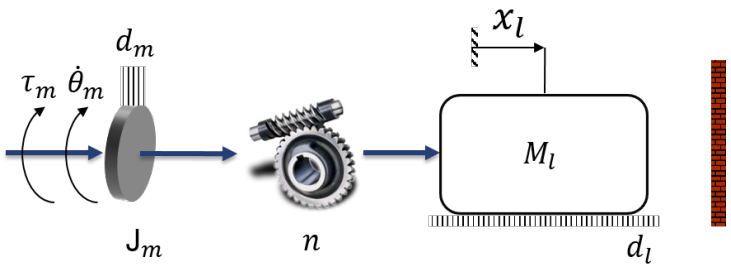

Figure 6.1: Collision scenario used to present the novel solution.

Trying to solve this problem and develop a solution which surpasses the friction approach, in this chapter we present an evolution of the Generalized Momenta algorithm which merges the accelerometers data with its approach. The performance are valued on a more complicate mechanical system, a robot arm.

6.1 IGM algorithm

To introduce the proposed method, let's resume the usual collision scenario, as well as it has been done for the FEEKF method (Figure 6.1).
A speed controlled actuator moves a cart with a mass M_l towards an obstacle at constant speed. The transmission is considered rigid and as components of energy dissipation a viscous friction term for the motor and load is taken into account.
We have seen the dynamics of the system before the collision occurs is given by

$$\tau_m = J_t\ddot{\theta}_m + d_t\dot{\theta}_m \tag{6.1}$$

where τ_m is the motor torque, $J_t = J_m + M_l n^2$ and $d_t = d_m + d_l n^2$ are respectively the overall inertia and the overall friction of the system. n is the transmission ratio.

Afterwards, we have seen that during the collision a term relative to the contact force appears in the equation,

$$\tau_m - F_c \cdot n = J_t \ddot{\theta}_m + d_t \dot{\theta}_m \tag{6.2}$$

Now that the scenario has been reminded, let's formulate the Generalized Momenta algorithm. Basing on the reference [17], it is possible to formulate the following observer:

$$\begin{aligned} \hat{\dot{p}} &= \tau_m - d_t \dot{\theta}_m - \hat{r} \\ \hat{r} &= K \cdot (\hat{p} - p) \end{aligned} \tag{6.3}$$

where we remind that $p = J_t \dot{\theta}_m$ is the momentum of mechanical system and r is the component-wise filtered version of the real impact force,

$$\hat{r} = \frac{K}{s + K} \cdot F_c n \tag{6.4}$$

with the gain K of the algorithm which sets the pole of the low-pass filter.

In the previous chapter, we saw two important facts about the Generalized Momenta algorithm. First, it shows a slower collision detection performance than the FEEFK. Second, the main reason behind this fact rests with the GM does not use the inertial information of the load, where the collision occurs. As proven in the chapter 4, the motor speed "feels" less impact dynamics in comparison the acceleration data at the load side.

Thus, the idea is to try of injecting the lost impact dynamics by the motor speed from the accelerometer. In other words, try to "accelerate" the motor speed.

To achieve that, we merge up the motor speed data with the accelerometer ones using a complementary filter. A low-pass filter for the motor speed data, while a high-pass filter for the accelerometer data. So, the new motor speed

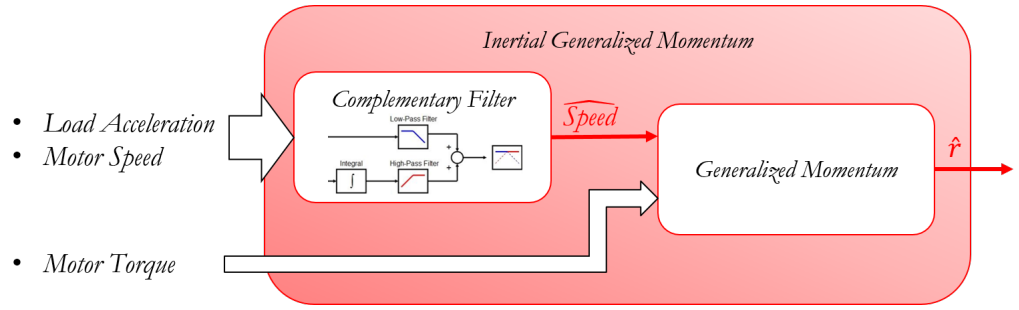

Figure 6.2: The structure of the IGM algorithm is briefly resumed in the figure. The motor speed and the acceleration permit to estimate a new motor speed, with larger frequency content. Then this parameter and the motor torque are used with the GM approach for the creation of the *signature* and the identification of the impact.

is given by

$$\hat{\dot{\theta}}_m = \frac{\ddot{x}_l}{n \cdot s} \cdot \frac{s^2}{s^2 + k_1 s + k_2} + \dot{\theta}_m \cdot \frac{k_1 s + k_2}{s^2 + k_1 s + k_2} \tag{6.5}$$

where k_i are constants which determine the cutoff frequency and damping of the second order filters. In Figure 6.2 we report the scheme of this new approach, that we name as: *Inertial-Generalized Momenta* algorithm (I-GM).

In conclusion, the novel solution combines the positive aspects of the Generalized Momenta with basic idea behind the FEEFKF approach, that is to take advantage of the inertial measure to speed up the dynamics of the others signals.

In the following section, we show the performance of the FEEKF algorithm compared to GM and its evolution, considering the collision application case of a robot arm.

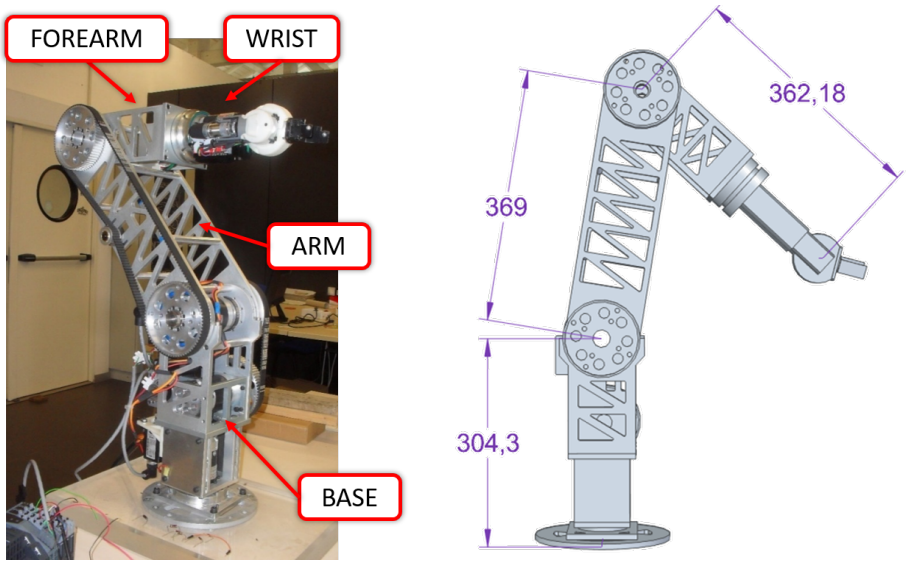

Figure 6.3: Laboratory's robot arm used for the application case.

6.2 Application case: collision detection with a robot arm

6.2.1 Problem description

The electromechanical system used to test the algorithms is a light robot arm used for researching activities in our laboratory. It is not a robust industrial robot. Thus, the types of collision trials, the speed and force of impact have been limited.

Like for the automatic access gate case, the goal is to detect in the minimum time a collision towards different types of obstacle, made of different material, thus different stiffness and capacity to absorb an impact. This lead to formulate two types of impact:

- *Stiff*: it relates to collisions between rigid objects – e.g. human bones or steel objects. In particular, rigid enough to generate high decelerations

in the load accelerometer measures.

- *Soft*: this type of impact refers to collisions with soft obstacles – e.g. obese people. The idea is to test the opposite scenario, where the impact dynamics is contained inside the bandwidth of the transmission and the deceleration values are low in way to reduce the effectiveness of the load accelerometer measures due to the noise.

In the following section, the description of the robot arm and the experimental setup is reported.

6.2.2 Experimental setup

The robot arm used is shown in Figure 6.3. It is 6 DoF robot with weight around 5 kg. The actuators of the wrist are collocated at the extremity of the forearm. The motors of the main links are not placed in the robot's joints, but in the robot base. Through reducers and belts, they command the angular position of the links. In particular, each transmission chain has been designed in way to obtain a constant relation between the motor rotation and the link absolute orientation:

$$\omega_{mi} = \frac{q_i}{n_i} \tag{6.6}$$

where n_i and q_i are respectively the ratio transmission and absolute angular position of the link-i. The actuators are trapezoidal brushless motors.

For our scopes, we consider only the link's motors which coordinate the robot space position. We do not use the wrist's motors, since they influence the end-effector orientation, that is not very relevant for the collision detection problem.

Furthermore, we test the algorithms on the arm and forearm motors for practical and cost reasons. Our system is a home-made light robot, mainly used for research activities on trajectory planning and control system theory. Since it has not been possible to remove the wrist, the most delicate part, we have been limited the trials at two types of collision: impact on the arm and forearm of the robot (Figure 6.8). In the section 6.2.4, we will give a description on the benchmark trials for test the algorithms.

About the sensing aspect, we have seen the algorithms require three information. The speed and torque of the motors, measured ahead of the transmission, and the motor accelerations estimated by load side. In particular, they are obtained from the following sensors:

- the motor speeds come from the motor encoder measures;
- the motor torques estimated by the PWM and the datasheet information. which absorb a part of the impact force. Unfortunately, the winding current measures are not available for type of motor brand used.
- The motor accelerations are measured by inertial measurement units placed on the links. Knowing sensor positions on links, l_{IMU_i}, it is possible to get the link angular accelerations,

$$\ddot{q}_i = \frac{a_{zi}}{l_{IMU_i}} \tag{6.7}$$

  and, as consequence, the motor acceleration:

$$\dot{\omega}_{mi} = \frac{\ddot{q}_i}{n_i} \tag{6.8}$$

In addition to these data and only for validation propose, the force of the

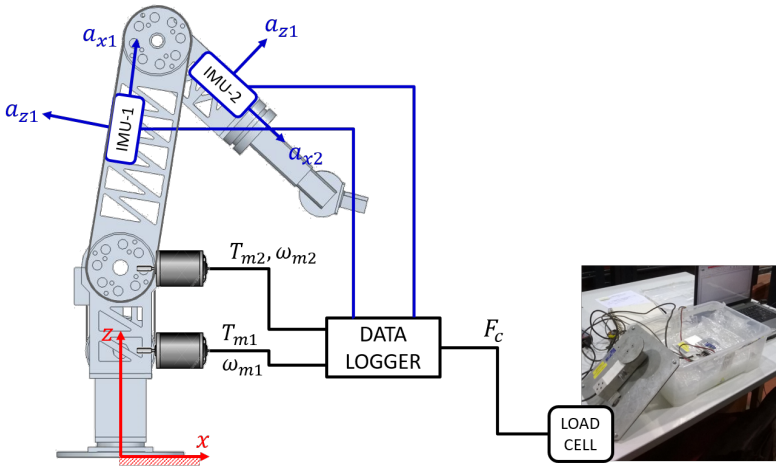

Figure 6.4: Schematic of the experimental layout. The positions of the IMU and the load cell reflect the real location during the tests.

impact is acquired using a load cell. This sensor permits to understand when the collision begins and, as a consequence, an evaluation of the time required by the algorithm to identify the impact. The load cell chosen has a stiffness of 500 N/mm which approximate the rigidity of human cranium.
The experimental layout described is shown in Figure 6.4.
The two type of collision defined in the previous section are recreated in this way:

- *Stiff*: using the load cell previously described;

- *Soft*: placing a rubber bumper in front of the load cell, which absorbs part of the impact force.

All these data are acquired using dedicated electronics which runs the algorithm in real-time. The embedded system permits to stop the robot in case of detection of the impact.

6.2.3 Collision detection algorithms

In this section the collision detection algorithms implemented for the robot arm are described.

As described in the second chapter, the general structure of a collision detection is composed by two parts.
The first part, called feature generation block, generates the collision detection signal – that is the information with which detecting the impact. The second part is the collision detection logic, which defines how to identify the collision.
In this work, we have developed two different feature generation algorithms: the Friction Estimation Extended Kalman Filter algorithm and the Inertial Generalized Momenta algorithm. Since both are based on the dynamic model of the system, first of all, the dynamic equations of the robot are reported. Followed by the description of the algorithms and the threshold generation.

Robot arm model

In Figure 6.5a is shown the parametrized model of the robot arm.
With the red axes is indicated the absolute reference system of our model. q_i are the absolute angular coordinate of the links, considered positive with anticlockwise rotation. l_i is the length of a link, while l_{Gi} is the position of the center of mass along the link-i. m_i and J_i are respectively the mass and rotational inertia of the link-i.

Now, let's proceed to calculate the robot dynamic model for the link of interest.
Exploding the system and applying the Newton-Euler approach, we get the

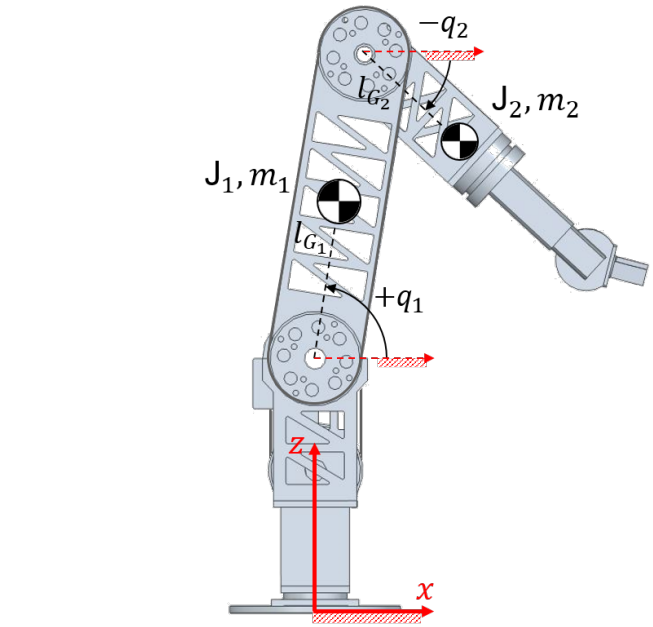

(a)

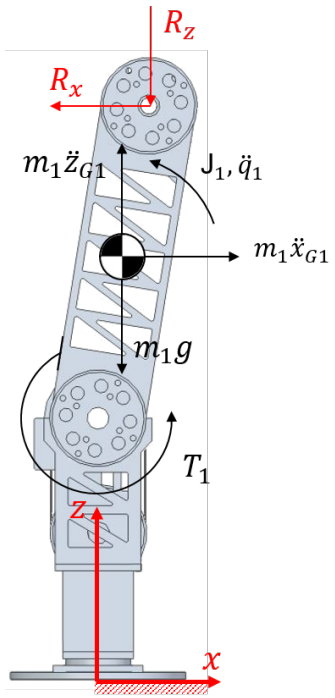

(b)

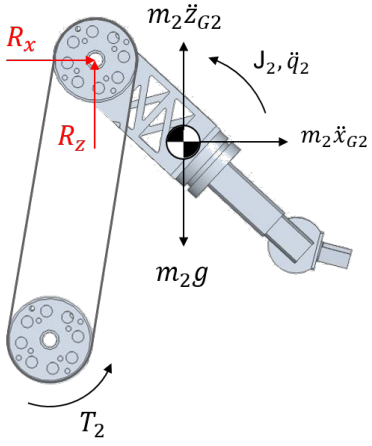

(c)

Figure 6.5: The figures illustrate the dynamic model of the robot arm. The Fig. (a) shows the parameterized model. The Fig. (b) reports the forces acting on the arm, while the Fig. (c) the forces acting on the forearm.

balance equations of the dynamic model:

$$\begin{aligned}\mathcal{T}_1 = {} & J_1\ddot{q}_1 + (g + \ddot{z}_{G1})\, m_2 l_{G1} \cos q_1 - m_1 \ddot{x}_{G1} l_{G1} \sin q_1 \\ & - R_x l_1 \sin q_1 + R_z l_1 \cos q_1\end{aligned} \tag{6.9}$$

$$\mathcal{T}_2 = J_2\ddot{q}_2 + (g + \ddot{z}_{G2})\, m_2 l_{G2} \cos q_2 - m_2 \ddot{x}_{G2} l_{G2} \sin q_2 \tag{6.10}$$

where,

- $m_i g$ terms are the weights of the link;-i
- $m_i \ddot{x_{Gi}}$, $m_i \ddot{z_{Gi}}$ are the inertia forces of the link-i;
- $J_i \ddot{q}_i$ are the torques of inertia of the link-i;
- $\mathcal{T}_i$ indicates the joint torque of the link-i.
- R_x and R_z are the internal reaction forces of the joint, which their expressions are given by,

$$R_x = m_2 \ddot{x}_{G2} \tag{6.11}$$

$$R_z = m_2 g + m_2 \ddot{z}_{G2} \tag{6.12}$$

What remains for obtaining the final expressions of the dynamic model is to rewrite the positions of the centers of mass in function of the link coordinates and calculate the accelerations. Thus, the position of the centers

of mass are,

$$x_{G1} = l_{G1} \cos q_1 \tag{6.13}$$

$$z_{G1} = l_{G2} \sin q_2 \tag{6.14}$$

$$x_{G2} = l_1 \cos q_1 + l_{G2} \cos q_2 \tag{6.15}$$

$$z_{G2} = l_1 \sin q_1 + l_{G2} \sin q_2 \tag{6.16}$$

Calculating the second derivate we get the accelerations,

$$\ddot{x}_{G1} = -l_{G1} \left(\ddot{q}_1 \sin q_1 + \dot{q}_1^2 \cos q_1 \right) \tag{6.17}$$

$$\ddot{z}_{G1} = \ l_{G1} \left(\ddot{q}_2 \cos q_2 - \dot{q}_2^2 \sin q_2 \right) \tag{6.18}$$

$$\ddot{x}_{G2} = -l_1 \left(\ddot{q}_1 \sin q_1 + \dot{q}_1^2 \cos q_1 \right) - l_{G2} \left(\ddot{q}_2 \sin q_2 + \dot{q}_2^2 \cos q_2 \right) \tag{6.19}$$

$$\ddot{z}_{G2} = l_1 \left(\ddot{q}_1 \cos q_1 - \dot{q}_1^2 \sin q_1 \right) + l_{G2} \left(\ddot{q}_2 \cos q_2 - \dot{q}_2^2 \sin q_2 \right) \tag{6.20}$$

Finally, substituting these last expressions in 6.9 and 6.10, we obtain the robot dynamic model,

$$\begin{aligned} \mathcal{T}_1 = &\left(J_1 + m_2 l_1^2 + m_1 l_{G1}^2 \right) \ddot{q}_1 + m_2 l_1 l_{G2} \cos\left(q_2 - q_1\right) \ddot{q}_2 - \\ &m_2 l_1 l_{G2} \sin\left(q_2 - q_1\right) \dot{q}_2^2 + \left(m_2 l_1 + m_1 l_{G1}\right) g \cos q_1 \end{aligned} \tag{6.21}$$

$$\begin{aligned} \mathcal{T}_2 = &\left(J_2 + m_2 l_{G2}^2 \right) \ddot{q}_2 + m_2 l_1 l_{G2} \cos\left(q_2 - q_1\right) \ddot{q}_1 + \\ &m_2 l_1 l_{G2} \sin\left(q_2 - q_1\right) \dot{q}_1^2 + m_2 l_{G2} g \cos q_2 \end{aligned} \tag{6.22}$$

As final step we include the actuating chain – the reducers and motor –

with their inertia and transmission ration,

$$\begin{aligned}\mathcal{T}_1 = &\left(\frac{J_{a1}}{n_1^2} + J_1 + m_2 l_1^2 + m_1 l_{G1}^2\right)\ddot{q}_1 + m_2 l_1 l_{G2}\cos\left(q_2 - q_1\right)\ddot{q}_2 - \\ &m_2 l_1 l_{G2}\sin\left(q_2 - q_1\right)\dot{q}_2^2 + \left(m_2 l_1 + m_1 l_{G1}\right) g\cos q_1\end{aligned} \tag{6.23}$$

$$\begin{aligned}\mathcal{T}_2 = &\left(\frac{J_{a2}}{n_2^2} + J_2 + m_2 l_{G2}^2\right)\ddot{q}_2 + m_2 l_1 l_{G2}\cos\left(q_2 - q_1\right)\ddot{q}_1 + \\ &m_2 l_1 l_{G2}\sin\left(q_2 - q_1\right)\dot{q}_1^2 + m_2 l_{G2} g\cos q_2\end{aligned} \tag{6.24}$$

where J_{ai} is the overall inertia of the actuating components, and $\mathcal{T}_i$ is redefined as the motor torque, τ_{mi}, reported at the joint,

$$\mathcal{T}_i = \frac{\tau_{mi}}{n_i} \tag{6.25}$$

IGM algorithm

In the section 6.1, we have seen the IGM is composed by two part. First, the complementary filter merges the motor speed and the inertial data at load side to obtain a new speed with higher frequency content. Then, having in input the motor torque and the new speed, GM generates the residual r for the collision detection.

Differently to the collision scenario, with which we have introduced the algorithm, we need to pre-process the inertial data before implementing the IGM approch. The inertial data are affected by the gravity acceleration, which requires to be removed. To achieve that, we use the angular position of the link to know how the gravity spans between the axes of the IMU

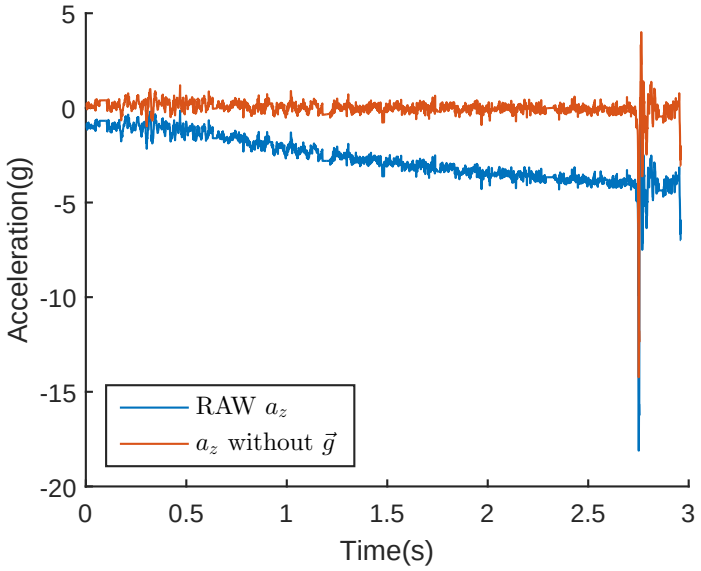

Figure 6.6: Comparison between the raw accelerometer measure and after its pre-processing.

sensors and through basic trigonometry relations it can be removed:

$$\bar{a}_{zi} = a_{zi} - a_{zi}cos(q_i) \tag{6.26}$$

The Figure 6.6 shows the result of the pre-processing for the arm's inertial measure along the z-axis, where it is possible to appreciate the difference between the signals. It is very clear the raw signal presents an offset due to the presence of the gravity. Then, during the rotation of the arm, the gravity along the axis grows. Observing the data, it is also possible to catch the direction of rotation of the robot arm.

Now, it is possible to apply the IGM algorithm. The complementary filter

for the robot arm is given by,

$$\hat{\dot{q}}_1 = \frac{\bar{a}_{z1}}{l_{IMU1}} \cdot \frac{s^2}{s^2 + k_1 s + k_2} + \dot{q}_1 \cdot \frac{k_1 s + k_2}{s^2 + k_1 s + k_2} \tag{6.27}$$

where $\dot{q}_1$ is obtained from motor speed ω_{m1} and the transmission ratio n_1. The residual of GM algorithm, always for the arm, is given by,

$$\begin{aligned} \hat{r}_1 =& K_1 \cdot \Bigg(\int \big(\mathcal{T}_1 - m_2 l_1 l_{G2} \cos(q_2 - q_1)\, \ddot{q}_2 - m_2 l_1 l_{G2} \cos(q_2 - q_1)\, \ddot{q}_2 \\ & + m_2 l_1 l_{G2} \sin(q_2 - q_1)\, \dot{q}_2^2 - \hat{r}_1 \big) dt - p_1 \Bigg) \end{aligned} \tag{6.28}$$

where the momentum p_1 is calculated by

$$p_1 = \left(\frac{J_{a1}}{n_1^2} + J_1 + m_2 l_1^2 + m_1 l_{G1}^2 \right) \hat{\dot{q}}_1 \tag{6.29}$$

The kinematic data of the joins are obtained from the motor ones through the transmission ratios.

The formulation of IGM for the forearm is given by,

$$\hat{\dot{q}}_2 = \frac{\bar{a}_{z2}}{l_{IMU2}} \cdot \frac{s^2}{s^2 + k_1 s + k_2} + \dot{q}_2 \cdot \frac{k_1 s + k_2}{s^2 + k_1 s + k_2} \tag{6.30}$$

and

$$\begin{aligned} \hat{r}_2 =& K_2 \cdot \Bigg(\int \big(\mathcal{T}_2 - m_2 l_1 l_{G2} \cos(q_2 - q_1)\, \ddot{q}_1 - m_2 l_1 l_{G2} \sin(q_2 - q_1)\, \dot{q}_1^2 \\ & - m_2 l_{G2} g \cos q_2 \dot{q}_2^2 - \hat{r}_2 \big) dt - p_2 \Bigg) \end{aligned} \tag{6.31}$$

where

$$p_2 = \left(\frac{J_{a2}}{n_2^2} + J_2 + m_2 l_{G2}^2 \right) \hat{\dot{q}}_2 \tag{6.32}$$

It is possible to note that we have written the algorithm at joints side, differently to the collision scenario in section 6.1. However, we underline that

nothing changes, since the speeds and torques of the joints still come from the motors.

FEEKF

In this section we formulate the FEEFK algorithm for robot arm. In particular, for the arm link since the approach is not applicable for the forearm link. In the Results section, the types of trials are described with explained the reason about its not-applicability.

Starting from the dynamic equation 6.21, let's add the virtual viscous friction term, representing the contact force:

$$\begin{aligned}\mathcal{T}_1 = &\left(\frac{J_{a1}}{n_1^2} + J_1 + m_2 l_1^2 + m_1 l_{G1}^2\right)\ddot{q}_1 + m_2 l_1 l_{G2}\cos(q_2 - q_1)\,\ddot{q}_2 - \\ &m_2 l_1 l_{G2}\sin(q_2 - q_1)\,\dot{q}_2^2 + (m_2 l_1 + m_1 l_{G1})\,g\cos q_1 + d_v \cdot \dot{q}_1\end{aligned} \tag{6.33}$$

where d_v is the virtual viscous coefficient.

Following [19] as a reference to apply the Extended Kalman Filter, let's formalize its main steps.
First, we define the state variables of the system, its input and the observations. Thus, the state variables are,

$$\boldsymbol{x} = \begin{cases} x_1 = d_v \\ x_2 = \ddot{q}_1 \\ x_3 = \dot{q}_1 \\ x_4 = q_1 \end{cases} \tag{6.34}$$

while the input u is the joint torque $\mathcal{T}_1$, which can be calculated from the motor torque measured and the transmission ration: $\mathcal{T}_1 = \frac{\tau_{m1}}{r_1}$. The observations

of the system are,

$$\boldsymbol{z} = \begin{cases} z_1 = \ddot{q}_1 = \dfrac{\bar{a}_{z1}}{l_{IMU1}} \\ z_2 = \dot{q}_1 = \omega_{m1} \\ z_3 = q_1 = \theta_{m1} \end{cases} \tag{6.35}$$

where ω_{m1} and θ_{m1} are respectively the speed and angular position of the motor. $\bar{a}_{z1}$ is the pre-processed acceleration, while l_{IMU1} is the sensor position along the arm link.

Hence, the discrete state space model of the arm link dynamics is:

$$\begin{cases} x_1(k+1) & = x_1(k) + w_1(k) \\ x_2(k+1) & = f_{x2} + w_2(k) \\ x_3(k+1) & = x_3(k) + T_s x_2(k) + w_3(k) \\ x_4(k+1) & = x_4(k) + T_s x_3(k) + w_4(k) \\ z_1(k) & = x_2(k) + v_1(k) \\ z_2(k) & = x_3(k) + v_2(k) \\ z_3(k) & = x_4(k) + v_1(k) \end{cases} \tag{6.36}$$

where,

$$\begin{aligned} f_{x2} = \Big(& u(k) - m_2 l_1 l_{G2} \cos\left(q_2 - x_4(k)\right) \ddot{q}_2 + \\ & m_2 l_1 l_{G2} \sin\left(q_2 - x_4(k)\right) \dot{q}_2^2 - \left(m_2 l_1 + m_1 l_{G1}\right) g \cos x_4(k) - \\ & x_1(k) \cdot x_3(k) \Big) \cdot \frac{1}{\frac{J_{a1}}{n_1^2} + J_1 + m_2 l_1^2 + m_1 l_{G1}^2} \end{aligned} \tag{6.37}$$

w_n represents the uncorrelated noise of the plant, v_m the uncorrelated noise in the measurement and T_s is the sampling time.

The second step consists in linearize our model and find the linearized matrix

F and H, requested for applying the EFK in accordance to [19]. Starting from the classic formulation in state space of a nonlinear system,

$$\begin{cases} \mathbf{x}(k+1) & = f(\mathbf{x}(k+1), \mathbf{u}(k)) \\ \mathbf{z}(k) & = h(\mathbf{x}(k), \mathbf{u}(k)) \end{cases}$$

The matrix F is given by,

$$\delta F = \frac{\delta f(x,u)}{\delta x} = \begin{bmatrix} 1 & 0 & 0 & 0 \\ F_{(2,1)} & 0 & F_{(2,3)} & F_{(2,4)} \\ 0 & T_s & 1 & 0 \\ 0 & 0 & T_s & 1 \end{bmatrix} \tag{6.38}$$

where

$$F_{(2,3)} = -\frac{x_3}{\frac{J_{a1}}{n_1^2} + J_1 + m_2 l_1^2 + m_1 l_{G1}^2} \tag{6.39}$$

$$F_{(2,3)} = -\frac{d_v}{\frac{J_{a1}}{n_1^2} + J_1 + m_2 l_1^2 + m_1 l_{G1}^2} \tag{6.40}$$

$$\begin{aligned} F_{(2,4)} = \Big(& g \sin(x_4)(l_2 m_3 + l_{G2} m_2) - l_2 l_{G3} m_3 \dot{q}_2^2 \cos(x_4 - q_3) + \\ & l_2 l_{G3} m_3 \ddot{q}_2 \sin(x_4 - q_2) \Big) \cdot \frac{1}{\frac{J_{a1}}{n_1^2} + J_1 + m_2 l_1^2 + m_1 l_{G1}^2} \end{aligned} \tag{6.41}$$

While the matrix H is,

$$\delta H = \frac{\delta h(x,u)}{\delta u} = \begin{bmatrix} 0 & 1 & 0 \\ 0 & 0 & 1 \end{bmatrix} \tag{6.42}$$

Finally, to complete the formulation the covariance matrix of the model

is defined as:

$$Q = I_{4x4} \cdot \boldsymbol{w} \tag{6.43}$$

$$R = I_{4x4} \cdot \boldsymbol{v} \tag{6.44}$$

where Q represents the covariance matrix related to the plant noise, while R is linked to the measurement noise. They are considered diagonal as simplified assumption. w and v are the variance vectors of the respective matrix.

Collision detection logic

With final goal to compare the performance of the two algorithms designed and the benchmark algorithm (the GM), we have developed a simple collision detection logic in way it does not influence the results.
Thus, based on a set of movements without impact, the threshold is created taking the mean of these curves and increasing it by a safe-factor, in this case the standard deviation multiplied by constant value.
Once the reference behavior is created the impact can be detected simply identifying when the collision detection signal exceeds the threshold.

In Figure 6.7a and 6.7a are reported respectively an example of activation for the FEEFKF and IGM algorithms.

6.2.4 Results

In this section we present the performance of the FEEKF and IGM algorithms for the application case considered. In particular, we compare our solutions with the *Generalized Momenta* algorithm used in Robotics and

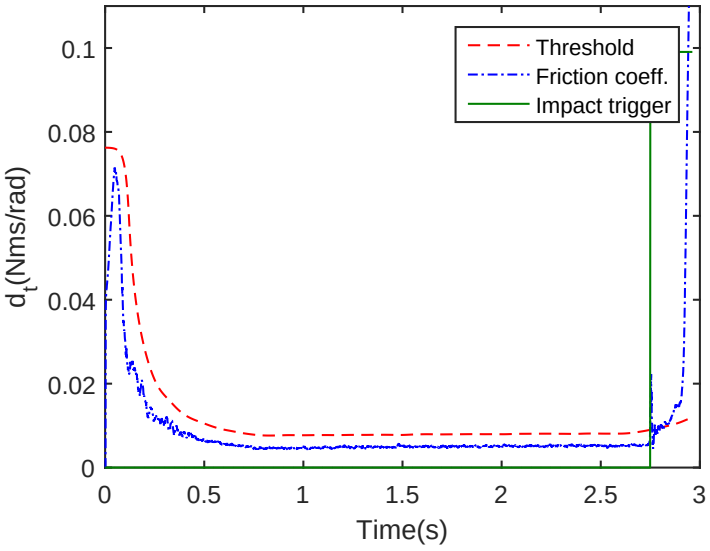

(a)

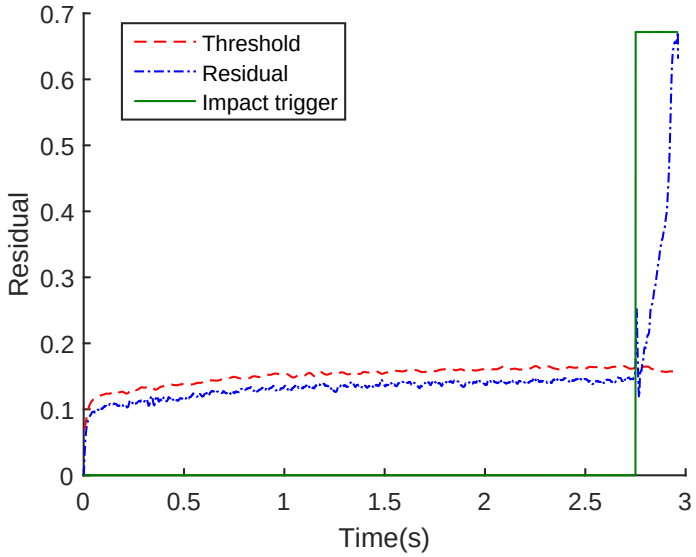

(b)

Figure 6.7: The figure illustrates how the FEEKF (a) and the IGM (b) algorithms identify the impact. In red (dashed line) is visible the *signature* created during the setting up of the system. In blue (dashed-dotted line) there is the friction coefficient estimated during a closing operation. In green (solid line) is visible the trigger which identifies the impact. It is clear that when the blue line exceeds the red one the impact is detected.

presented in the first chapters of this thesis.

It is important to underline the method used to generated the threshold for methods is the same. Therefore, the only difference in performance between the algorithms is given by the different data about the collision contained in the measure, or in the main information with which the threshold is generated.

The benchmark used to test the performance consists in two trials. In the first trial the collision occurs on the robot arm as shown in Figure 6.8a. The link starts its movement with an orientation of 45 degree and impacts with a joint constant speed of 16 degree per second. The forearm during the motion is kept perpendicular to the ground, $q_2 = 90°$. The aim with this trial is to test the algorithms for the arm motor.
In the second trial the collision occurs on the forearm, close to the wrist, as shown in Figure 6.8b. The robot arm starts with an orientation of 45 degree and impacts with a joint constant speed of 16 degree per second. The forearm during the motion is kept parallel to the ground, $q_2 = 0°$. The aim with this trial is to test the algorithms for the forearm motor.
With the last trial emerges an important issue about the applicability of the FEEKF algorithm. Since the forearm is kept at constant orientation, its motor speed is zero and the friction estimation approach does not work. During the motion it always estimates a viscous friction force equal to zero, thus an infinity value of the viscous friction coefficient which implies an impossibility of detecting the collision.
This might be a good application example of the FEEKF algorithm limit, since the mechanical system is actually in movement and a collision occurs, but, due to the transmission, the motor speed is zero and the event cannot be detect.

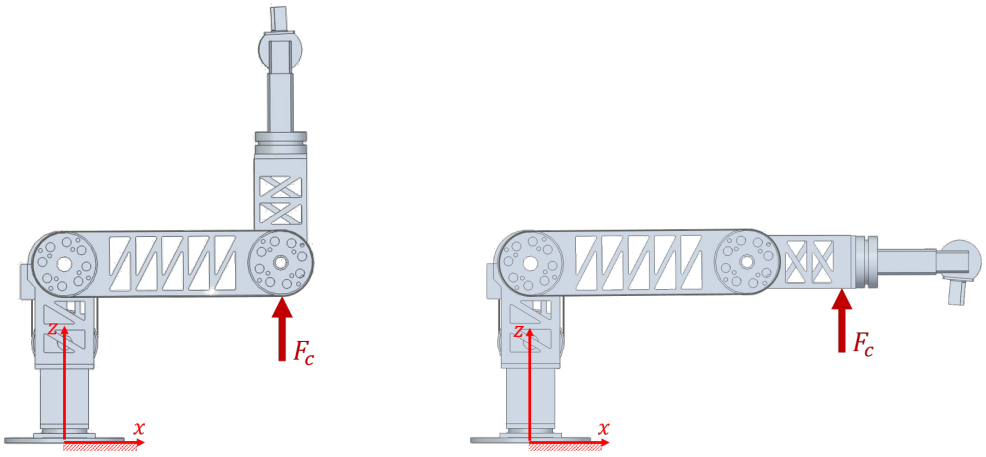

(a) (b)

Figure 6.8: The figures illustrate the types of collision performed for testing the algorithms on the robot arm. (a) shows the TRIAL-1, the collision on the arm. (b) shows the TRIAL-2, the collision on the forearm.

Thus, with the first trial are tested all the algorithms, while with the second are compared only the IMG and GM algorithms.

Stiff impact

The trigger activations for the stiff impact which, recalling the concept, represents a collision with a rigid object, are shown in figure 6.9 and the performance of the algorithms are summarized in the table 6.1.

For the first trial, the FEEKF algorithm is the fastest to detect the collision. It identify a collision occurred after 10 milliseconds. 20 milliseconds later, the trigger of Inertial Generalized Momenta sets off. As for the automatic gate application case, The GM algorithm identifies the collision much later compared to the others, since it doesn't have any measure at load side, where the collision occurs.

For the second trial, the novel GM is faster than the classic GM about 48 milliseconds. it is interning to note that, although FEEFKF is not always

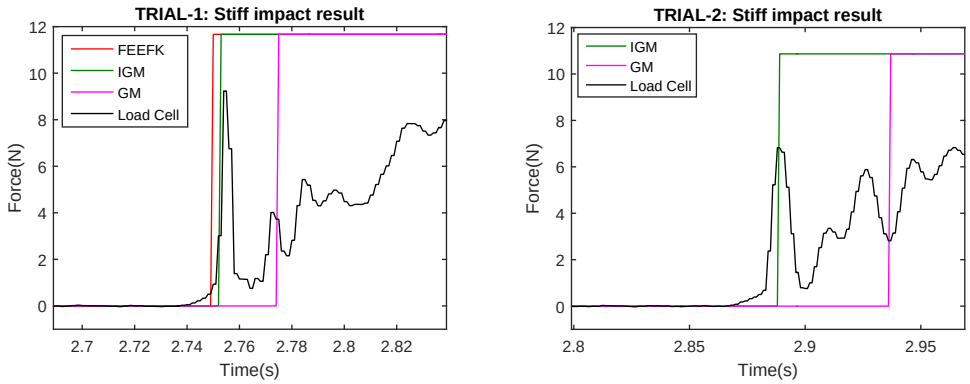

(a) (b)

Figure 6.9: Triggers of the IGM algorithm for the stiff impact. (a) is for the collision on the arm, (b) is for the collision on the forearm. The red line is the FEEKF, the green line is the IGM algorithm and the violet line the GM algorithm. The black continuous line is the force of the impact measured by the load cell.

applicable, it show the best performance.

Algorithm type	TRIAL-1: activation time (ms)		TRIAL-2: activation time (ms)	
	Mean	Std deviation	Mean	Std deviation
FEEKF	10	3.2	-	-
IGM	13	2.1	19	3
GM	35	5	67	10

Table 6.1: Performance of the algorithms in case of stiff impact. The mean and the std deviation are computed using 30 impact test.

Soft impact

The performance of the algorithms for the stiff impact are summarized in Table 6.2, whilst in Figure 6.10 the activations of the triggers are shown.

As for the automatic access gate case, the effect of the bumper is very

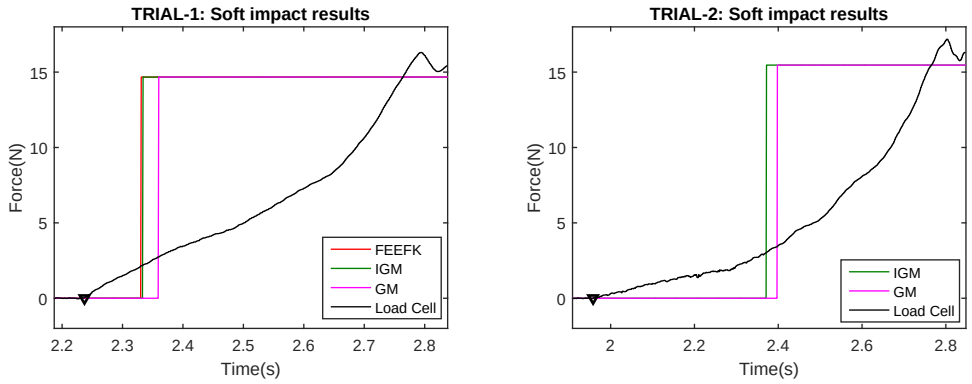

(a) (b)

Figure 6.10: Triggers of the IGM algorithm for the soft impact. (a) is for the collision on the arm, (b) is for the collision on the forearm. The green line is the IGM algorithm and the violet line the GM algorithm. The black continuous line is the force of the impact measured by the load cell.

visible.

Comparing the trend of the load cell between the two types of collision for the first trial, taken as example, we can see the signal is very smooth in the soft impact than the rigid case.

Though it does not appear so clearly, for both the trials the first algorithm to identify the impact is, again, the FEEKF which is able to perfectly mix the information from the accelerometer, the torque and speed.

Some milliseconds later, we get the IGM, while the worst performance are achieved by the benchmark algorithm.

Considerations

It is important to note the results confirm the main conclusions obtained with the gate application case. The solutions which perform better and are more robust for the different collisions are those which merge the load inertial measures with the motor ones, that are the torque and the speed.

Indeed, the algorithm which shows the worse performance is the Generalized

Algorithm type	TRIAL-1: activation time (ms)		TRIAL-2: activation time (ms)	
	Mean	Std deviation	Mean	Std deviation
FEEKF	93	2.6	-	-
IGM	96	1.9	412	5.3
GM	122	10.5	438	7.2

Table 6.2: Performance of the algorithms in case of soft impact. The mean and the std deviation are computed using 30 impact test.

Momenta, which does not use the accelerometer data.

The IGM e FEEKF algorithms present comparable results. The first approach seems performs a little better, however it has the drawback of not being always applicable, as for the collision trial on the forearm.

6.3 Conslusion

Starting from the Generalized Momenta approach, in this chapter we have developed a its evolution which takes the advantages from its older version and the FEEKF solution.
In particular, it shows similar performance to the FEEFK approach without have the drawback of the applicability when the motor speed is zero or the system is motionless. We called it as *Inertial Generalized Momenta* collision detection algorithm.

Summarizing, as the FEEKF algorithm, it uses the following sensor:

- position sensor at motor side – e.g. encoders;
- inertial measurement unit position at load side;
- finally, an information related to the control action of the regulator.

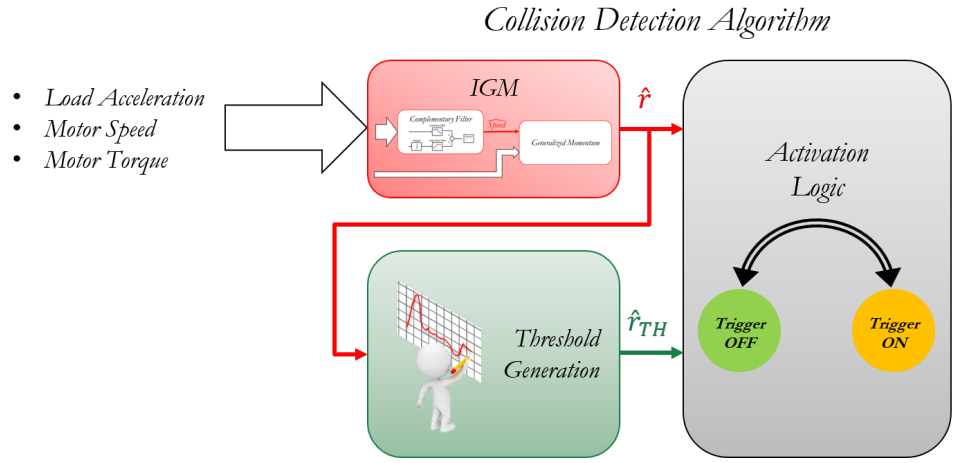

Figure 6.11: The structure of the IGM algorithm is briefly resumed in the figure. The torque, the angular speed and the acceleration permit to estimate the residual. Then this parameter is used for the creation of the *signature* and the identification of the impact.

In conclusion, in Figure 6.11 we reports the final structure of the IGM collision detection algorithm.

we propose

Chapter 7

Conclusions

This work focused on the collision detection issue for industrial application, trying to contribute with different aspects: from modeling, sensors and algorithms.

The goal of a collision detection algorithm is to identify a collision in a way to reduce the force generated. Thus, rapidity is crucial characteristic of the algorithm.

After investigating in literatures the physics of the phenomenon, its modeling approaches and the current collision detection schemes,we analyzed the impact dynamics in a generic actuated system, finding the sensors which give the optimal tradeoff between feasibility, costs and information about the collision event. Summarizing, the sensors are:

- position sensor at motor side – e.g. encoders;
- inertial measurement unit positioned at load side, close to the collision occurs;
- an information related to the control action of the regulator.

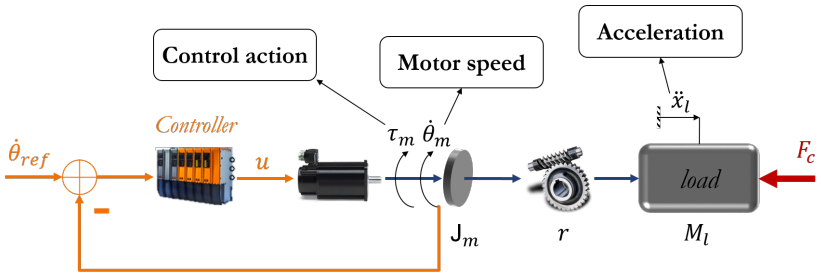

Figure 7.1

Considering as example a mechanical system actuated by an electrical motor, in Figure 7.1 we highlights the information used.

Basing on these results, afterward we developed and tested two new collision detection algorithms.

The first, it is the *Friction Estimation Extended Kalman Filter*. As the name suggests, the core of this approach is to use the EK filtering to estimate a virtual viscous coefficient, used to model the collision event, and detect the impact as a virtual changing of the mechanical system wear.
Analyzing its performance respect the *General Momenta algorithm*, the currently best recognized collision detection solution used in Robotics, we saw our solution is the fastest independently the physical characteristic of the collision – i.e. stiff impacts or soft impacts.
Further, we saw it presents a drawback about its applicability. The algorithm works only when the actuator is in movement.

To surpass this problem, we proposed also a second solution based on General Momenta approach and the FEEKF idea of merging the accelerometer information with the others two data, the actuator speed and effort. In particular, using a complementary filter we got a good estimate of the speed at the load during the collision. Using this signal with GM we obtained an relevant improvement of its performance, so much to be almost equivalent to the FEEKF solution. We named it: *Inertial Generalized Momenta*.

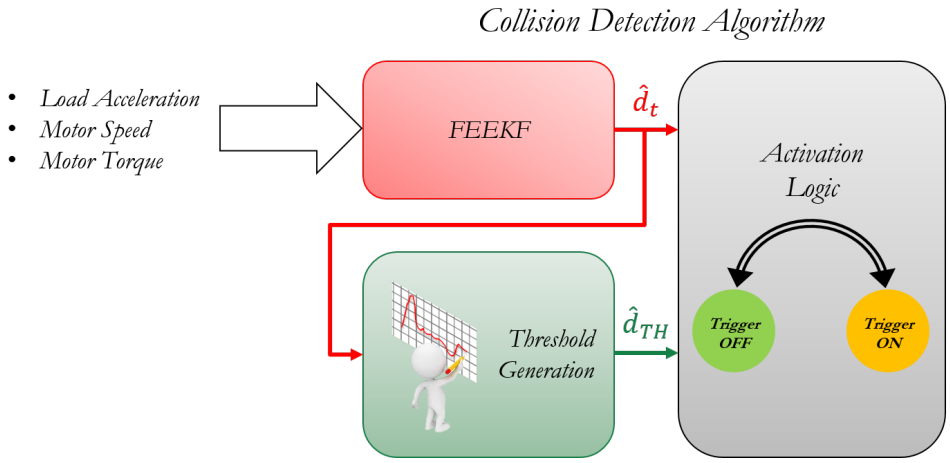

Figure 7.2: The structure of the algorithm is briefly resumed in the figure. The torque, the angular speed and the acceleration permit to estimate the friction coefficient. Then this parameter is used for the creation of the *signature* and the identification of the impact.

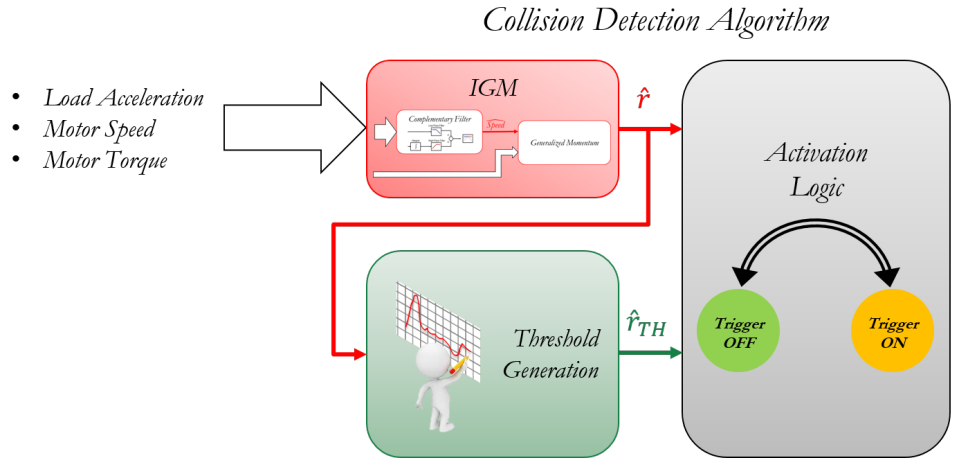

Figure 7.3: The structure of the IGM algorithm is briefly resumed in the figure. The torque, the angular speed and the acceleration permit to estimate the residual. Then this parameter is used for the creation of the *signature* and the identification of the impact.

In conclusion, we reports the final schemes of the new proposed algorithms 7.2 7.3.

Bibliography

[1] *PC-Crash: A simulation program for vehicle accident*. Technical manual, ver. 6.2, 2002.

[2] E Abele, M Dervisopoulos, and M Kreis. Beeinflussbarkeit von lebenszykluskosten durch wissensaustausch. produzieren mit blick auf die lebenszykluskosten. *wt Werkstatttechnik online*, 96:447–454, 2006.

[3] Eberhard Abele, Christian Brecher, SC Gsell, A Hassis, and D Korff. Steps towards a protection system for machine tool main spindles against crash-caused damages. *Production Engineering*, 6(6):631–642, 2012.

[4] Eberhard Abele and Dennis Korff. Avoidance of collision-caused spindle damages-challenges, methods and solutions for high dynamic machine tools. *CIRP Annals-Manufacturing Technology*, 60(1):425–428, 2011.

[5] GEES Andrea. *Accelerometer-enhanced speed estimation for linear-drive machine tool axes*. PhD thesis, Citeseer, 1996.

[6] P. Barkan. *Impact design, in: Mechanical Design and Systems Handbook, Section 31*. McGraw-Hill, 1974.

[7] A Bicchi and G Tonietti. Fast and soft arm tactics: dealing with the safety–performance tradeoff in manipulators design and control. *IEEE Robotics and Automation Magazine, Special Issue on Safety Among Us*, 11:23–24, 2004.

[8] R.M. Brach. *Mechanical Impact Dynamics: Rigid Body Collisions*. John Wiley and Sons, 1991.

[9] G Byrne and GE ODonnell. An integrated force sensor solution for process monitoring of drilling operations. *CIRP Annals-Manufacturing Technology*, 56(1):89–92, 2007.

[10] Alessandro De Luca and Raffaella Mattone. An adapt-and-detect actuator fdi scheme for robot manipulators. In *Robotics and Automation,*

2004. Proceedings. ICRA'04. 2004 IEEE International Conference on, volume 5, pages 4975–4980. IEEE, 2004.

[11] Alessandro De De Luca and Raffaella Mattone. Actuator failure detection and isolation using generalized momenta. In *Robotics and Automation, 2003. Proceedings. ICRA'03. IEEE International Conference on*, volume 1, pages 634–639. IEEE, 2003.

[12] Hans-Jörg Dennig. Entwicklung einer schnell schaltenden bremse und kupplung für linearbewegungen zum überlastschutz in werkzeugmaschinen. 2009.

[13] Michele Ermidoro. *Control and estimation problems based on inertial measurements in industrial mechatronic systems*. PhD thesis, University of Bergamo, 2015.

[14] G Gilardi and I Sharf. Literature survey of contact dynamics modelling. *Mechanism and machine theory*, 37(10):1213–1239, 2002.

[15] Werner Goldsmith. *Impact, the Theory and Physical Behaviour of Colliding Solids*. Edward Arnold Ltd., 1960.

[16] Yves Gonthier. Contact dynamics modelling for robotic task simulation. 2007.

[17] Sami Haddadin. *Towards safe robots: approaching Asimov's 1st law*, volume 90. Springer, 2013.

[18] Sami Haddadin, Alin Albu-Schäffer, Alessandro De Luca, and Gerd Hirzinger. Collision detection and reaction: A contribution to safe physical human-robot interaction. In *Intelligent Robots and Systems, 2008. IROS 2008. IEEE/RSJ International Conference on*, pages 3356–3363. IEEE, 2008.

[19] Simon S Haykin, Simon S Haykin, and Simon S Haykin. *Kalman filtering and neural networks*. Wiley Online Library, 2001.

[20] Gerd Hirzinger, Norbert Sporer, A Albu-Schaffer, M Hahnle, R Krenn, A Pascucci, and Markus Schedl. Dlr's torque-controlled light weight robot iii-are we reaching the technological limits now? In *Robotics and Automation, 2002. Proceedings. ICRA'02. IEEE International Conference on*, volume 2, pages 1710–1716. IEEE, 2002.

[21] W Stamps Howard and Vijay Kumar. A minimum principle for the dynamic analysis of systems with frictional contacts. In *Robotics and Automation, 1993. Proceedings., 1993 IEEE International Conference on*, pages 437–442. IEEE, 1993.

[22] KH Hunt and FRE Crossley. Coefficient of restitution interpreted as damping in vibroimpact. *Journal of applied mechanics*, 42(2):440–445, 1975.

[23] KH Hwang and AA Shabana. Effect of mass capture on the propogation of transverse waves in rotating beams. *Journal of sound and vibration*, 186(3):495–525, 1995.

[24] Rolf Isermann. Modellgestutzte uberwachung und fehlerdiagnose technischer systeme-teil 1. *Automatisierungstechnische Praxis*, 38(5):9–20, 1996.

[25] Rolf Isermann. *Fault-diagnosis systems: an introduction from fault detection to fault tolerance*. Springer Science & Business Media, 2006.

[26] Thomas R Kane and David A Levinson. *Dynamics: theory and applications*. McGraw Hill, 1985.

[27] YA Khulief and AA Shabana. Dynamic analysis of constrained system of rigid and flexible bodies with intermittent motion. *Journal of Mechanisms, Transmissions, and Automation in Design*, 108(1):38–45, 1986.

[28] YA Khulief and AA Shabana. Impact responses of multi-body systems with consistent and lumped masses. *Journal of Sound and Vibration*, 104(2):187–207, 1986.

[29] Kyung-Soo Kim, Keun-Ho Rew, and Soohyun Kim. Disturbance observer for estimating higher order disturbances in time series expansion. *Automatic Control, IEEE Transactions on*, 55(8):1905–1911, 2010.

[30] Peter R Kraus and Vijay Kumar. Compliant contact models for rigid body collisions. In *Robotics and Automation, 1997. Proceedings., 1997 IEEE International Conference on*, volume 2, pages 1382–1387. IEEE, 1997.

[31] HM Lankarani and PE Nikravesh. A contact force model with hysteresis damping for impact analysis of multibody systems. *Journal of Mechanical Design*, 112(3):369–376, 1990.

[32] Johann Marcus Marci. *De proportione motus: seu regula sphygmica ad celeritatem et tarditatem pulsuum ex illius motu ponderibus geometricis librato absque errore metiendam*. Bilina, 1967.

[33] DB Marghitu. The impact of flexible links with solid lubrication. *Journal of sound and vibration*, 205(5):712–720, 1997.

[34] Matthew T Mason and Yu Wang. On the inconsistency of rigid-body frictional planar mechanics. 1987.

[35] Khalid Mirza, Mark D Hanes, and David E Orin. Dynamic simulation of enveloping power grasps. In *Robotics and Automation, 1993. Proceedings., 1993 IEEE International Conference on*, pages 430–435. IEEE, 1993.

[36] Hamid Movahedi-Lankarani. Canonical equations of motion and estimation of parameters in the analysis of impact problems. 1988.

[37] R Neugebauer, P Klimant, and M Witt. Realistic machine simulation with virtual reality. *Procedia CIRP*, 3:103–108, 2012.

[38] R Neugebauer, P Klimant, and V Wittstock. Virtual-reality-based simulation of nc programs for milling machines. In *Global Product Development*, pages 697–703. Springer, 2011.

[39] JP Nobre, AM Dias, and R Gras. A study on elasto-plastic impact friction. *Wear*, 230(2):133–145, 1999.

[40] H Palas, WC Hsu, and AA Shabana. On the use of momentum balance and the assumed modes method in transverse impact problems. *Journal of vibration and acoustics*, 114(3):364–373, 1992.

[41] Gunter Pritschow and Sascha Rock. "hardware in the loop" simulation of machine tools. *CIRP Annals-Manufacturing Technology*, 53(1):295–298, 2004.

[42] William Franklin Riley and Loren W Zachary. *Introduction to mechanics of materials*. Wiley New York, 1989.

[43] Thomas Rudolf, Christian Brecher, and Frank Possel-Dolken. Contact-based collision detection-a new approach to avoid hard collisions in machine tools. In *International Conference on Smart Machining Systems*, 2007.

[44] Marco Schumann, Marco Witt, and Philipp Klimant. A real-time collision prevention system for machine tools. *Procedia CIRP*, 7:329–334, 2013.

[45] Bruno Siciliano and Oussama Khatib. *Springer handbook of robotics*. Springer Science & Business Media, 2008.

[46] Scott Smith. Post-processing should not work. *Cutting Tool Engineering*, 61(8), 2009.

[47] Guido Stoeppler, Thomas Menzel, and Steve Douglas. Hardware-in-the-loop simulation of machine tools and manufacturing systems. *Computing & Control Engineering Journal*, 16(1):10–15, 2005.

[48] Dan Stoianovici and Yildirim Hurmuzlu. A critical study of the applicability of rigid-body collision theory. *Journal of Applied Mechanics*, 63(2):307–316, 1996.

[49] William James Stronge. *Impact mechanics*. Cambridge university press, 2004.

[50] WJ Stronge. Unraveling paradoxical theories for rigid body collisions. *Journal of Applied Mechanics*, 58(4):1049–1055, 1991.

[51] Moncef Tagina et al. A novel fault detection approach combining adaptive thresholding and fuzzy reasoning. *arXiv preprint arXiv:1203.5454*, 2012.

[52] Goodier JN Timoshenko SP. *Theory of elasticity*. McGraw-Hill, New York, 1970.

[53] Tomonori. Collision prevention method for machine tool operating part.

[54] MA Veluswami and FRE Crossley. Multiple impacts of a ball between two plates-part 1: Some experimental observations. *Journal of Engineering for Industry*, 97(3):820–827, 1975.

[55] Yin-Tien Wang and Vi-jay Kumar. Simulation of mechanical systems with multiple frictional contacts. *Journal of Mechanical Design*, 116(2):571–580, 1994.

[56] Yu Wang and Matthew T Mason. Two-dimensional rigid-body collisions with friction. *Journal of Applied Mechanics*, 59(3):635–642, 1992.

[57] Leo J Windecker. Impact resistant composite structure, November 4 1980. US Patent 4,232,069.

[58] Y Yamada, Y Hirasawa, SY Huang, and Y Umetani. Fail-safe human/robot contact in the safety space. In *Robot and Human Communication, 1996., 5th IEEE International Workshop on*, pages 59–64. IEEE, 1996.

[59] Yoji Yamada, Yasuhiro Hirasawa, Shengyang Huang, Yoji Umetani, and Kazutsugu Suita. Human-robot contact in the safeguarding space. *IEEE/ASME transactions on mechatronics*, 2(4):230–236, 1997.

[60] AS Yigit, AG Ulsoy, and RA Scott. Dynamics of a radially rotating beam with impact, part 2: experimental and simulation results. *Journal of Vibration and Acoustics*, 112(1):71–77, 1990.

[61] J Zhang, SK Ong, and AYC Nee. Design and development of an in situ machining simulation system using augmented reality technology. *Procedia CIRP*, 3:185–190, 2012.